Petrography, ore mineral paragenesis, and gold deportment of the Twin Hills Gold Deposit, central Namibia.

Johannes Sales (2508821)

School of Geosciences, University of the Witwatersrand, Johannesburg, South Africa

08 June 2023

Supervisor: Prof. Paul Nex

A Thesis submitted to the Faculty of Science, University of the Witwatersrand, Johannesburg, in fulfillment of the requirements for the degree of Master of Science.

Plagiarism Declaration

University of the Witwatersrand, Johannesburg

School of Geosciences

SENATE PLAGIARISM POLICY

Declaration by Students

I Johannes Sales (Student number: 2508821) am a student registered for Master of Science in the year 2022. I hereby declare the following:

- **I am aware that plagiarism (the use of someone else's work without their permission and/or without acknowledging the original source) is wrong.**
- **I confirm that ALL the work submitted for assessment for the above course is my own unaided work except where I have explicitly indicated otherwise.**
- **I have followed the required conventions in referencing the thoughts and ideas of others.**
- **I understand that the University of the Witwatersrand may take disciplinary action against me if there is a belief that this in not my own unaided work or that I have failed to acknowledge the source of the ideas or words in my writing.**

Signature:  **Date: 08 June 2023**

Abstract

The Twin Hills Gold Deposit is an orogenic gold deposit hosted within the metamorphic turbidites of the Kuiseb Formation in the Southern Central Zone of the Damara Belt. This study aimed to understand the petrography of the host rocks, the formation of the ore minerals and asses the deportment of the Twin Hills Gold Deposit. Methods used in this study included drill core logging, transmitted and reflected light microscopy and scanning electron microscopy (SEM) based TESCAN Integrated Mineral Analyzer (TIMA). The host rocks are characterized by graded bedding with gradations ranging from pelitic mica-rich interbeds to psammitic quartz-rich interbeds, together forming interbedded metagreywacke. The interbedded metagreywacke is the main host unit of the gold mineralization and is made up of quartz, biotite, muscovite, plagioclase, orthoclase and cordierite. The ore mineral assemblage at the Twin Hills Gold Deposit is characterized by the prescence of gold and three major sulphide minerals namely, pyrrhotite, arsenopyrite, and pyrite. Gold mineralization at the Twin Hills Gold Deposit is associated with two main hydrothermal alterations, namely, potassic alteration and silicification. This research suggests at least three stages of mineralization within the Twin Hills Gold Deposit. The first stage is the diagenetic stage, which involved the enrichment of diagenetic arsenian pyrite (Py_0) in the turbiditic sediments with gold and other trace elements via the exhalation of reduced, deep-seated Au-As enriched H_2S-rich basinal brines onto the sea floor. The second stage involved the release of gold initially locked up within the arsenian pyrite (Py_0) crystal lattice into the metamorphic fluids and the subsequent precipitation of free gold (Au_1) from the gold bearing fluids via phase separation due to a drop in fluid pressure. This resulted in the formation and concentration of disseminated gold to economic grades within the metagreywacke. The third stage is the quartz veining stage, which was characterized by increased permeability and advanced fluid flow due to

progressive metamorphism and deformation. This stage was responsible for the remobilization of fine gold grains (Au_1) that were disseminated within the groundmass of the metagreywacke and concentrating them into the biotite selvages. This stage is also presumed to be responsible for the exsolution of gold from the arsenopyrite crystal lattice resulting in very fine gold (Au_2) grains included within arsenopyrite crystals (Asp_2). The third stage led to the further upgrading of the gold grades to higher economic levels. The gold deportment analyses revealed three modes of occurrences of gold within the Twin Hills deposit. This includes gold disseminated within the groundmass, gold grains disseminated within biotite selvages associated with quartz veinlets and gold grains included within arsenopyrite crystals. This study recommends a two stage recovery procedure to ensure optimum gold recovery, this includes gravity separation methods followed by cyanide leach process. The outcomes of this research further reiterate the importance of the Kuiseb Formation meta-turbidites as a significant fertile source for gold and mineralizing fluids in sediment hosted gold deposits in the Damara Belt. A sediment hosted gold deposit model should be adopted in conjunction with the mineral systems approach in identifying targeting vectors in exploration programs. This exploration approach should also be applied to other meta-sediment hosting stratigraphic sequences within the Damara Belt such as the Arandis and the Okonguarri Formations. These stratigraphic horizons have proven gold fertility as they host the only two currently producing gold mines in Namibia, the Navachab gold mine and the Otjikoto gold mine.

Acknowledgments

Firstly, I would like to express my heartfelt gratitude to Osino Resources Corp. (Osino) for funding my studies. This project would not have been possible without their generous support. I will forever be grateful for this. Words cannot express my gratitude to my supervisor, Prof. Paul Nex, for his guidance, patience, and constant feedback throughout this journey.

I would like to express my deepest appreciation to Jon Andrew for supporting my ambition to undertake this MSc journey and for the meticulous review and discussions of my research work. I am incredibly grateful to Dave Underwood for his continuous support, constructive discussions, and mentorship during my studies. My heartfelt appreciation goes to Wynand Slabbert for his unending support, belief in me, and always ensuring that I had all I needed for my studies. This journey has been a smooth one due to your momentous contributions. I am very grateful. I would like to thank the senior management at Osino for their technical and professional contribution to my growth (Edwin Daweti, Theresia Malobela, Werner Schuckmann, Svetlana Loubser, Malakia Iindombo, and Linda Hishoono).

Special thanks to Silke Van Heerden and Maria Kambazembi for your enormous support with the logistics of my travels to and from Johannesburg over the past two years. My journey has indeed been smooth due to your significant contributions; I am very grateful.

I would like to thank Prof. Benjamin Mapani for his support, mentorship, and assistance with some of the earliest interpretations of the petrography results.

I would like to extend my sincere thanks to Prof. Grant Bybee and Dr. Nonkuselo Madlakana for your assistance with the TIMA analysis in the Wits Automated Mineralogy Lab.

Many thanks to Leonidas Vonopartis and Senamile Dumisani for assistance with analyses in the Wits Imaging and Microscopy Lab.

I am also thankful to my classmates who made my time at Wits a fantastic experience (Lovemore Mauled, Leahn-Pieterse, Sitwala Mulonda, Karina Ndalulilwa, Kapalakasha Mulenga, Connie Setladi, Mietha Du Plessis, Ompile Phala, Bruno Bartolomeu, Jason Borrett, Jumien Peceur and Paula Mabena.

I am also thankful to Josia Shilunga for the interesting discussions and advice with the writing of the thesis. Thank you for always inspiring me to keep pushing for excellence.

I would like to thank my colleagues at Osino for your advice, proofreading, and moral support (Sakaria Thomas, Job Nghipandulwa, Albertina Mwandingi, Nailoke Shali and Tangeni Nantana).

Lastly, I would be remiss in not mentioning my family; their belief in me and unwavering support has kept me motivated to achieve my goals.

Table of Contents

List of Figures

List of tables

Chapter 1

Introduction

1.1 Background and Research rationale

The Damara Belt has proven to have a significant mineral endowment, especially in west central Namibia, where a number of gold occurrences are known, and a diverse range of commodities such as gold, uranium, lithium, tin, tantalum, and tourmaline are mined (Steven, 1992).

The Damara Belt has significant potential for hosting orogenic gold-type deposits. Several gold deposits and occurrences from historical to recent discoveries have been recorded within the Damara Belt, e.g Navachab, Otjikoto, Ondundu, Onguati, Goldkuppe and Twin Hills.(Figure 1).

There are, however, only two gold-producing mines currently in Namibia, namely QKR Navachab gold mine and B2Gold's Otjikoto gold mine. It is the author's opinion that the Damara Belt has been underexplored for orogenic gold-type deposits. The discovery of the Twin Hills gold deposit by Osino Resources Corp. (Osino) in 2019 and the recent discovery of significant gold mineralization at Kokoseb by Wia Gold Limited in 2022 further highlight this point and shows the significant potential for further discovery of similar mineralization within the Damara Belt.

1.1.1 Orogenic Gold Deposits

Orogenic gold deposits are a distinctive class of deposits that are epigenetic, structurally hosted lode-gold deposits in metamorphic terranes with unique temporal and spatial associations with collisional orogens (Groves, et al.,, 1998; Goldfarb, et al., 1998; Goldfarb, et al., 2001) (Figure 2).This group of deposits has significant unifying geological and geochemical features, amongst

which are tectonic setting, structural controls, conditions of formation and ore and alteration parageneses (Groves, et al.,, 1998; Goldfarb, et al., 1998; Goldfarb, et al., 2001; Kisters, 2005; Wulff, et al., 2010; Goldfarb & Groves, 2015; Gloyn-Jones, 2018). Mafic and ultramafic rocks (e.g., in the greenstone belts) or metamorphosed marine sedimentary sequences commonly host orogenic gold mineralization. (Goldfarb, et al., 2001; Wulff, et al., 2010).

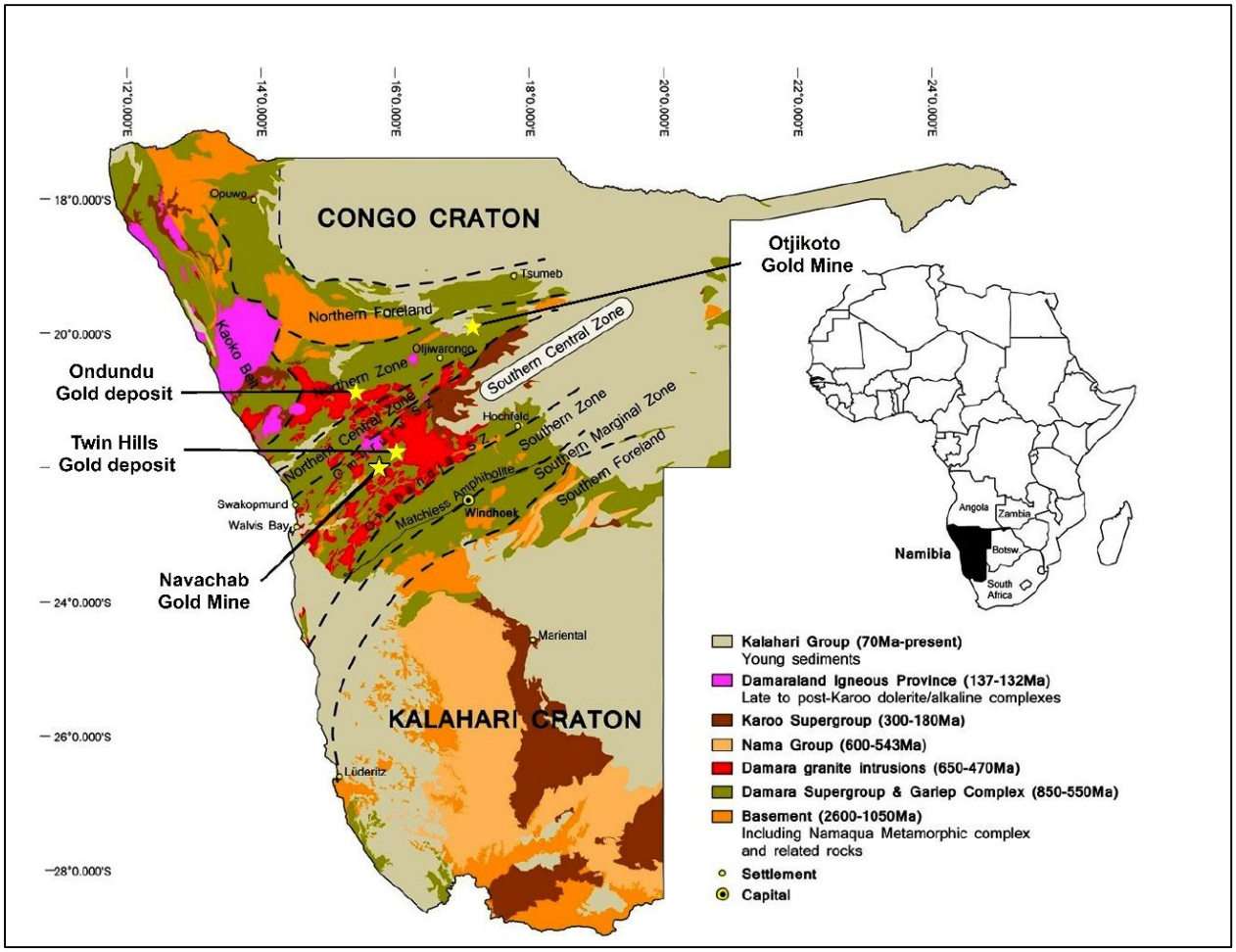

Figure 1 Geological map of Namibia showing the tectonostratigraphic domains of the Damara Belt and some of the significant gold deposits within the Damara Belt (Modified after Vollgger, et al., 2015).

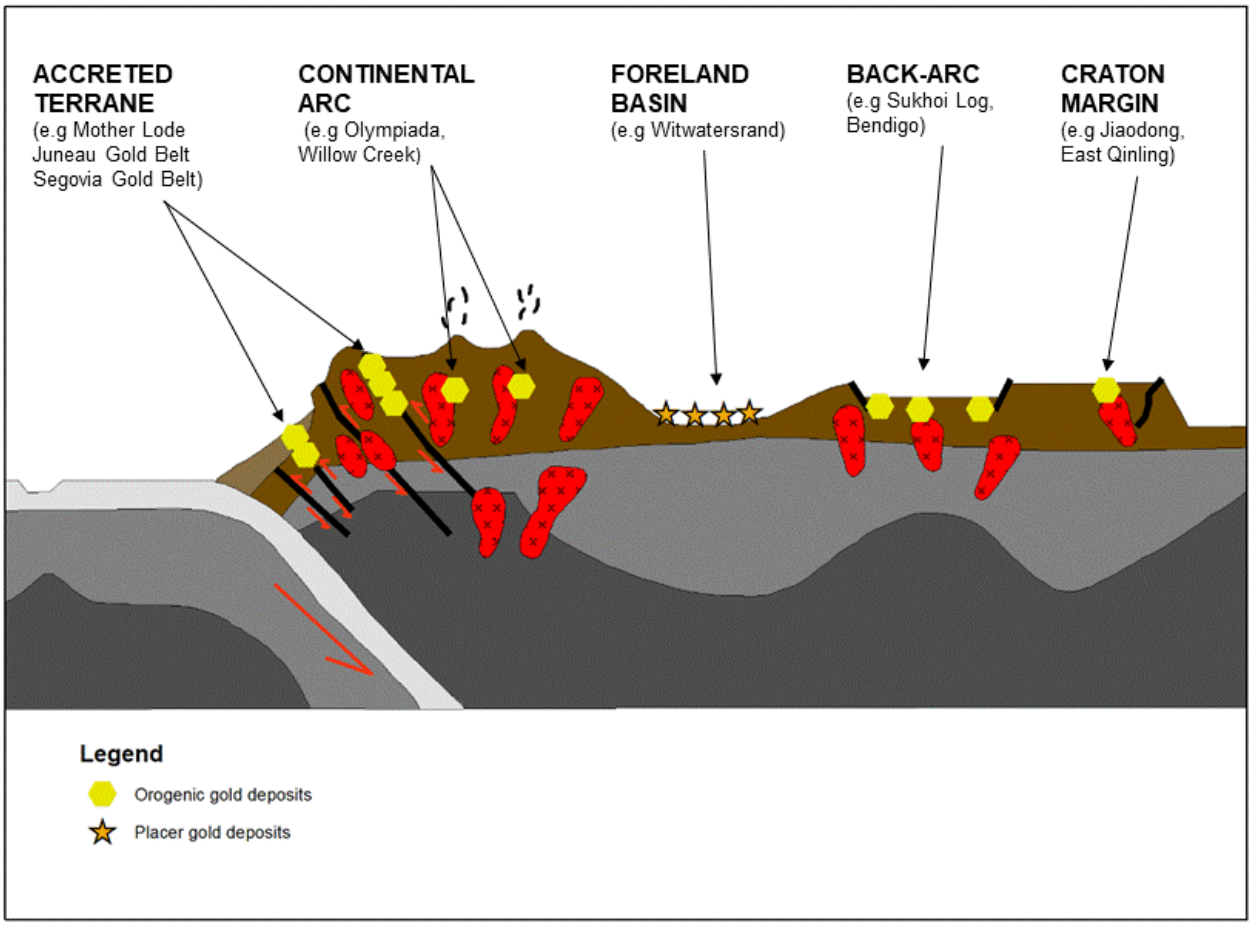

Figure 2 A schematic cross-section depicting the tectonic setting of known orogenic and related placer gold deposits, i.e., the back-arc regions of an active continental margin and along sheared cratonic margins (Modified after (Goldfarb & Groves, 2015).

Mineralising fluids are formed as metamorphic fluids by thermal gradients during orogenesis, where temperatures reach about 400-500°C by dehydration of the source rocks during prograde metamorphism (Goldfarb, et al., 2001; Wulff, 2008). The source rocks typically contain syngenetic sulphide minerals (e.g., in greenstones and marine sedimentary sequences), in which the sulphur is partly released into the metamorphic fluids. The sulphur-bearing hydrothermal fluids transport a significant amount of gold along major, deep-seated structures (e.g., major shear interbeds and thrust faults) (Goldfarb, et al., 2001).

The gold is eventually deposited in secondary and tertiary fault structures at shallower crustal levels of the uplifting orogeny (Goldfarb, et al., 2001; Wulff, 2008). A ubiquitous spatial and temporal association of orogenic gold deposits with granitoids has been explained as a result of temperatures exceeding 700°C in and below gold bearing fluid source area and forming both fluid and melt, of which the latter crystallizes into granitoids (Goldfarb, et al., 2001).

1.1.2 The Twin Hills Gold Project

The Twin Hills Gold Project (Twin Hills) is located within the southern Central Zone (sCZ) of the Damara Belt in Namibia. The project area lies south of the Omaruru Lineament and is about 20-55 km east-northeast of the Navachab Gold Mine (Geldenhuys & Hetherington, 2021). The project area is underlain by meta-sedimentary rocks of the Swakop Group. The Swakop Group units in the project area are characterized by biotite schists and calc-silicate rocks of the Arandis Formation, dolomitic and calcitic marbles of the Karibib Formation, and schistose quartz feldspar mica meta-greywackes and meta-pelites of the Kuiseb Formation (Figure 3).

The Twin Hills Project includes a series of gold discoveries along the crustal-scale Karibib Fault Zone (KFZ) on the southern margin of the Karibib Basin (Geldenhuys & Hetherington, 2021) (Figure 3). Osino Resources Corp. (Osino) interpreted the KFZ from regional magnetic data to have a strike length of over 100km (Underwood, 2020) (Figure 3 and Figure 4). Osino have located gold mineralization along the KFZ for over 20km of strike length. The Twin Hills Gold Deposit is located in the calcrete-covered central portion of the KFZ, at a structural jog and secondary structures splaying off the KFZ (Geldenhuys & Hetherington, 2021) (Figure 5). Geochemical sampling over Twin Hills Gold Deposit targeted the hard pan part of the calcrete. Anomalous

samples returned gold concentration ranging from 20 to >300 ppb Au. The deposit is characterized by a cluster of gold mineralized interbeds associated with the variably magnetic schists of the Kuiseb Formation, with the gold mineralization mainly associated with arsenopyrite, pyrrhotite, and pyrite (Underwood, 2020).

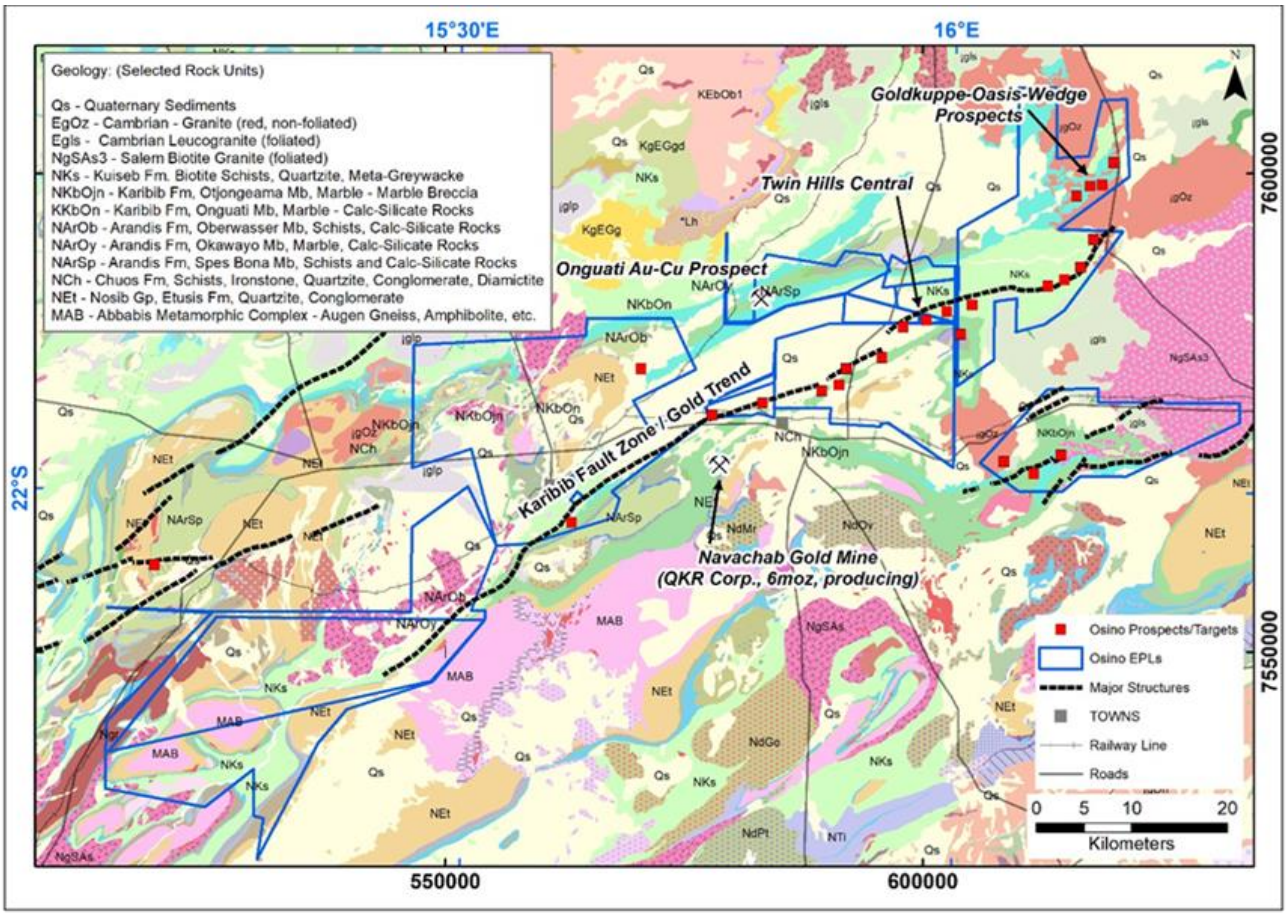

Figure 3 Geology of the Twin Hills Project Area and location of the Osino targets with reference to the Karibib Fault Zone (KFZ) (Underwood, 2020).

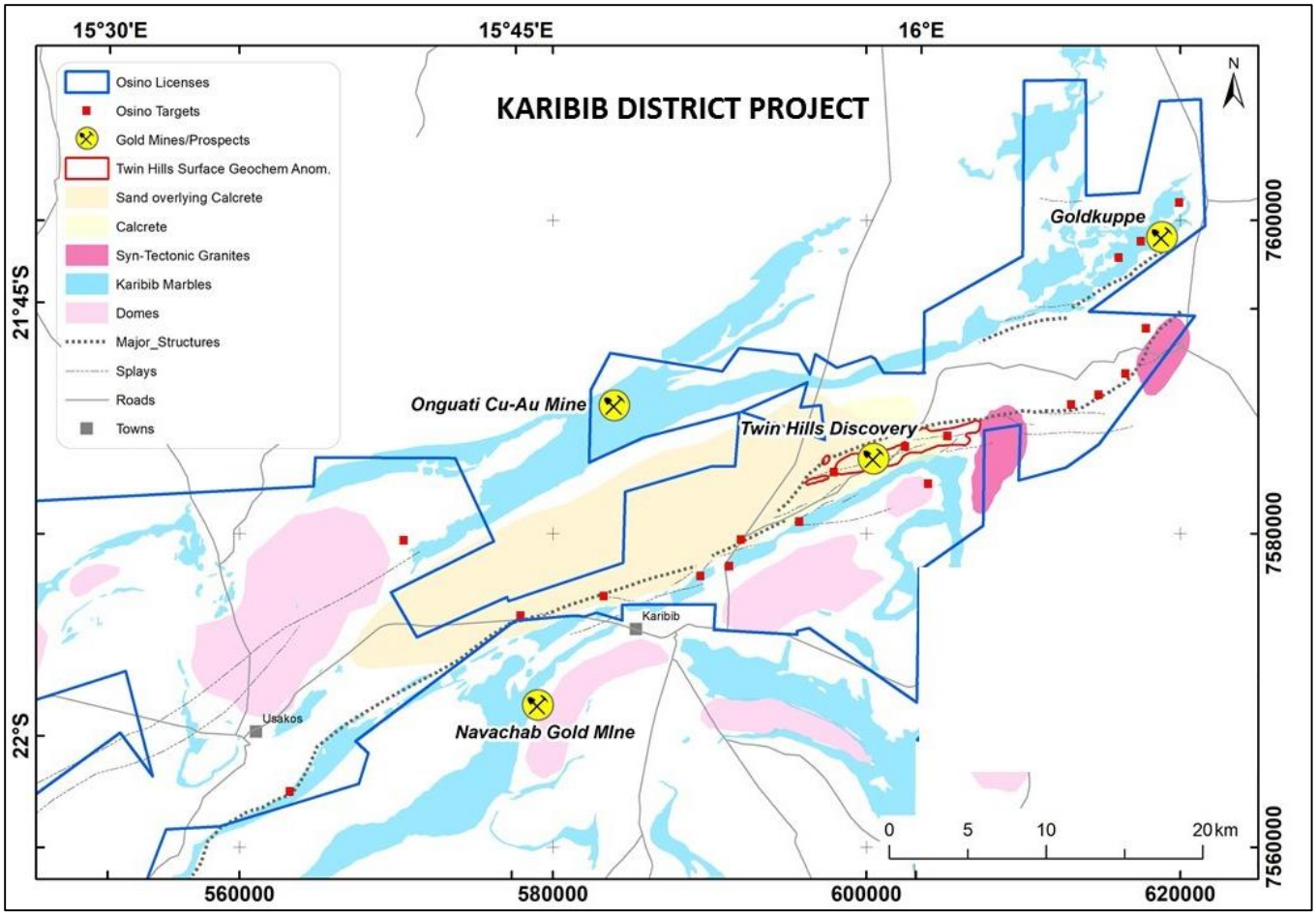

Figure 4 The Karibib Fault Zone (KFZ) on the southern margin of the Karibib Basin. The Twin Hills Gold Deposit is located on splays off the KFZ. Notable gold deposits and occurences are also indicated. (Source: Osino Resources Corp, 2021).

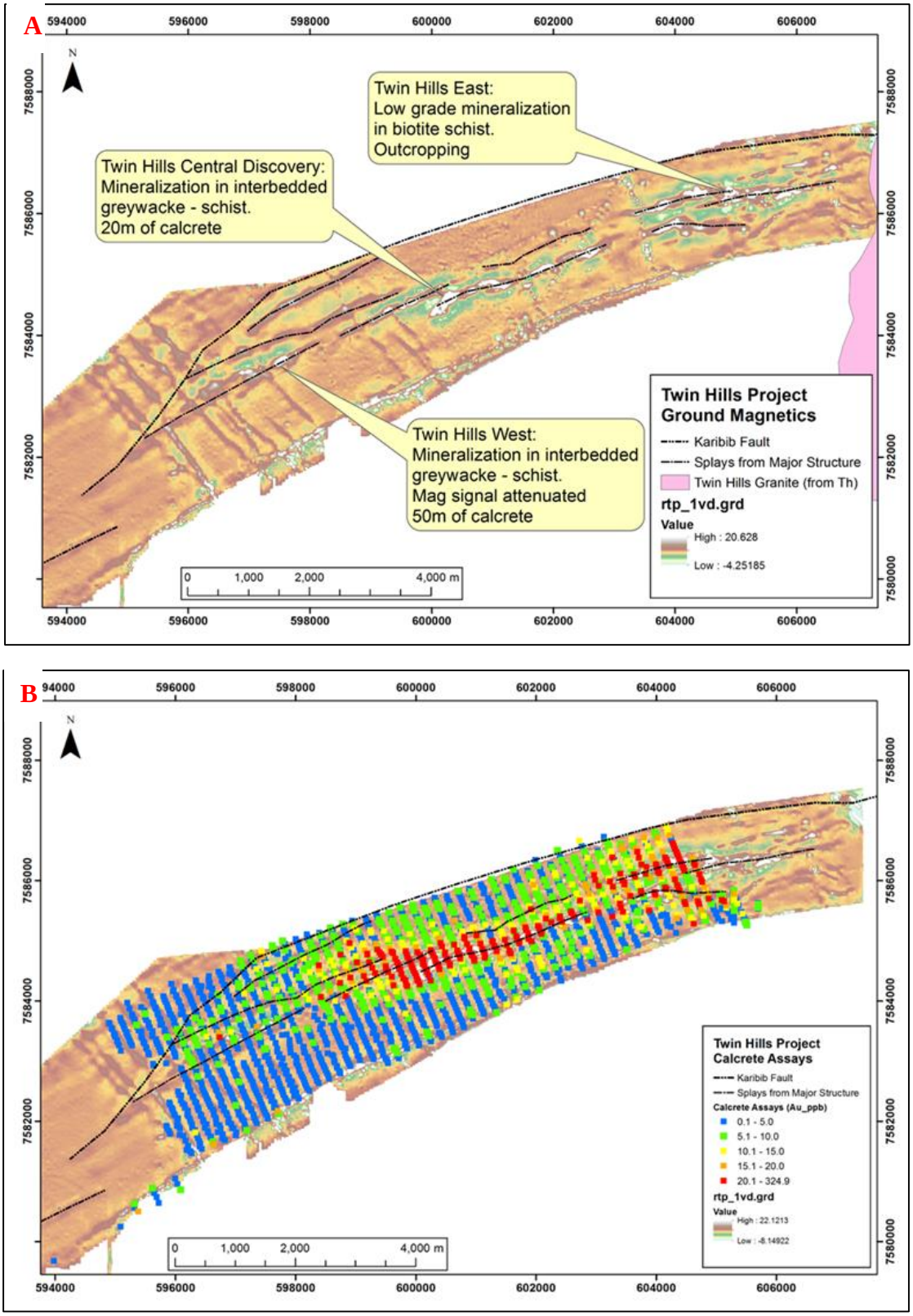

Figure 5 Depiction of the Karibib Fault Zone from A)Delineation of the KFZ and associated splays. B)Anomalous calcrete assays over the Twin Hills project. (Source: Osino Resources Corp. 2021)

1.2 Location of the Study Area

The study area is located in the Karibib district, west central Namibia, about 22km northeast of the town of Karibib.

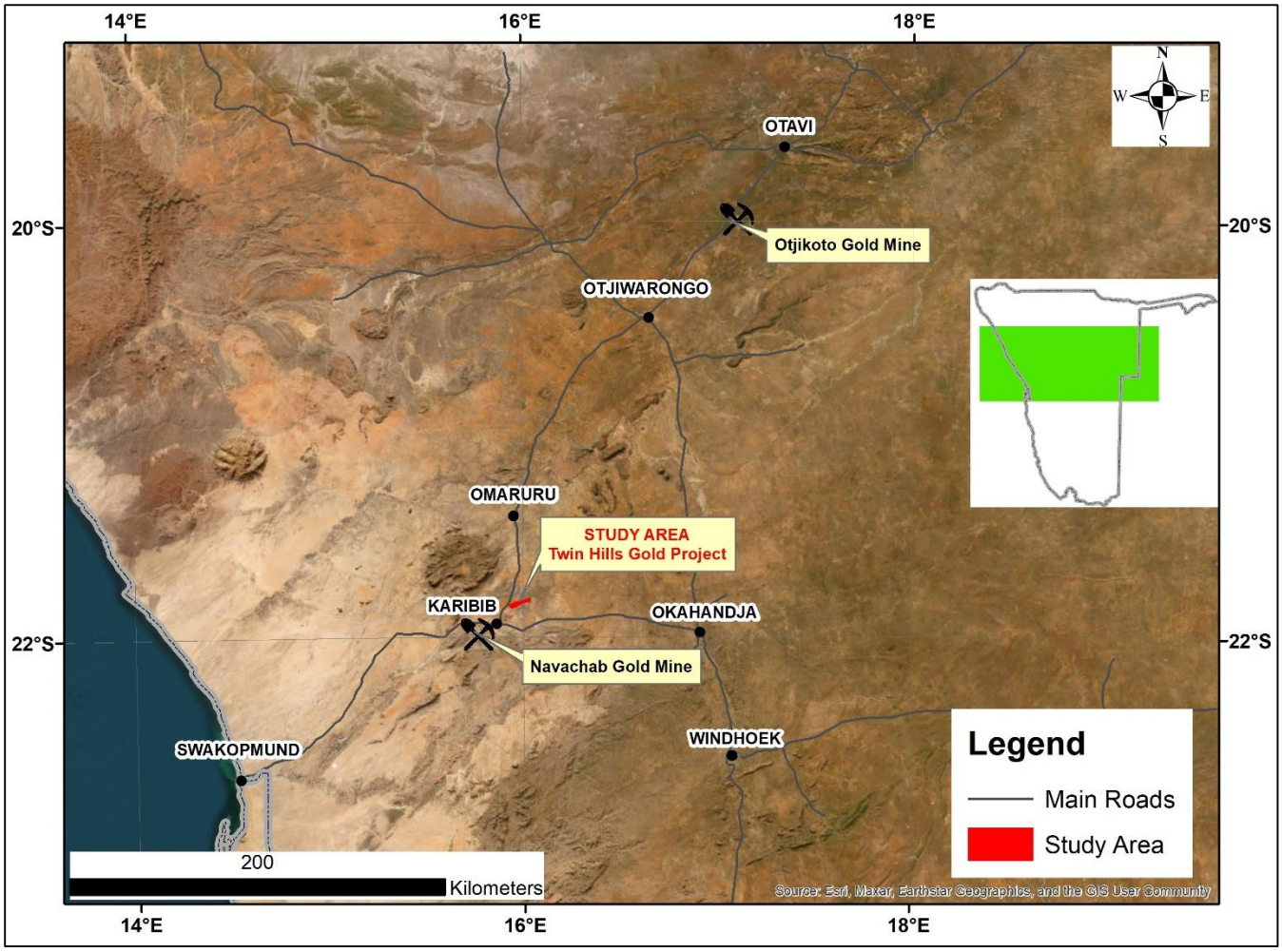

Figure 6 Google Earth Image showing the location of the study area in relation to surrounding major towns and the locations of the two gold-producing mines in Namibia. Source: Esri, Maxar, Earthstar Geographics, and the GIS User Community).

1.3 Problem Statement & Aims

The Twin Hills Gold Deposit was discovered in mid-2019, and little academic research has been carried out on the project to date. This study aims to understand the petrography of the host rocks, the formation of ore minerals, and to investigate a case for multiple stages of mineralization due to multiple modes of occurrence of ore minerals. The study also aims to conduct a comprehensive gold deportment study on the gold mineralization at Twin Hills. The study further seeks to establish a genetic model and the relative timing of mineralization for the Twin Hills Gold Deposit.

1.4 Objectives

The objectives of this research project are as follows:

- To produce detailed petrographic descriptions of the host rocks, mineralogy and alteration.
- To produce a detailed paragenetic sequence of the ore minerals at Twin Hills Gold Deposit.
- To investigate a case for multiple stages of mineralization by identifying, quantifying, and grouping different generations of sulphides and gold minerals.
- To quantify and describe the main alteration types at Twin Hills Gold Deposit.
- To carry out a comprehensive gold deportment study by locating and describing the gold-containing particles, their grain size, association, liberation, and free surface area.
- To explain the consistent association of pyrite with pyrrhotite and arsenopyrite in the deposit.
- To investigate the metamorphic grade in the Twin Hills area.
- To establish a genetic model and the relative timing of mineralization for the Twin Hills Gold Deposit.

Chapter 2

Regional Geology

2.1 Regional Geology of the Damara Belt

2.1.1 The Damara Belt

The amalgamation of continents to form the Gondwana supercontinent in the Neoproterozoic resulted in a widespread orogenic episode characterized by orogenic belts which formed as sutures between the continents (Miller, 1983; Miller, 2008; Gray, et al., 2007). This episode is called the Pan-African orogenic event because these belts are located within and around Africa, but are also known in South America, India and Antarctica.

The Damara Orogen in Namibia represents the suture of the collision between the Congo and Kalahari Cratons of Southern Africa and the Rio de la Plata Craton of South America (Gray, et al., 2006) (Figure 7). The Damara Orogen comprises of three component arms that define a three-pronged orogenic system (Gray, et al., 2007). These components include a N-S trending coastal branch made up of the northern Kaoko and southern Gariep Belts, and a NE-trending intracratonic branch, the Damara Belt (Miller, 1983; Miller, 2008; Gray, et al., 2006; Gray, et al., 2007).

The Damara Belt is subdivided into several distinct tectonostratigraphic interbeds on the basis of stratigraphy, structure, metamorphic grade, plutonic rocks, geochronology, and aeromagnetic expression (Miller, 1983; Miller, 2008). The main tectonostratigraphic interbeds identified by Miller, (2008) include the Northern Platform (NP), Northern Zone (NZ), Central Zone (CZ), Okahandja Lineament Zone (OLZ), Southern Zone (SZ), Southern Margin Zone (SMZ) and Southern Foreland (SF) (Figure 8).

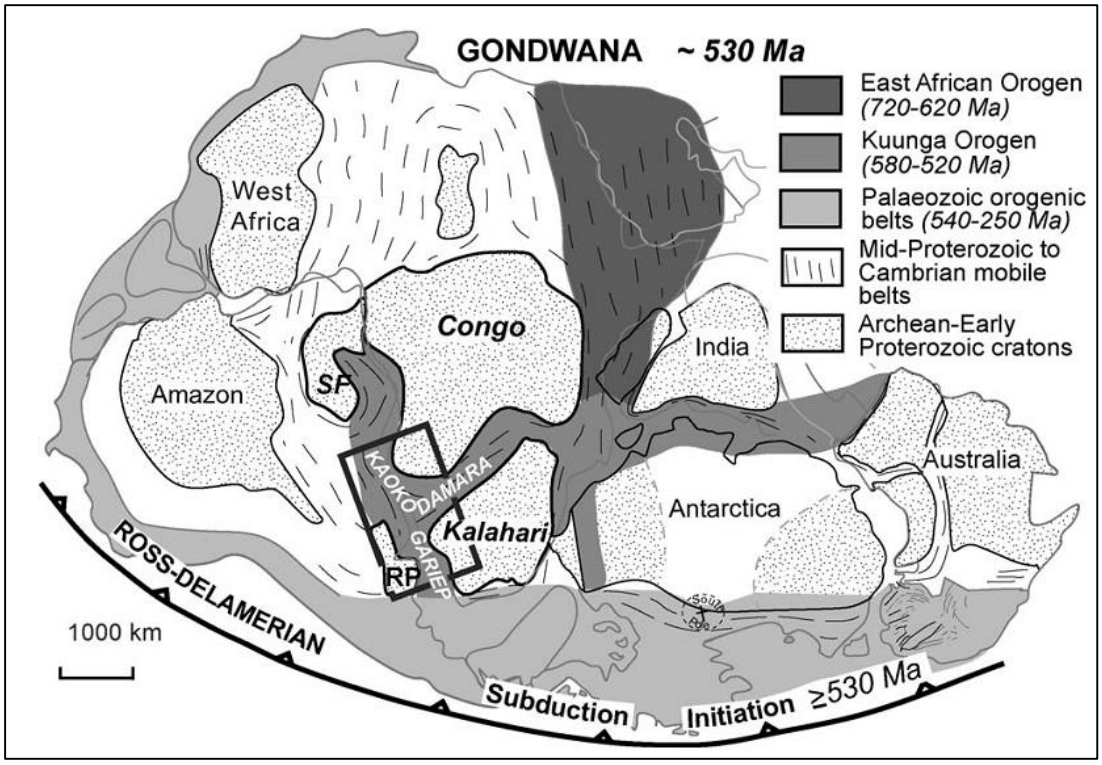

Figure 7 Showing the Gondwana supercontinent with emphasis on the positions of the Congo, Kalahari, and Rio de la Plata (RP) amongst a mosaic of other cratons linked by a set of Pan-African-Brasiliano fold belts (Gray, et al, 2006).

2.1.2 The Central Zone

The Central Zone (CZ) is a tectonostratigraphic entity of the Damara Belt, characterized by low pressure and high temperature (Puhan, 1983; Steven, 1992; Miller, 1983; Kisters, 2005; Miller, 2008). It is is comprised of calcareous and pelitic metasediments and minor volcanics, which were initially deposited in a back-arc basin on a passive continental margin that rested on the pre-Damaran basement rocks (Miller, 1983; Steven, 1992; Oliver, 1995; Oliver, 2014). The magnetically defined Omaruru Lineament (OmL) -Waterberg Fault separates the CZ into the northern Central Zone (nCZ) and southern Central Zone (sCZ) (Miller, 1983; Steven, 1992 Creus, 2011).

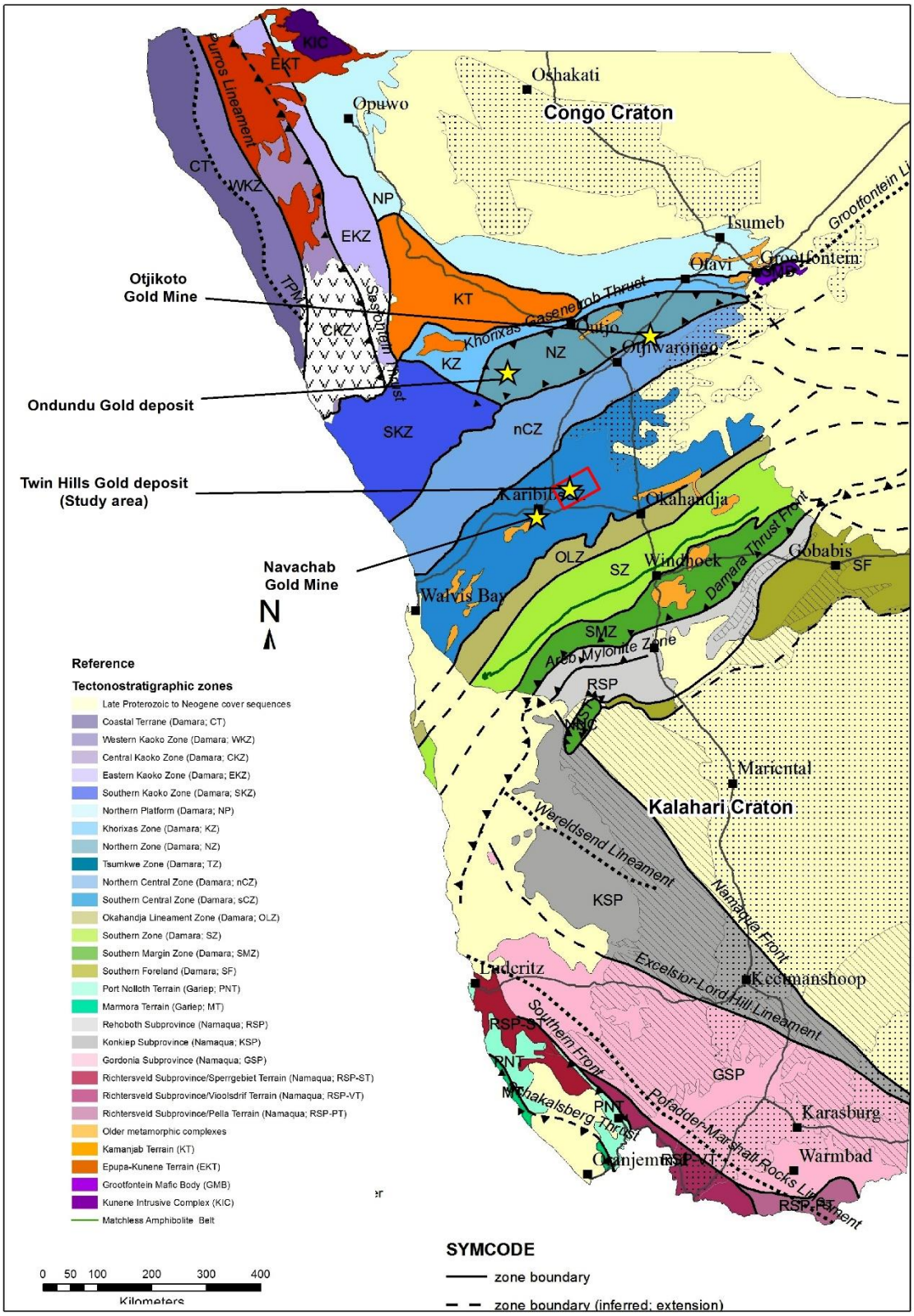

Figure 8 Map showing the main tectonostratigraphic interbeds of the Damara orogeny. (Source:Geological survey of Namibia. Modified after (Miller, 1983; Miller, 2008)).

The northern Central Zone (nCZ)

The nCZ is comprised of lower shallow marine carbonates, which are overlain by deep water sediments and turbidites. It is magnetically quiet as opposed to the sCZ, which is magnetically disturbed (Miller, 1983; Steven, 1992). Three phases of deformation have been recorded in most of the area (Miller, 1983).

The southern Central Zone (sCZ)

The sCZ is mainly comprised of continental and shallow marine metasediments, which overlie a 1.7–2.0Ga granite gneiss basement inlier transected by numerous east-northeast trending auriferous megashears (Steven, 1992). These structures controlled the localization of hydrothermal fluids in the overlying supracrustal rocks. Steven (1992) attributes the northeast trending structural fabric and domes in the central zone to the third deformation episode and granitic intrusions.

The sCZ is separated from the Southern Zone (SZ) by the Okahanja Lineament Zone (OLZ) (Miller, 1983; Miller, 2008; Creus, 2011) (Figure 8).

2.2 Lithostratigraphy of the southern Central Zone

2.2.1 The Abbabis Metamorphic Complex (1.9Ga)

The Abbabis Metamorphic Complex is the basement underlying the metasedimentary units of the Damara Supergroup. The Abbabis Metamorphic Complex is a granitic gneiss complex made up of ortho- and paragneisses, schists, quartzites and amphibolites. Jacob, et al, (1978) determined the first U-Pb age for the Abbabis Metamorphic Complex using zircons from the granite-gneisses, which yielded a concordia age of ±1925Ma.

2.2.2 Damara Supergroup in the southern Central Zone

The lithologies of the Nosib and Swakop Groups constitute the Damara Supergroup in the southern Central Zone (Table 1).

Nosib Group

The Nosib Group in the CZ is divided into the lower Etusis Formation and and the overlying Khan Formation. The Etusis Formation is comprised of metaquartzites, arkoses, and conglomerates which are considered to either be in unconformable contact or tectonic contact with the basement (Brandt, 1985; Oliver, 1995). The Etusis formation is believed to represent a fluvio-deltaic sedimentary sequence derived from the erosion of the preexisting granitic basement (Miller, 1983; Steven, 1992). The Khan Formation is believed to be a succession of marly sediments now metamorphosed into a pyroxene-amphibole bearing feldspathic quartzite (Steven, 1992).

Swakop Group

The Rossing Formation forms the lowermost stratigraphic unit of the Swakop Group, and it is comprised of marbles and calcsilicates. The glaciogenic mixtite and associated banded iron formation (BIF) of the Chuos Formation overlies the Rossing Formation (Miller, 1983; Miller, 2008; Brandt, 1985; Steven, 1992). The Arandis Formation, which overlies the Chuos Formation, is divided into three distinct members (Miller, 2008). The lowermost Spes Bona Member (Lower Arandis Formation) is comprised of an intercalated succession of biotite schists, calc-silicate rocks, and minor volcanics.

Table 1 General stratigraphy of the Damara Supergroup in the Central Zone of the Damara Belt with selected significant gold occurrences highlighted (Underwood, 2020).

Group	Formation	Member	Lithologies	Significant Au Occurrences
Swakop	Kuiseb		Metaturbidites and biotite schists and minor calc-silicate rocks and marble	Okawayo 146, Ondundu, Sandamap Noord 115, Osino's Twin Hills Project
	Karibib	Onguati	Quartzite, schist, calc-silicate rock, marble	
			Calcitic and dolomitic marble and minor calc-silicate rocks and schist	Navachab 58 (Grid A), Goldkuppe, Onguati, Albrechtshöhe 44
		Otjongeama	dolomitic calcite marble, calcitic marble, and dolomite, calc-silicate rocks, biotite schists	
	Ghaub	Omusema	amphibolites (only present in SCZ)	
		Daheim	continental mafic volcanic rocks (only present in SCZ)	Daheim 106
		Kachab	phyllitic schist/dropstone bearing siliciclastic rocks	
	Arandis / Okonguarri	Oberwasser / Upper	Biotite schist, calc-silicate rocks, and minor felsic volcanic rocks	Epako 38 Otjikoto?
		Okawayo / Middle	Calcitic marble Schists and calc-silicates	Navachab Mine, Kranzberg South 113 Otjikoto
		Spes Bona / Lower	Biotite schist, calc-silicate rocks, and minor felsic volcanic rocks	Navachab 58 (Eastern Interbeds)
	Chuos		Glaciogenic mixtite, Banded Iron Formation	
	Rössing		Dolomitic marble, minor calc-silicate rocks, and calcitic marble	
Nosib	Khan		Pyribole calc-silicate rocks, minor biotite schist, graphite schist, and marble	
	Etusis		Feldspathic quartzite, grit and minor calc-silicate rocks and schist	Nordenburg 76
Abbabis Metamorphic Complex				

The succession continues upwards with the Okawayo Member (Middle Arandis formation), which is made up of different marbles often intercalated with calc-silicate bands. The Oberwasser Member (Upper Arandis Formation) is made up of biotite schists, often with calc-silicate bands (Miller, 2008). The Ghaub Formation overlies the Arandis formation, and is made up of metavolcanics and diamictites. The Ghaub Formation is overlain by the lowermost Karibib formation unit known as the Otjongeama Member, which is made up of marbles, dolomitic marbles, dolomites, and minor calc-silicate bands (Miller, 2008). The Karibib Formation forms an essential stratigraphic marker in the Southern Central Zone (Wulff, 2008). The Onguati Member (Upper Karibib Kormation) is considered to be the transition zone from the shelf-type sedimentatary environment of the Karibib Formation to the pelagic sedimentation environment of the Kuiseb Formation and is characterized by schist, quartzites, calc-silicates, marbles, and mafic tuff units (Petzel, 1988; Miller, 2008; Wulff, 2008). The Kuiseb Formation consists of a thick succession of quartz-biotite schists with minor intercalated calc-silicate bands and lenses (Petzel, 1988; Miller, 2008; Wulff, 2008).

2.2.3 Intrusive Rocks

Large masses of plutonic rocks have repeatedly intruded the lithologies of the Abbabis Metamorphic Complex and the Damara Supergroup throughout the course of the orogen's metamorphic and structural evolution (Brandt, 1985) . Five groups of major plutonic rock groups are classified within the Central Zone. The first group is characterized by red, inhomogeneous, syntectonic granites which occur with the Nosib Group or Basement rocks (Miller, 1983; Brandt, 1985; Steven, 1992). These granites are limited to the western part of the Central Zone, where the degree of metamorphism was higher than in the eastern part. The second group of plutonic rocks constitutes red and grey homogenous syntectonic granites that are not confined to any stratigraphic

level thence are found throughout the Central Zone. The Salem granites forms the third group of plutonic rocks, and are grey (often reddish), fine to coarse, and crystalline to porphyritic. The Salem-type granite is almost exclusively associated with the Kuiseb Formation (Miller, 1983; Brandt, 1985; Steven, 1992). The fourth group is characterized by the post-tectonic granites of the Donkerhoek intrusion. The fifth group is characterized by syn to post tectonic leucogranites, pegmatitic alaskites, and pegmatites that occur as sheets at various stratigraphic levels (Miller, 1983; Brandt, 1985; Steven, 1992). Figure 9 shows the lithologies of the Damara supergroup and intrusions within the Twin Hills Project area.

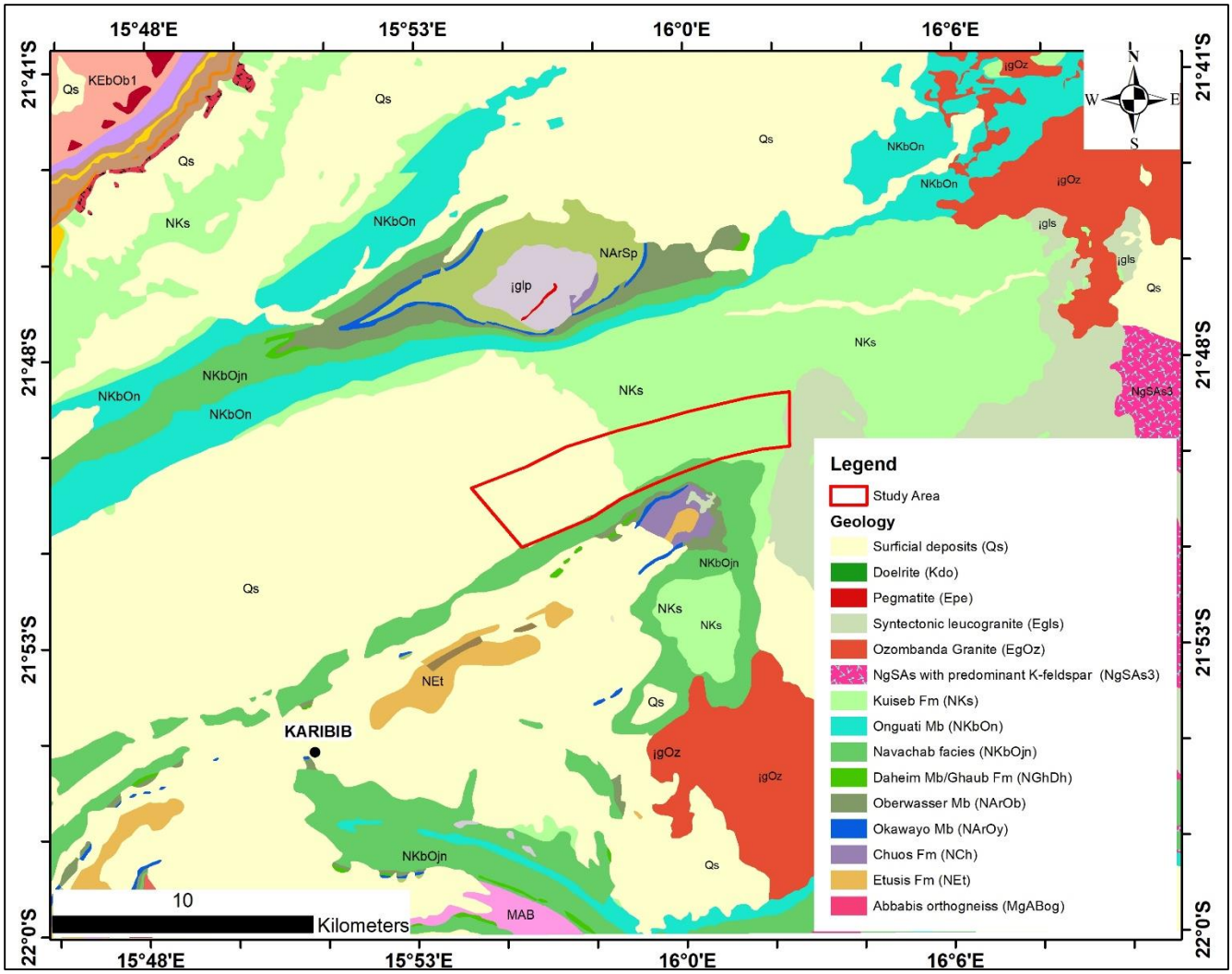

Figure 9 Geological map showing the local Geology underlying the Twin Hills Gold Project area (GSN Published Geology Map, 1:250,000 scale, Sheet 2114 – Omaruru; Sheet 2116 – Okahandja).

2.3 Metamorphism in the Central Zone

The lithologies in the Central Zone (CZ) were metamorphosed by two major thermal events (Miller, 1983). The first metamorphic event is characterized by a biotite-sillimanite-calc-silicate mineral assemblage at about 600Ma. The second metamorphic event is late to post D3 and is characterized by garnet-cordierite mineral assemblage at about 530 Ma (Miller, 1983; Petzel, 1988). The temperatures of metamorphism increased inwards from the margins of the orogen towards the Central Zone. Puhan, (1983) determined the P-T conditions of metamorphism in the central zone using the dolomite-calcite solvus thermometry on the forsterite + diopside + tremolite + dolomite + calcite mineral assemblage and recorded temperatures ranging from 555°C-645°C from the Karibib to the Swakopmund area respectively.

2.4 Structural Geology of the Southern Central Zone

A polyphase deformational history of up to three deformational episodes has been recorded in the CZ (Miller, 1983; Oliver, 1995). The first deformational episode (D_1) is believed to be the result of the collision and subduction of the Kalahari craton beneath the Congo craton at about 580Ma. D_1 is characterized by upright folds (F_1) initially oriented SE-NW, low angle thrusts, and an association with the development of a bedding subparallel penetrative foliation, (S_1) (Kasch, 1983; Oliver, 1995; Creus, 2011). The second deformational episode, (D_2), resulted from the progressive convergence between the Kalahari and Congo cratons circa 550 – 540Ma. NNE-SSW oriented D_2 deformation refolded the F_1 folds to produce an interference pattern of domes, and sharp keels generally oriented NE-SW, low angle thrusting and the development of an S_2 foliation axial planar to the F2 folds (Kasch, 1983; Oliver, 1995; Miller, 2008; Creus, 2011). The third deformational

episode, (D_3), is believed to mark the final collisional stage between the Congo and Kalahari cratons at circa 540Ma (Miller, 1983; Miller, 2008; Creus, 2011).

D_3 is characterized by upright, NE trending, SE verging domes that resulted in the NE trending structural grain of the southern central zone (Miller, 1983; Miller, 2008; Creus, 2011).

Mapping of the dome structures in the Central Zone has shown that a significant ductile shear zone named the Khan River Detachment separates the ~ 2Ga granitic gneiss basement from the overlying Damara supracrustal rocks (Oliver, 1995). The domes are thought to have formed due to a combined crustal NW-SE compression and a SW-NE extension following the collision of the Kalahari and Congo cratons (Oliver, 1995). This provides an alternative interpretation of dome formation rather than being formed by a fold interference pattern.

Chapter 3

Methodology

The samples that were selected for this study were collected from drill core. A total of 14 boreholes were selected for this study. These boreholes were drilled across four sections of the Twin Hills deposit, which include The Bulge, Twin Hills Central, Clouds and Twin Hills West (Figure 10). The samples were collected across the four main lithological units at Twin Hills, and included unaltered, unmineralized zones as well as the mineralized and highly altered zones. This was done in order to obtain petrographic descriptions that are representative of the deposit.

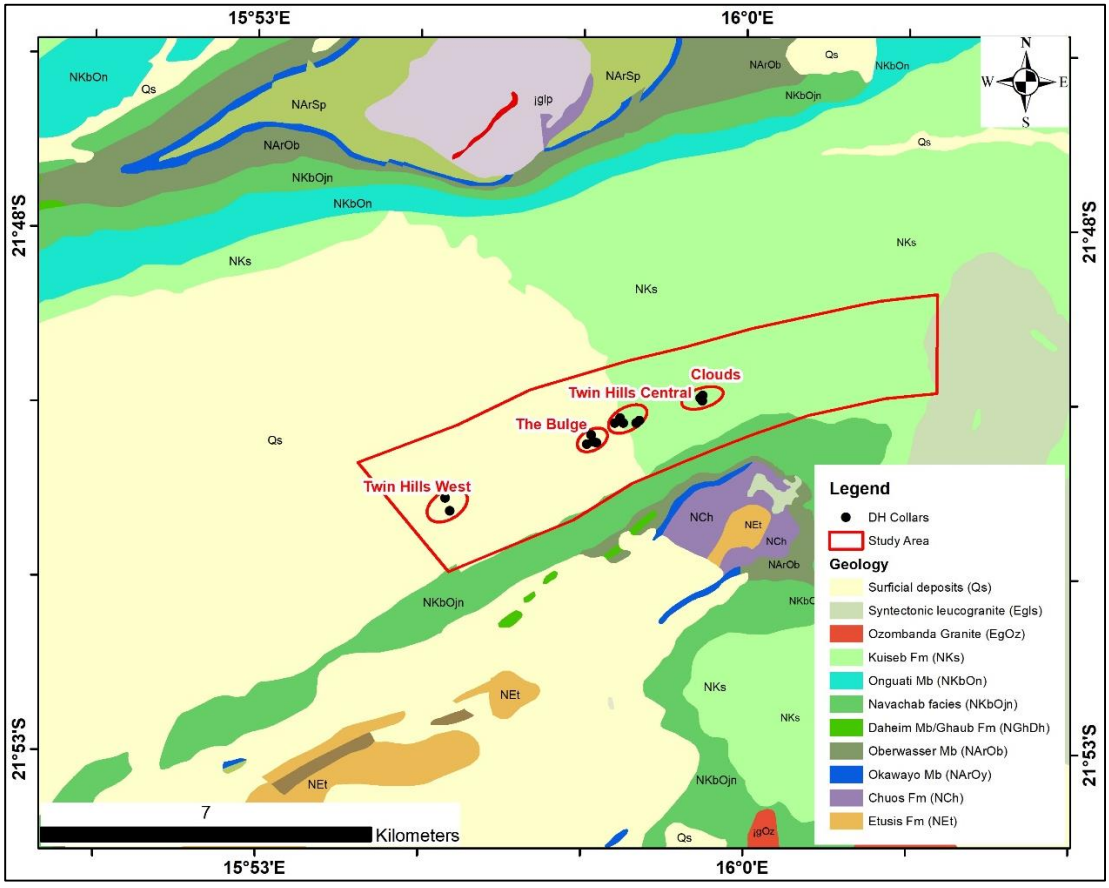

Figure 10 Geological map showing the geology of the study area and the location of the boreholes that were sampled for this study. (GSN Published Geology Map, 1:250,000 scale, Sheet 2114 – Omaruru).

3.1 Petrography

Petrographic studies involved the detailed examination and description of hand specimen samples from drill core from the Twin Hills Gold Deposit. The petrographic studies entailed detailed descriptions of the different lithological units, ore minerals, and the different modes of occurrence of the ore minerals. Detailed descriptions of the different alteration types were also carried out.

A total of 24 polished thin section samples were prepared to investigate the optical properties of rock forming and ore minerals. The polished section areas on the drill core were selected such they were representative of all the lithological units, the altered and unaltered zones as well as the mineralized and un-mineralized zones.

An Olympus microscope (BX-50) was used to study the petrographic properties of the minerals. The rock-forming minerals were studied in transmitted light, while the ore minerals were studied in reflected light.

3.1.1 Preparation of the polished thin sections

The following sections provides a brief overview on how the polished thin sections were prepared.

The polished thin section area was demarcated on the drill core. A slab was then cut out of the drill core using a diamond saw. The slab was labeled and then polished until one surface became smooth. A glass slide was then glued to the polished surface of the slab using epoxy. The protruding part of the slab was then cut off from and the reminder of the section was polished until it reached the target thickness of 30 microns.

3.2 Automated Scanning Electron Microscopy Analysis

3.2.1 TESCAN Integrated Mineral Analyzer (TIMA)

The TESCAN Integrated Mineral Analyzer (TIMA) is a scanning electron microscope (SEM) based on an automated mineralogical analysis system. The TIMA was used to identify the different mineral phases in the polished thin sections based on the backscattered electron (BSE) intensity and chemical composition. False color mineral maps and element maps were created to generate quantitative textural data obtained using energy dispersive spectroscopy (EDS). A total of six polished thin-section samples were selected for TIMA analysis. These samples were primarily selected for a gold deportment study, which aimed to locate and describe the gold containing particles, their grain size, association, liberation, and free surface area. Sample preparation for the TIMA analysis involved polishing and applying a thin layer (10nm) of carbon on the surface of the polished thin section sample using the Q150T ES carbon coater from Quorum at the School of Geoscience (WAMLAB) at the University of the Witwatersrand. Phase maps and elemental maps of minerals were quantified by energy-dispersive X-ray spectroscopy (EDS) using the VEGA3 SEM instrument and the VEGA3 X64 TESCAN TIMA 2.4.0. software.

The beam conditions during quantitative analyses on the VEGA3 X64 TESCAN SEM were 25kV accelerating voltage, 43µA emission current, with a working distance of 21.33mm, a specimen beam current of 17.68nA, and a spot size of 590.00nm with an absorption current of <1pA. The scanning resolution varied between 1 and 7 µm per pixel. High-resolution scanning of 1 µm was primarily carried out in areas that were identified to have very fine-grained gold grains included within arsenopyrite crystals.

Chapter 4

Petrology and Mineralization

4.1 Petrographic Descriptions of the Lithologic Units

Detailed petrographic descriptions were carried out to establish a systematic, petrographic characterization of the host rocks, mineralization and alteration at the Twin Hills Gold Deposit. The petrographic descriptions were carried out on samples collected from unaltered, unmineralized rock units as well as the mineralized and highly altered rock units. The work presented below is the outcome of the description of the four main lithologic units at the Twin Hills Deposit. These lithologies include metagreywacke, cordierite metagreywacke, biotite schist and cordierite schist. These lithologies can be broadly grouped into two main units, the mineralized unit which is dominantly made up of the metagreywacke and the unmineralized, footwall which is dominantly made up of the cordierite schist (Figure 11).

4.1.1 Metagreywacke

Metagreywacke is the main host unit to gold mineralisation at the Twin Hills Gold Deposit. This unit is grey, fine-grained, and exhibits a moderate to highly defined schistosity (Figure 12 and Figure 13). The mineralogy of the metagreywacke is dominantly made up of quartz, biotite, muscovite, and feldspars (mainly plagioclase and minor orthoclase (Figure 14). The estimated mineral abundances for the major mineral phases are quartz 40%, plagioclase 20%, biotite 15%, orthoclase 7% and muscovite 4%. The feldspars are not easily identified in drill core samples nor in transmitted light microscopy but were adequately identified and quantified by energy–dispersive X-ray spectroscopy (EDS) analysis in the TESCAN Integrated Mineral Analyzer (TIMA). The composition of the metagreywacke can be classified in terms of a gradation from pelitic, mica-rich

interbeds to psammitic, quartz-rich interbeds. This classification reflects the turbidite nature of the metagreywacke.

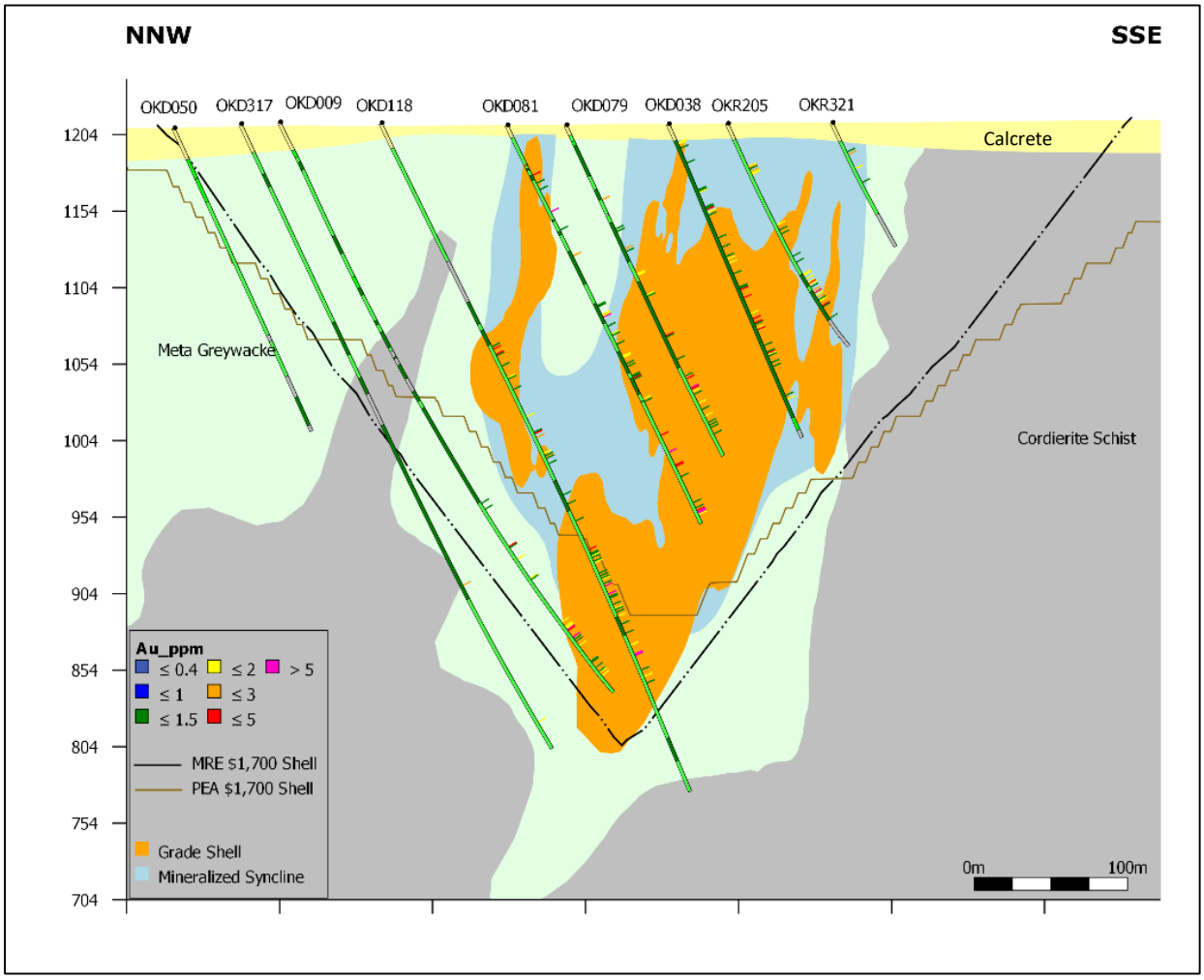

Figure 11 Cross section across some of the boreholes used in this study that were drilled at the Bulge section of the Twin Hills Deposit.

The metagreywacke can be divided into two main sub-lithologies based on bedded versus massive texture. The former is referred to as the interbedded metagreywacke (IMGK), and the latter is referred to as the massive meta-greywacke (MGWK) (Figure 15). The interbedded metagreywacke has graded bedding with relatively coarser, quartz-rich bases and finer mica-rich tops.

Figure 12Photographs of borehole core showing A) Interbedded metagreywacke in a pelitic zone. B) Interbedded metagreywacke in a psammitic zone with coarser beds, graded bedding characterized by coarser, quartz-rich bases, and finer mica-rich tops.

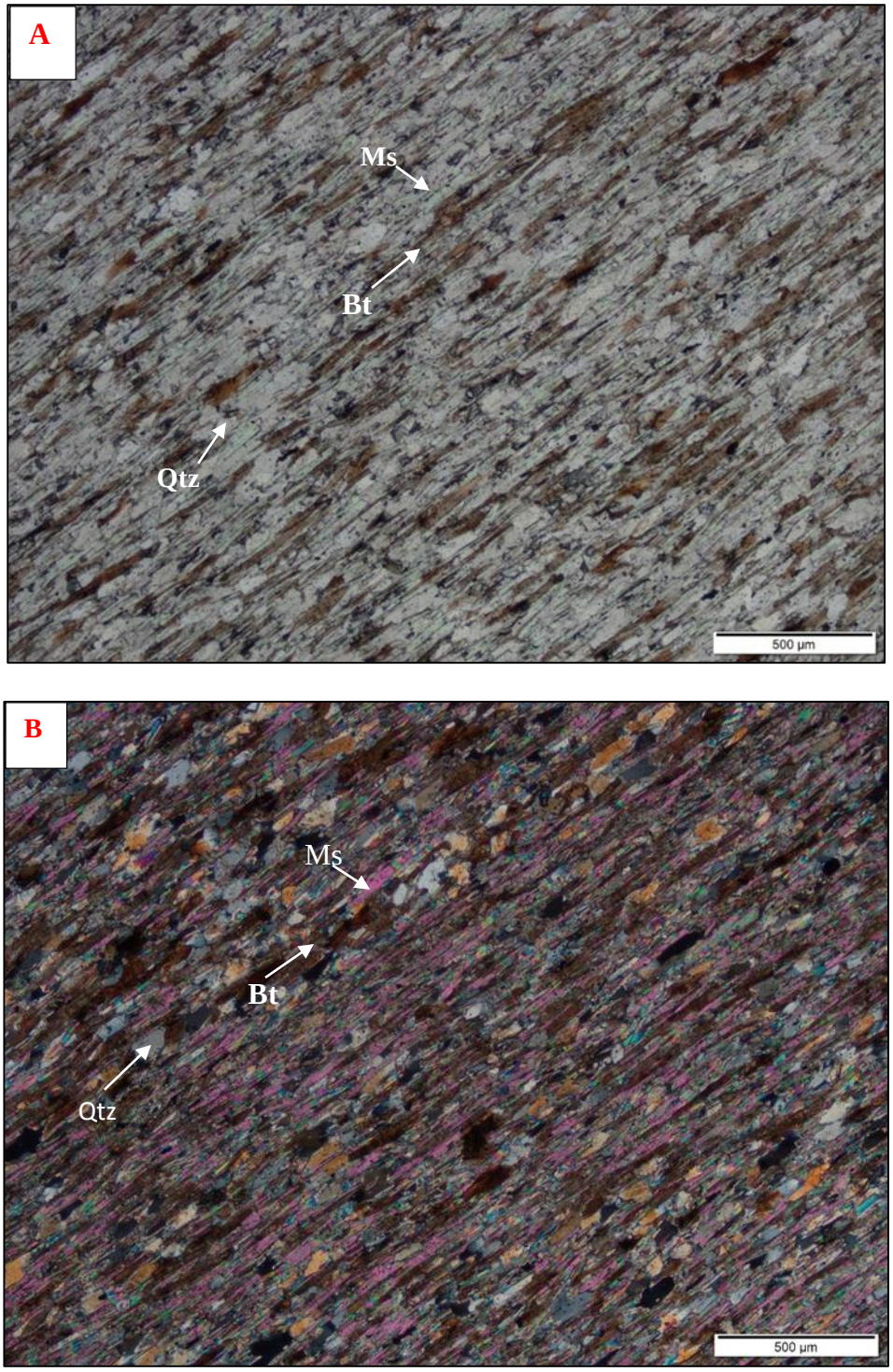

Figure 13 Photomicrographs of borehole core samples of interbedded metagreywacke A) Well developed schistosity in the pelitic interbeds of the interbedded metagreywacke. The mineralogy is dominantly comprised of biotite, muscovite, and quartz. Plane polarized light (PPL) (Magnification:4X). (Sample JS20- OKD211, 152.65m). B) Crossed polarized light (XPL) view of A.

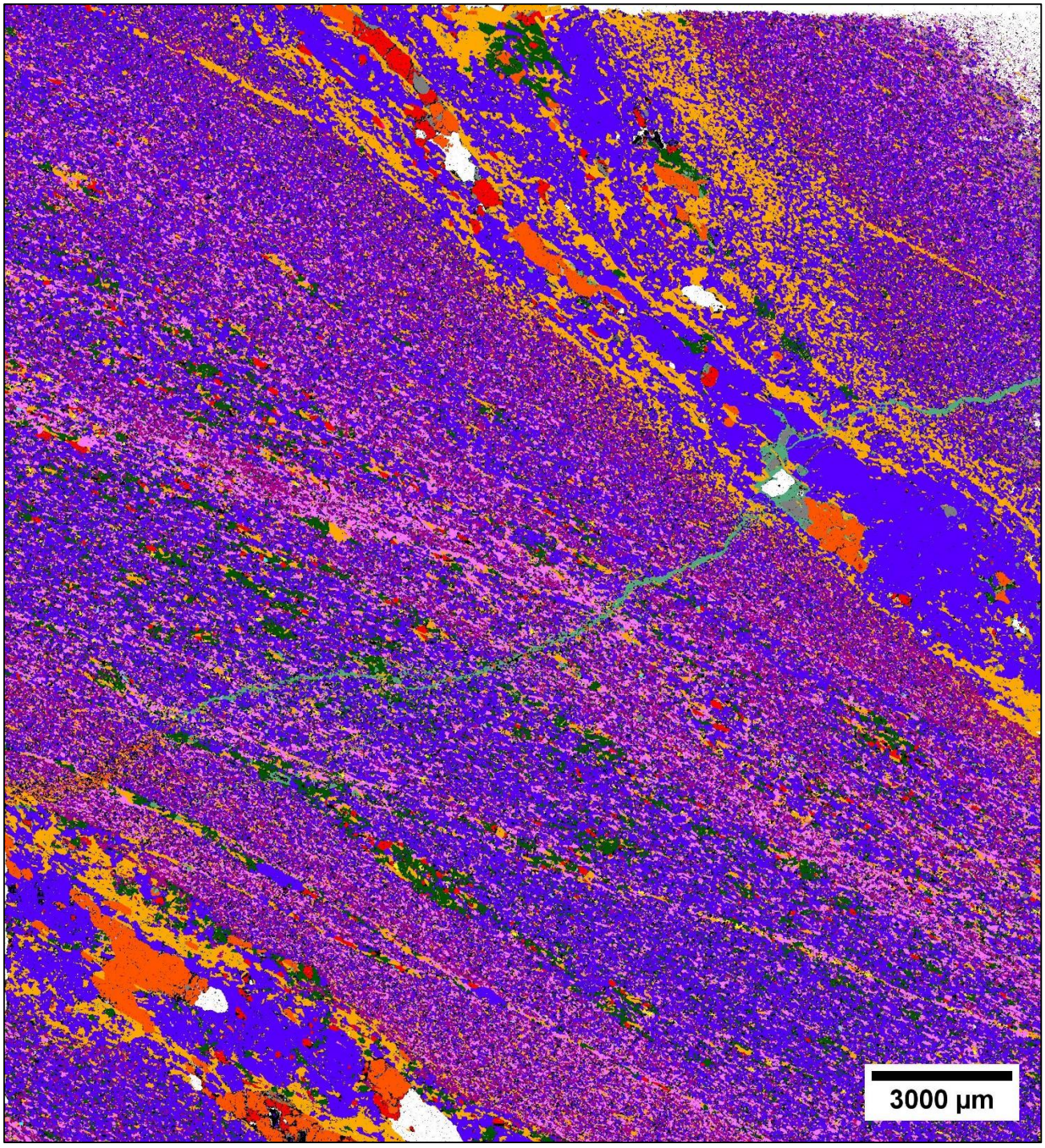

Figure 14 Mineral Phase map showing dominant mineral phases in the interbedded metagreywacke (Sample JS18-OKD211, 120.67m). Phase map produced by the TESCAN Integrated Mineral Analyzer (TIMA).

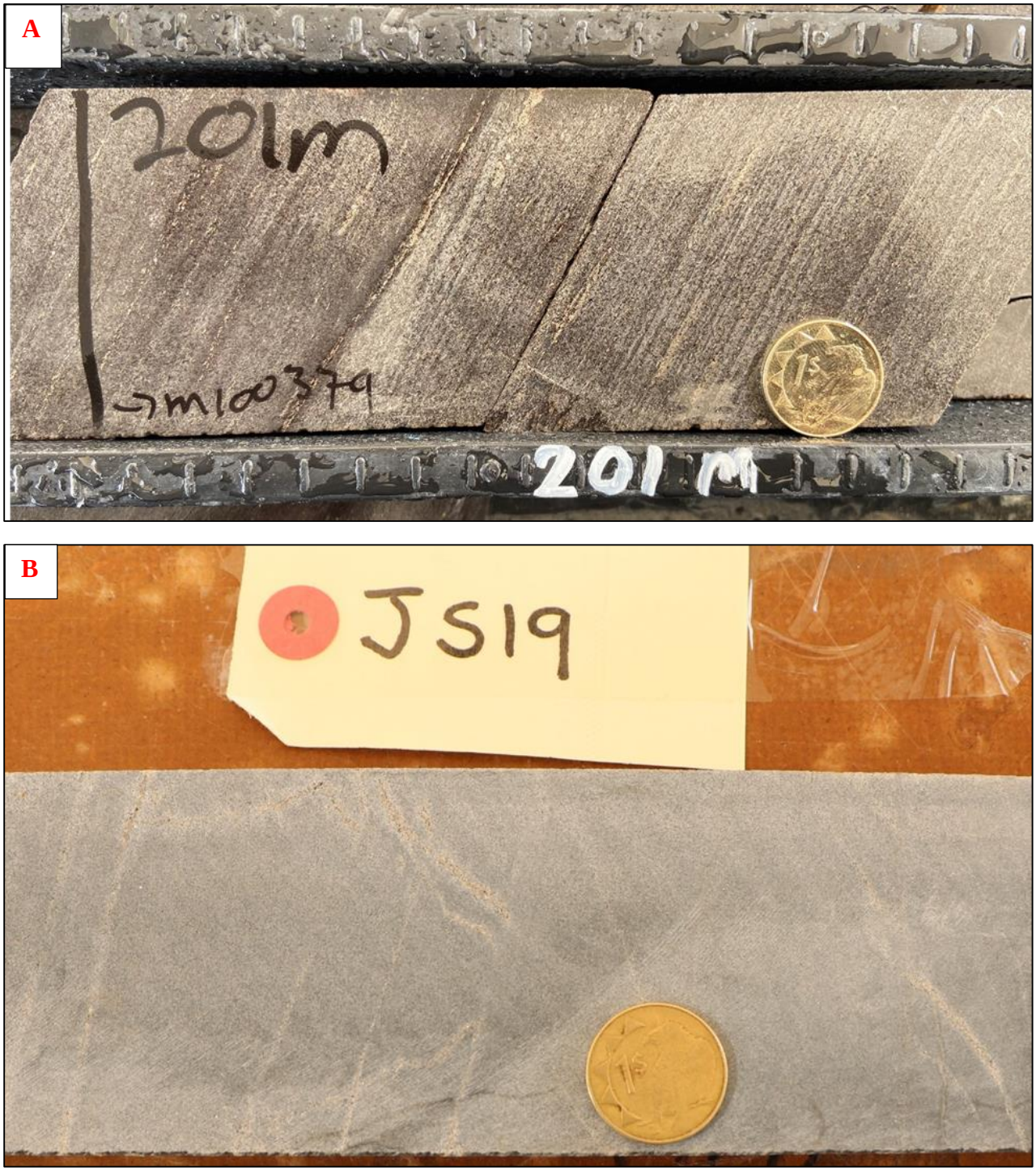

Figure 15 Photographs of borehole core showing A) Interbedded metagreywacke (IMGK) in a pelitic zone with graded bedding characterized by pale, quartz-rich bases, and dark grey, mica-rich tops. B) Massive metagreywacke (MGWK) with distinctive low to moderate schistosity and significantly higher quartz abundance and minor micaceous minerals.

4.1.2 Cordierite Metagreywacke

The cordierite metagreywacke is grey, fine-grained, and exhibits a porphyroblastic texture with cordierite porphyroblasts. The size of the cordierite porphyroblasts in the cordierite metagreywacke are quite small (<2mm diameter) (Figure 16). Fine-grained cordierite porphyroblasts mainly occur in the more psammitic interbeds of the metagreywacke whilst the coarse grained porphyroblasts occur in the pelitic interbeds. In transmitted light microscopy, pressure shadows are seen where mica laths wrap around the cordierite porphyroblasts (Figure 17). The cordierite metagreywacke often grades into the more pelitic cordierite schist. Minor amounts of pyrite and pyrrhotite have been identified in the cordierite metagreywacke, however no significant gold mineralization was identified in this unit.

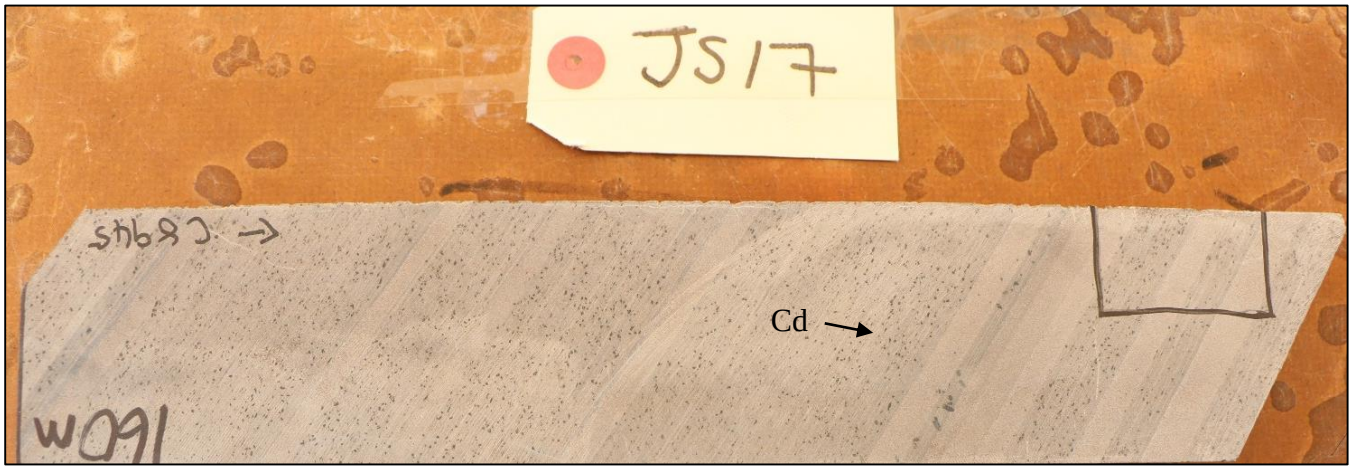

Figure 16 Photographs of borehole core showing cordierite metagreywacke with distinctive, fine-grained cordierite porphyroblasts (dark spots).

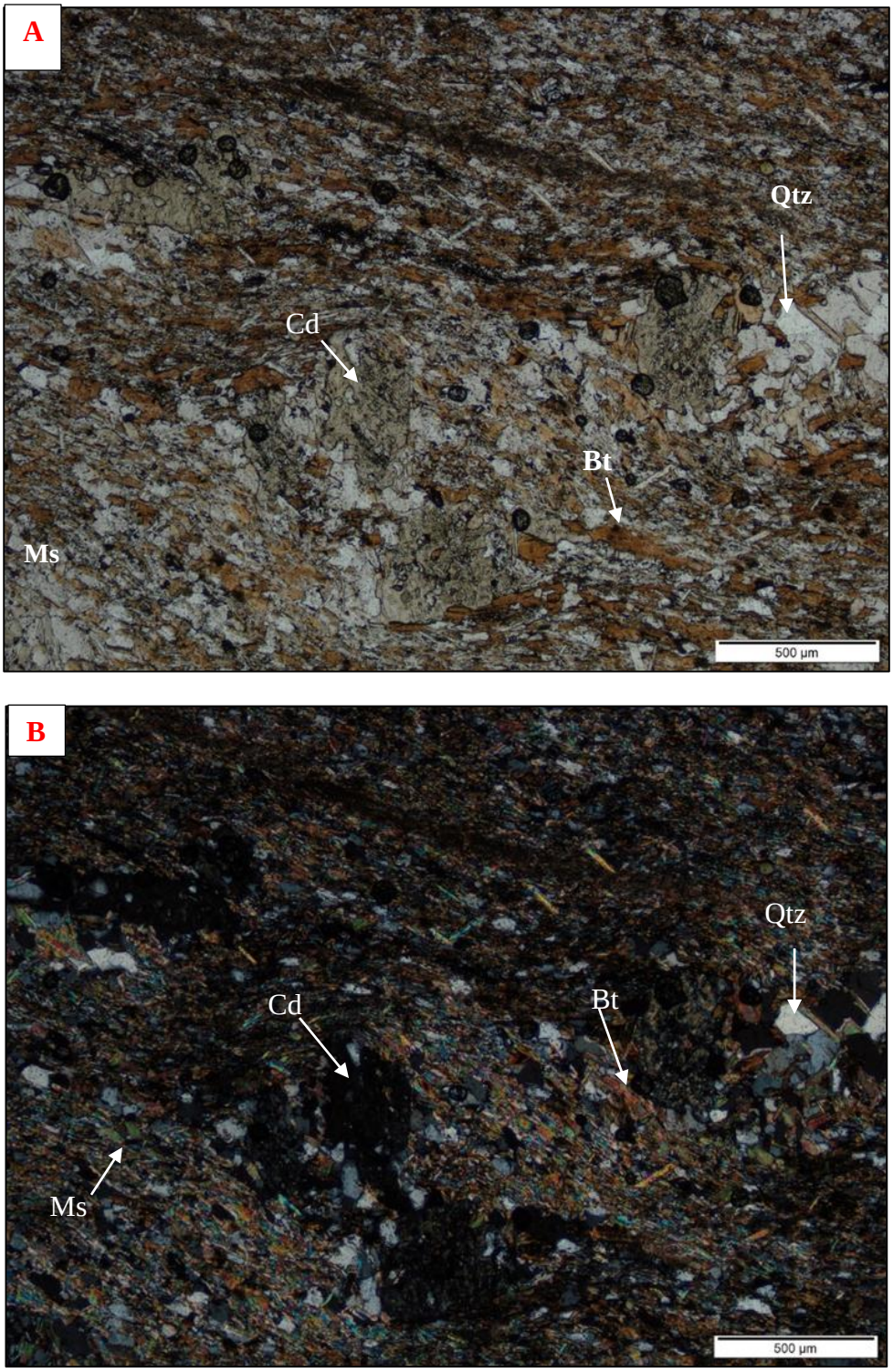

Figure 17 Photomicrographs of cordierite metagreywacke showing A) Mica laths forming pressure shadows around cordierite. Plane polarized light (PPL). (Magnification:4X). (Sample JS17-OKD019, 159.7m). B) Crossed polarized light (XPL) view of A.

4.1.3 Biotite Schist

The biotite schist is grey, fine-grained, highly schistose, and exhibits a finely laminated texture (Figure 18). The mineralogy of the biotite schist consists of biotite, muscovite, and quartz which contribute to a distinctive lepidoblastic texture (Figure 19). The estimated mineral abundances for the major mineral phases include 40% quartz, 20% biotite, and 10% muscovite. The unit is characterized by an alternation between darker, biotite-rich laminae and lighter quartz and muscovite-rich laminae. The biotite schist usually occurs as a thin bed at the base of the metagreywacke and grades into the cordierite schist. The sulphide mineral content decreases significantly within this unit when compared to the metagreywacke. A minor amount (≤1%) of pyrite and pyrrhotite are usually found within the biotite schist.

Figure 18 Biotite schist with distinctive mm scale laminae and highly schistose texture.

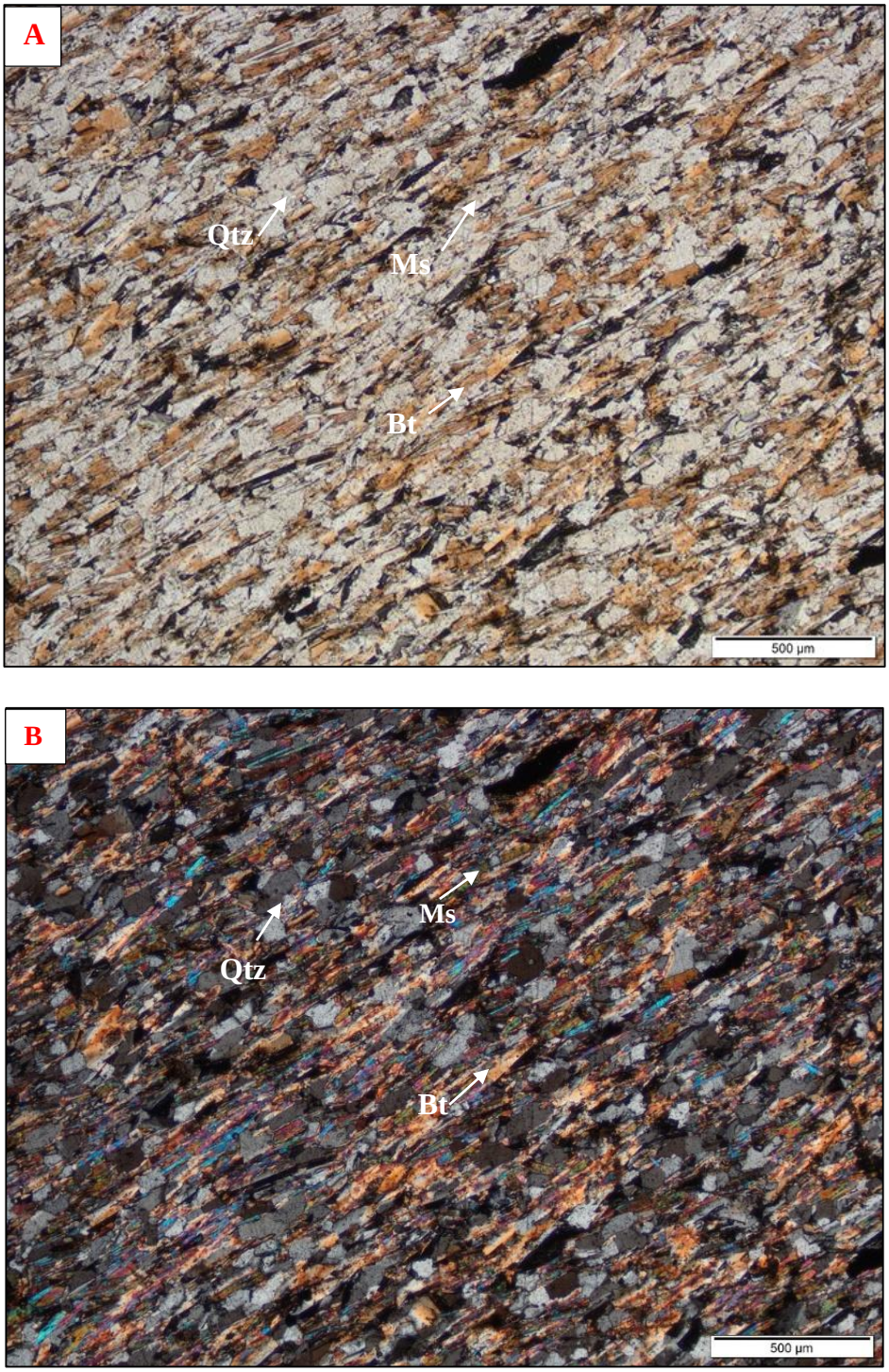

Figure 19 Photomicrographs of the biotite schist showing A) Highly pronounced schistosity, predominantly composed of quartz and biotite, contributing to the overall lepidoblastic texture. PPL (Magnification:4X). (Sample JS24 -OKD034 @ 256.50 m). B) Crossed polarized light (XPL) view of A.

4.1.4 Cordierite Schist

The cordierite schist is grey, fine-grained, and has a prominent porphyroblastic texture characterized by very coarse cordierite porphyroblasts up to 5 mm size (Figure 20). The mineralogy of the cordierite schist consists of cordierite, quartz, biotite, and muscovite. A distinct schistosity is indicated by the alignment of biotite laths around the cordierite grains, forming pressure shadows (Figure 21). This unit is not mineralized and is considered to be the footwall at the Twin Hills Gold Deposit. Some minor amounts of pyrrhotite and pyrite are often found within this unit.

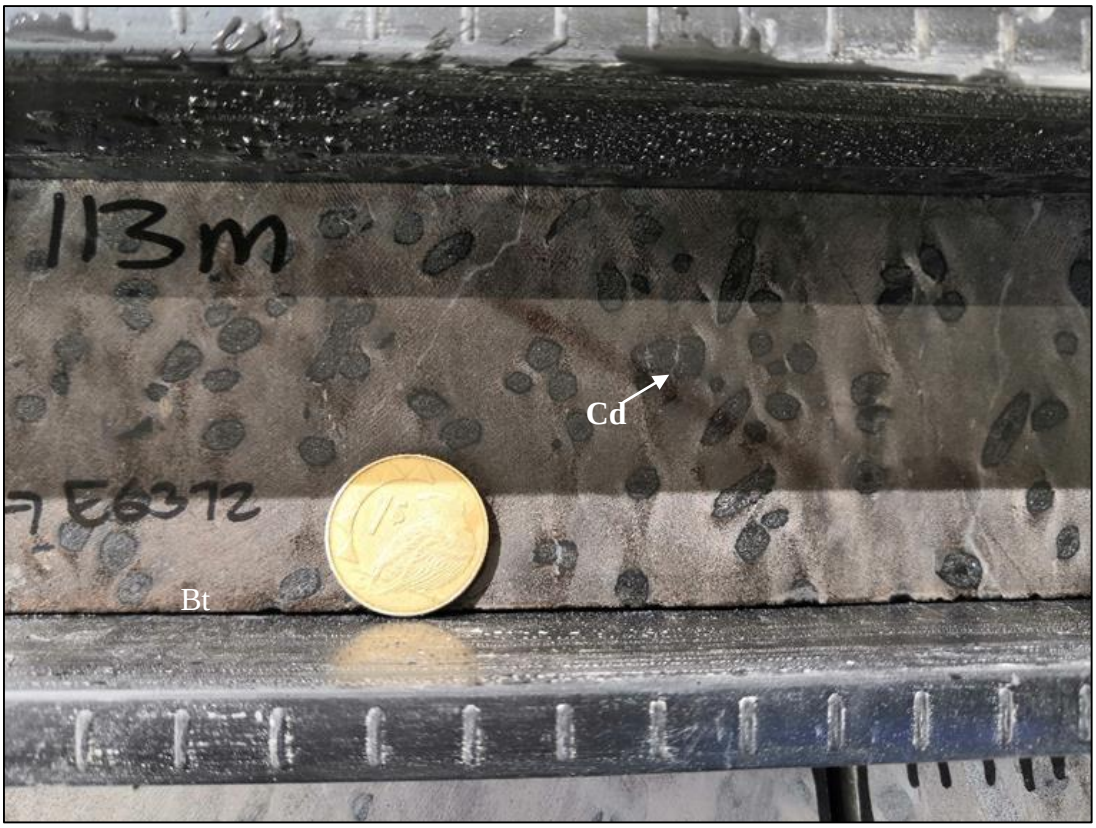

Figure 20 Very coarse (~3mm) cordierite porphyroblasts in cordierite schist.

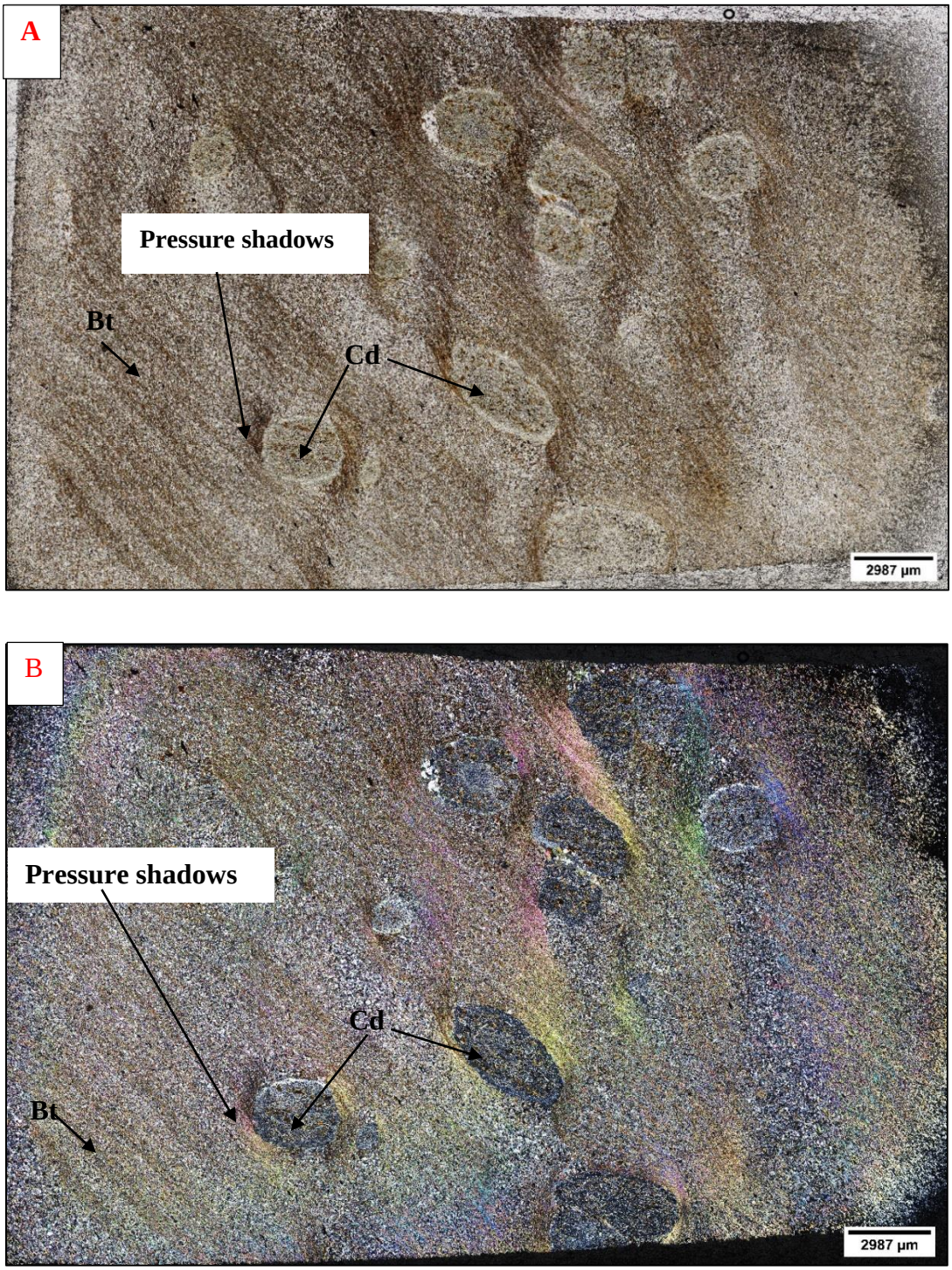

Figure 21 Photomicrographs of the cordierite schist showing A) Porphyroblastic texture with pressure shadows created by mica laths wrapping around the cordierite porphyroblasts. PPL. (Magnification:4X). (Sample JS16- OKD037 - 254.40m. B) Crossed polarized light (XPL) view of A.

4.2 Ore Mineralogy

The major sulphide minerals at the Twin Hills Gold Deposit include pyrrhotite, arsenopyrite, and pyrite. Pyrrhotite is the most abundant (1 - 5%), followed by arsenopyrite (1 -3%) and pyrite (1 – 2%). Minor amounts of lollingite have been identified mainly as inclusions within coarse, euhedral arsenopyrite crystals associated with quartz veins. Minor oxides such as magnetite and hematite have also been identified using the TESCAN Integrated mineral analyzer (TIMA). Gold grains have been identified within the metagreywacke's groundmass, the biotite selvages surrounding quartz veinlets, and as inclusions within arsenopyrite.

4.2.1 Styles of Mineralisation

There are three different styles of mineralization found within the rocks at the Twin Hills Deposit. These include disseminated sulphides, sulphides in veinlets and stringers, and sulphides associated with quartz veins. Gold grains occur as disseminated within the groundmass and biotite selvages and as inclusions within arsenopyrite crystals.

- **Sulphides Disseminated within the Groundmass**

Mineralization in the groundmass is characterized by the presence of two main sulphide minerals disseminated within the groundmass, namely pyrrhotite, and arsenopyrite. The quantity of disseminated sulphides is significantly higher in the metagreywacke than in the more pelitic rocks such as the biotite schist and the cordierite schist.

Pyrrhotite occurs as fine to medium-grained, anhedral crystals disseminated within the groundmass of the metagreywacke. Some fine-grained pyrrhotite crystals in the groundmass are deformed and therefore stretched along the long axis parallel to foliation (Figure 22). The elongated pyrrhotite is usually concentrated in the more pelitic interbeds of the metagreywacke.

Figure 22 Fine-grained, elongated pyrrhotite (Po), elongate parallel to foliation.

Arsenopyrite occurs as fine to medium-grained, euhedral to subhedral, often prismatic crystals disseminated within the groundmass of the metagreywacke. Minor arsenopyrite crystals are observed in the more pelitic interbeds of the metagreywacke. These minor arsenopyrite crystals in the more pelitic interbeds are often elongated and aligned parallel to the foliation (Figure 23). The quantity of the arsenopyrite grains increases significantly in the more psammitic units of the metagreywacke. The arsenopyrite grains in the psammitic interbeds of the metagreywacke are often randomly oriented (Figure 24). Fine-grained arsenopyrite crystals often form coarse, subhedral to anhedral aggregate crystals disseminated within the groundmass. Pyrite crystals are very scarce in the groundmass.

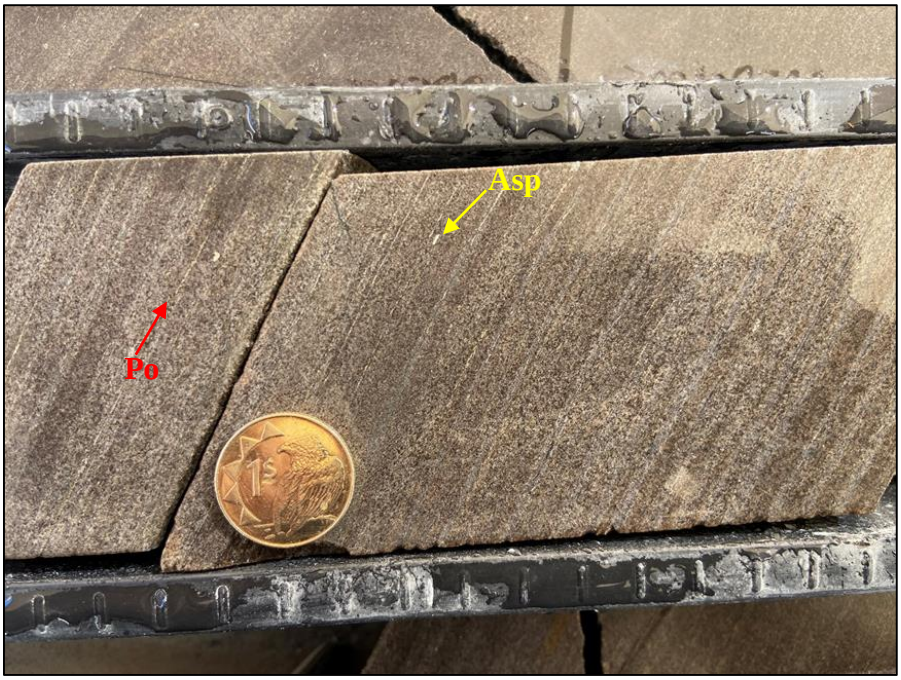

Figure 23Very minor arsenopyrite (Asp), aligned along foliation, similar to the stretched pyrrhotite (Po).OKD395 @218m Clouds East section of the Twin Hills Gold Deposit.

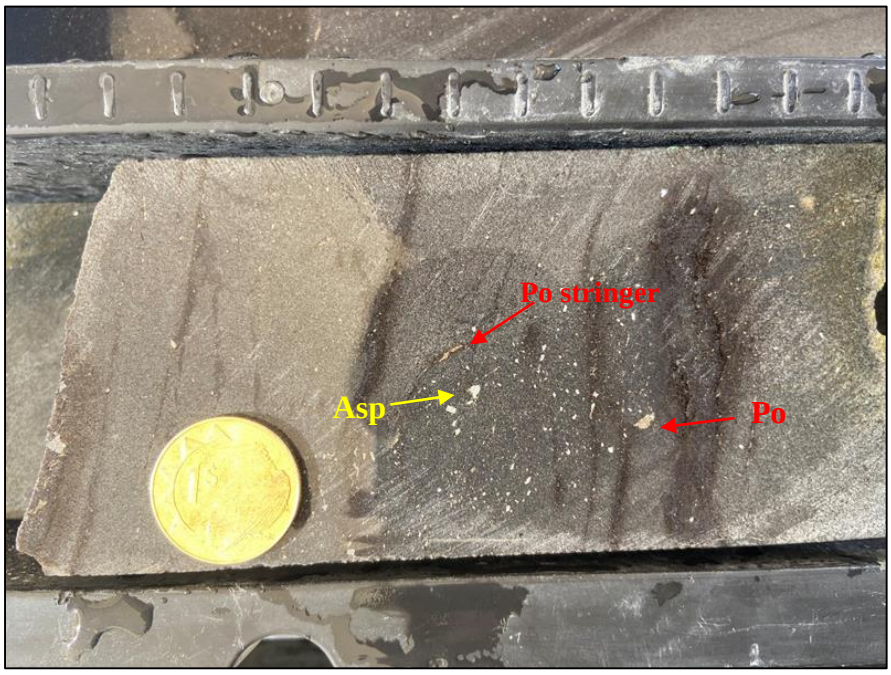

Figure 24Randomly oriented fine-grained, acicular arsenopyrite (Asp) and medium-grained Asp and Po aggregate grains also disseminated within the groundmass of the quartz-rich psammitic interbeds. Po stringer. OKD396 @240m. – Bulge section of the Twin Hills Gold Deposit.

- **Sulphide Veinlets and Stringers**

Pyrrhotite and arsenopyrite often form veinlets and stringers within the groundmass of the metagreywacke and within the quartz veinlets (Figure 25). The arsenopyrite veinlets are made up of euhedral, rhomb-shaped arsenopyrite crystals (Figure 26). The Sulphide veinlets are usually fine-grained in the groundmass and become medium to coarse-grained adjacent to and within quartz veins. Pyrrhotite and arsenopyrite veinlets and stringers are often parallel to the foliation in the groundmass and can be either parallel or cross-cutting the foliation when associated with quartz veinlets (Figure 27). Pyrite typically only forms veins and stringers in quartz veins (Figure 28). A close relationship exists between arsenopyrite and pyrrhotite crystals in the sulphide veinlets and stringers, where arsenopyrite crystals are often included or marginally attached to pyrrhotite grains. Pyrite veinlets also occur as fine to coarse (<1mm to 2mm), euhedral crystals in calcite veins.

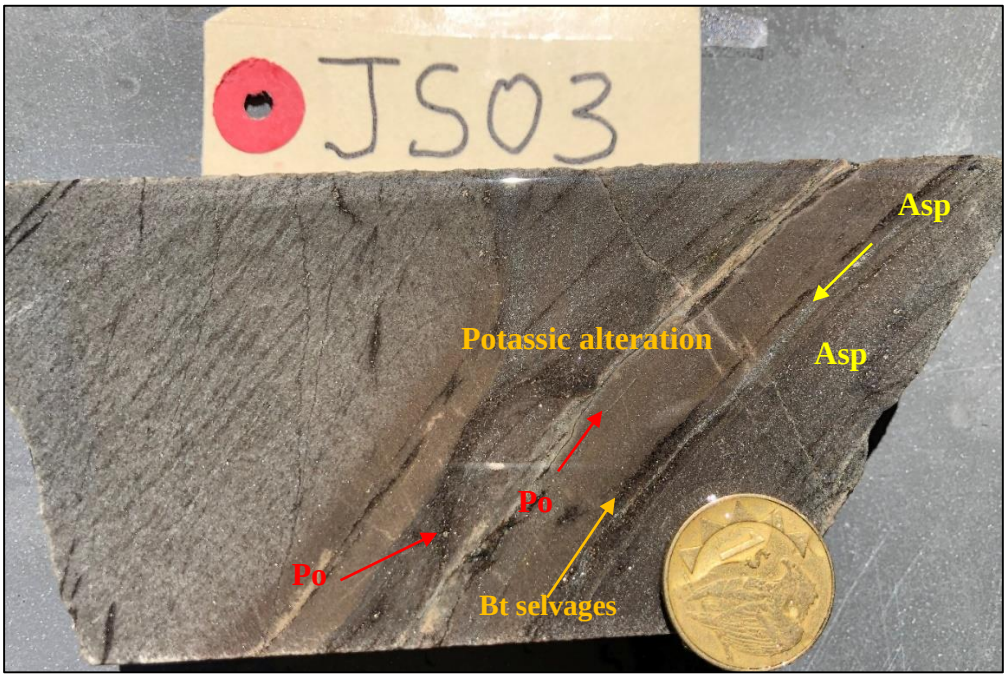

Figure 25 Arsenopyrite (Asp) and pyrrhotite (Po) veinlets and stringers within the groundmass of the interbedded metagreywacke. The veinlets and stringers are strongly associated with quartz veinlets with biotite selvages. The photo also shows strongly pottasic altered IMGK with fine-grained disseminated arsenopyrite and pyrrhotite crystals.

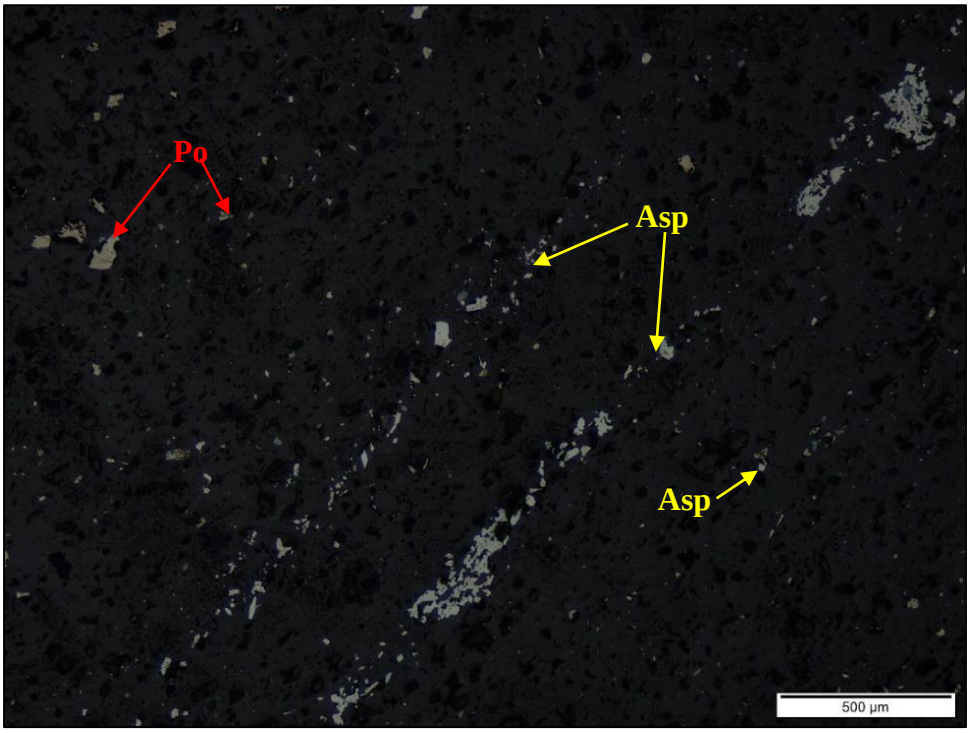

Figure 26 Reflected-light photomicrograph showing euhedral, rhomb-shaped arsenopyrite crystals forming veinlets. Arsenopyrite and pyrrhotite crystals are also disseminated within the groundmass. (Magnification:4X). (SampleJS03 – OKD118 @176.42 m; Twin Hills Central section of the Twin Hills Gold Deposit.

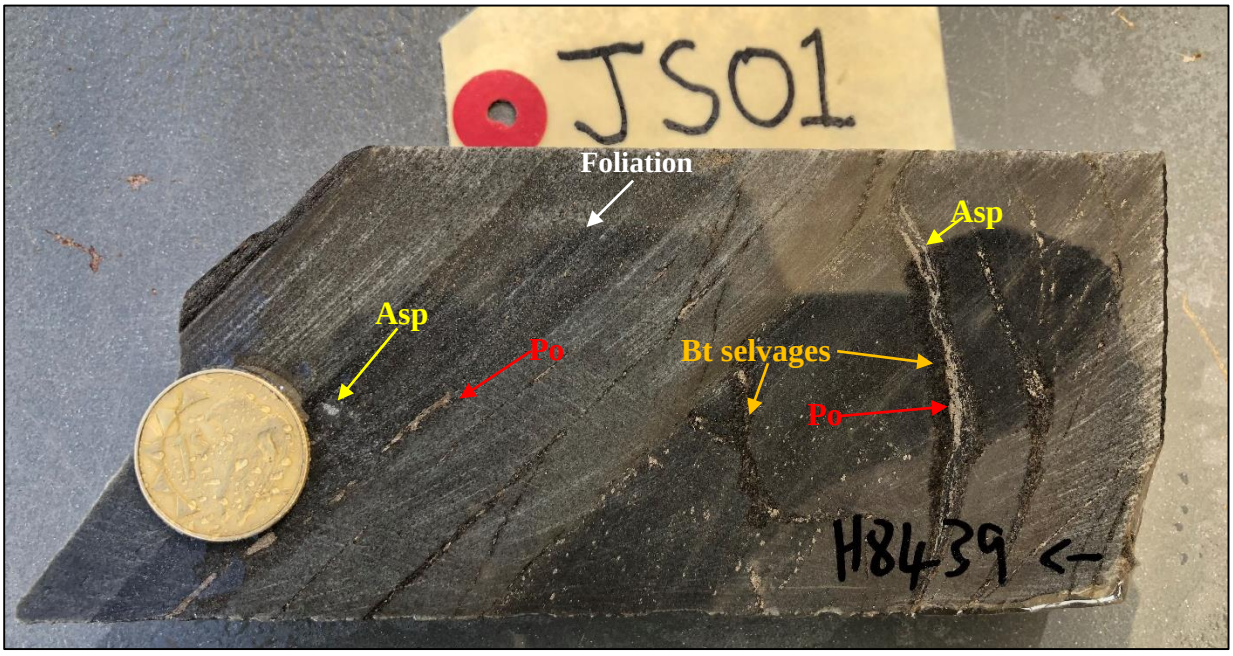

Figure 27 Showing fine-grained pyrrhotite and arsenopyrite crystals disseminated within the groundmass of the psammitic interbedded metagreywacke. Pyrrhotite stringers sub-parallel to foliation in the groundmass. Pyrrhotite and arsenopyrite veinlets are associated with millimeter-scale quartz veinlets with biotite that cross-cut foliation.

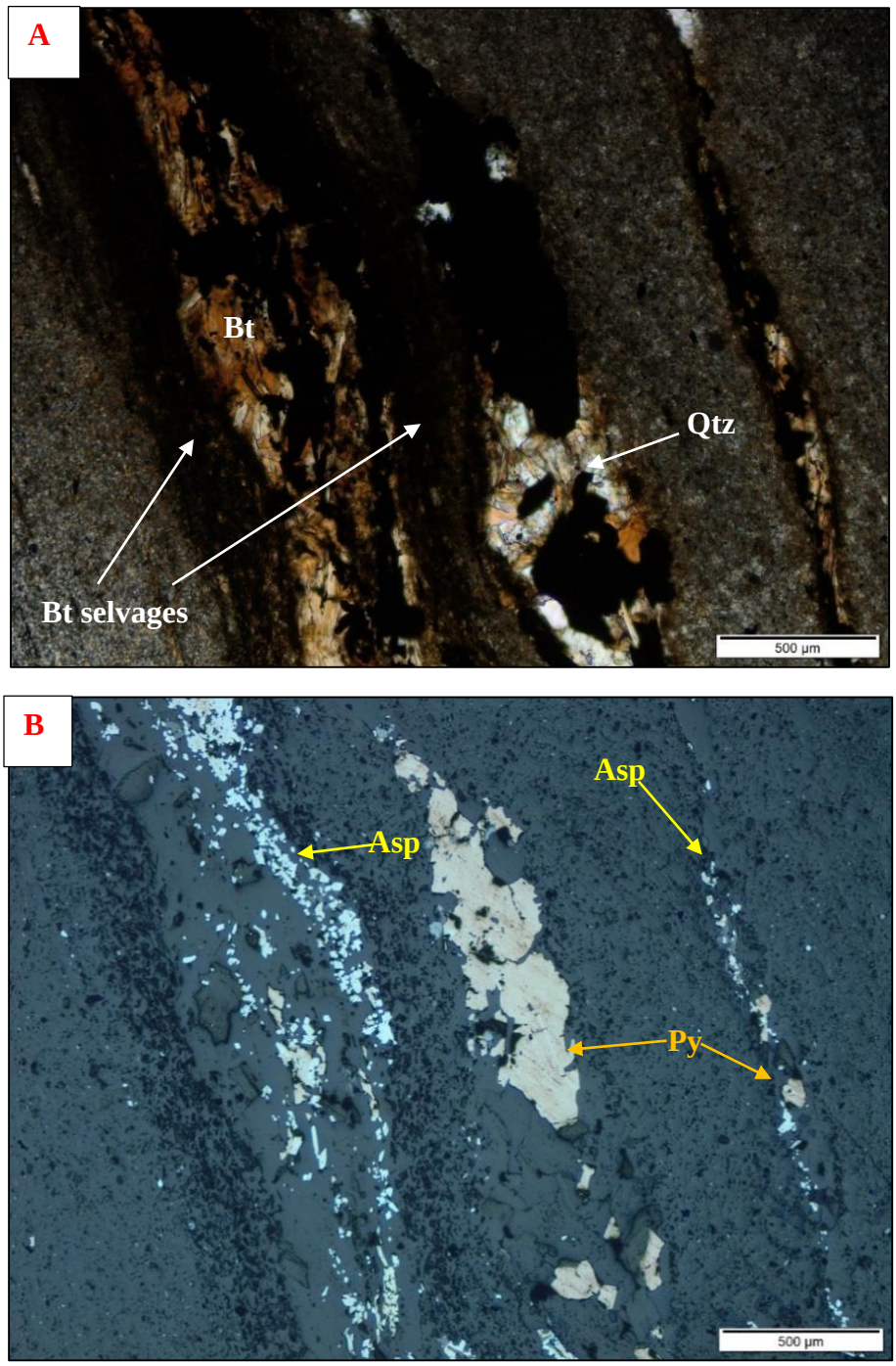

Figure 28 Photomicrographs of veinlets and stringers showing A) Quartz veinlets with biotite selvages characterized by coarser biotite laths and quartz grains. In contrast, the groundmass consists of fine-grained quartz and biotite laths. Transmitted light microscopy. PPL. (Magnification:4X). B) Euhedral arsenopyrite rhombs forming stringers and subhedral pyrite grains. Py occurs to be in the core of the vein. Reflected light microscopy. (Magnification: 4X). (SampleJS23 – OKD038 @104.89m; Twin Hills Central section of the Twin Hills Gold Deposit.).

- **Quartz Sulphide Veinlets**

Quartz veinlets are often associated with the three main sulphide phases: pyrrhotite, arsenopyrite, and pyrite. Sulphides within and marginal to the quartz veinlets are usually much coarser, grained, and euhedral than the equivalent sulphides in the groundmass (Figure 29 and Figure 30

Figure 30 Photomicrographs of quartz sulphide veinlets showing A) Quartz veins with coarse opaque sulphide minerals. Transmitted light microscopy. PPL. B) Coarse pyrite and arsenopyrite crystals forming veins and stringers within the quartz vein. Reflected light microscopy. (SampleJS18 – OKD211 @120.67m; Clouds East section of the Twin Hills Gold Deposit.).

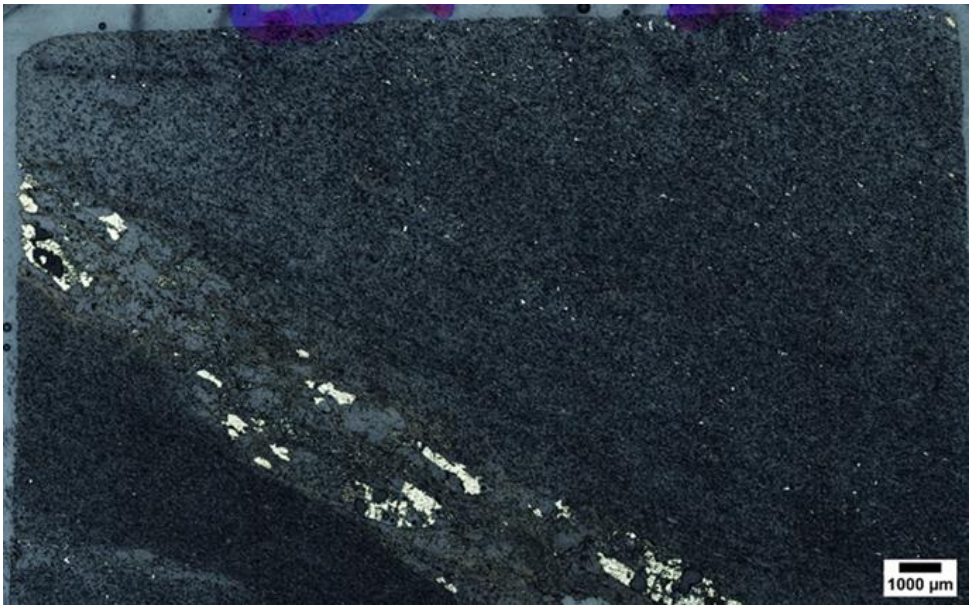

). The quartz veinlets with biotite selvages are strongly associated with arsenopyrite and pyrrhotite, where they occur as fine to medium grained crystals and often form veinlets and stringers (Figure 31). Some of the sulphide-bearing quartz veinlets cross-cut the dominant foliation (Figure 32A and B). Fine pyrrhotite crystals are often included within coarse, euhedral arsenopyrite and pyrite crystals in the quartz veins (Figure 33 A and B). Minor grains of lollingite are also included within coarse, euhedral arsenopyrite crystals (Figure 34).

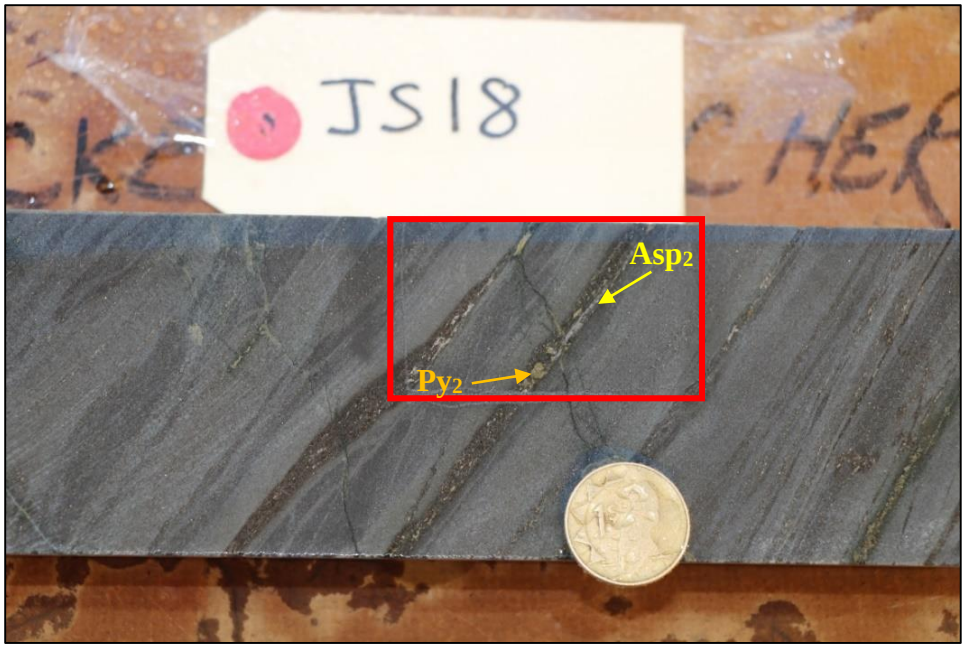

Figure 29 Boudinaged quartz veins with biotite selvages with coarse pyrite, and arsenopyrite stringers hosted within light grey (bleached) fine grained and interbedded metagreywackey. (SampleJS18 – OKD211 @120.67m; Clouds East section of the Twin Hills Gold Deposit.).

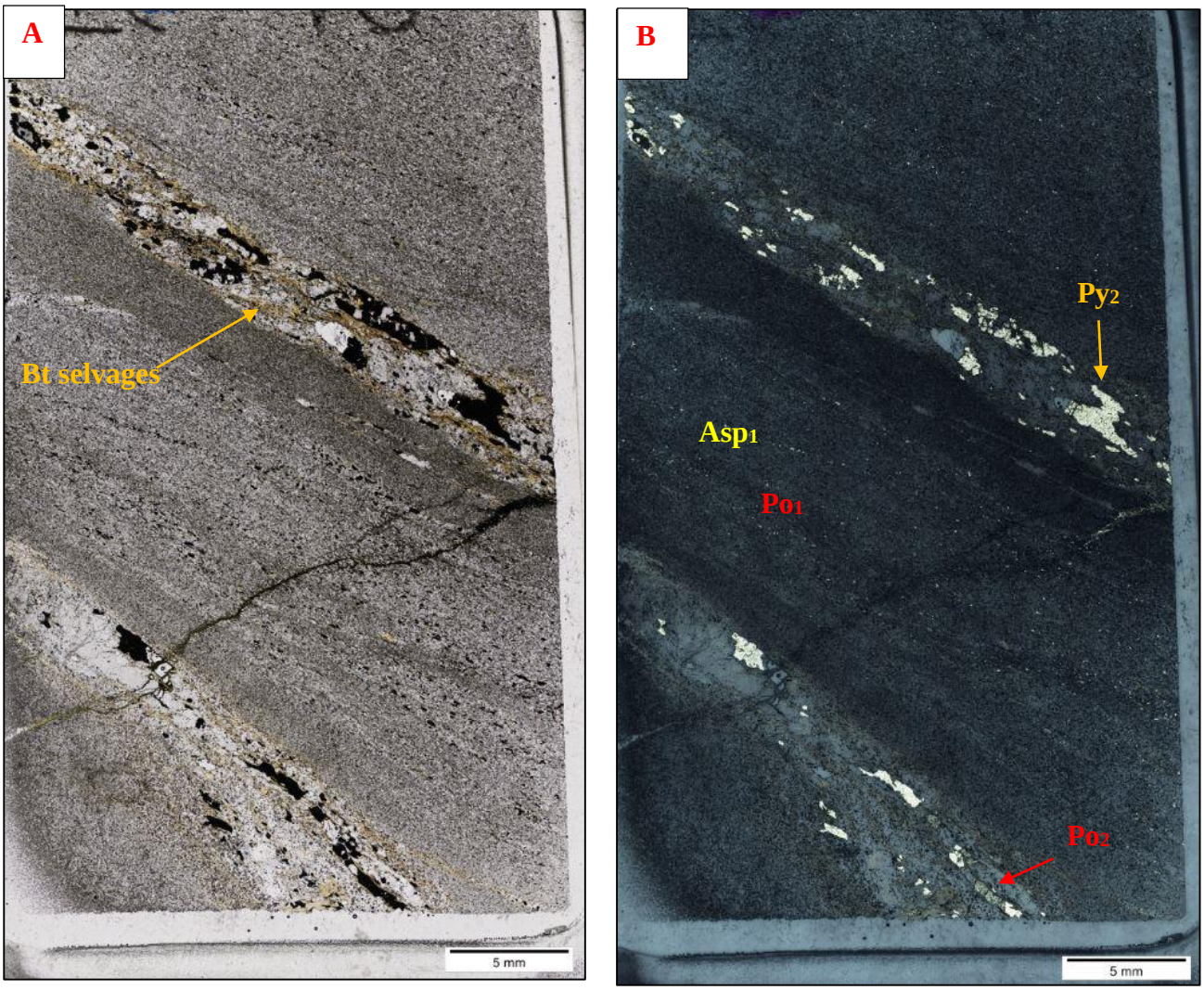

Figure 30 Photomicrographs of quartz sulphide veinlets showing A) Quartz veins with coarse opaque sulphide minerals. Transmitted light microscopy. PPL. B) Coarse pyrite and arsenopyrite crystals forming veins and stringers within the quartz vein. Reflected light microscopy. (SampleJS18 – OKD211 @120.67m; Clouds East section of the Twin Hills Gold Deposit.).

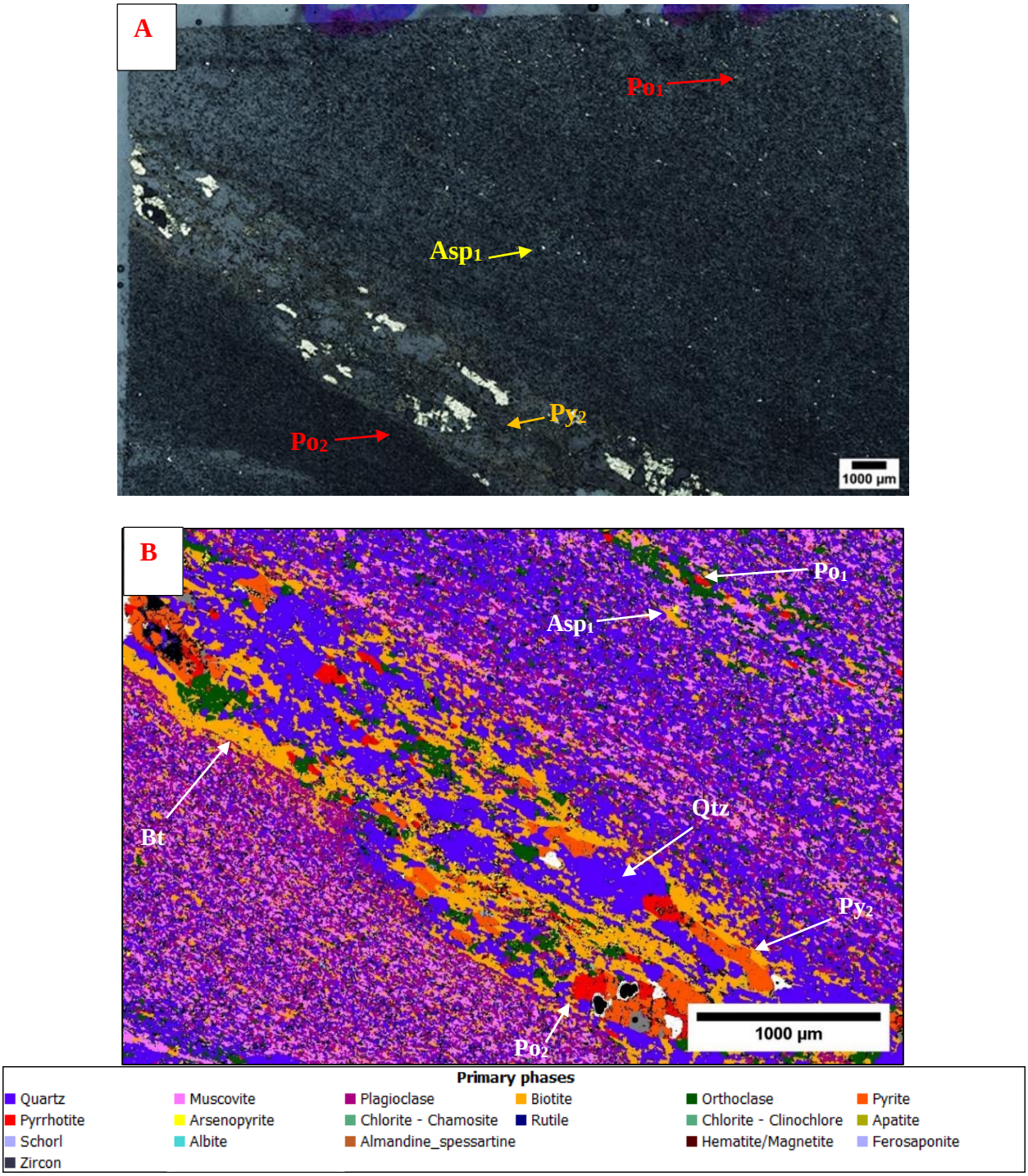

Figure 31 Photomicrograph and mineral phase map of a quartz sulphide vein showing A) Coarse-grained pyrite and pyrrhotite stringers within a quartz vein. Fine-grained arsenopyrite and pyrrhotite disseminated within the groundmass. Reflected light microscopy. B) The dominant mineral phases within the quartz vein. Coarse-grained pyrite, pyrrhotite stingers, and fine-grained arsenopyrite stringers are mainly within the biotite selvages. (SampleJS18 – OKD211 @120.67m; Clouds East section of the Twin Hills Gold Deposit.).

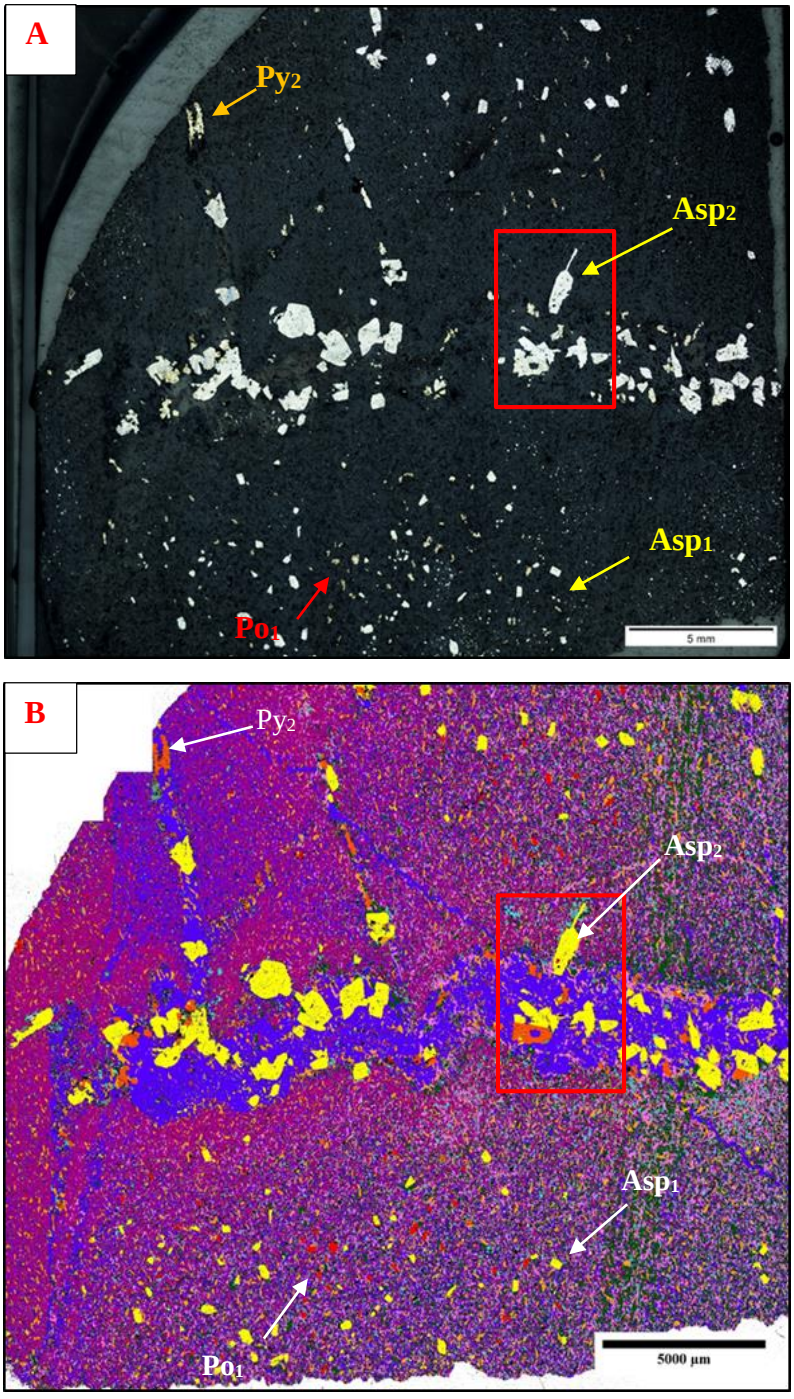

Figure 32 Photomicrograph and mineral phase map of a quartz sulphide vein showing A) Fine-grained arsenopyrite and pyrrhotite disseminated within the groundmass of the metagreywacke. Coarse-grained, euhedral Asp and Py within the quartz vein cross-cuts foliation. Reflected light microscopy. B) Mineral phase map. (SampleJS07 – OKD142 @218.75m; Clouds East section of the Twin Hills Gold Deposit).

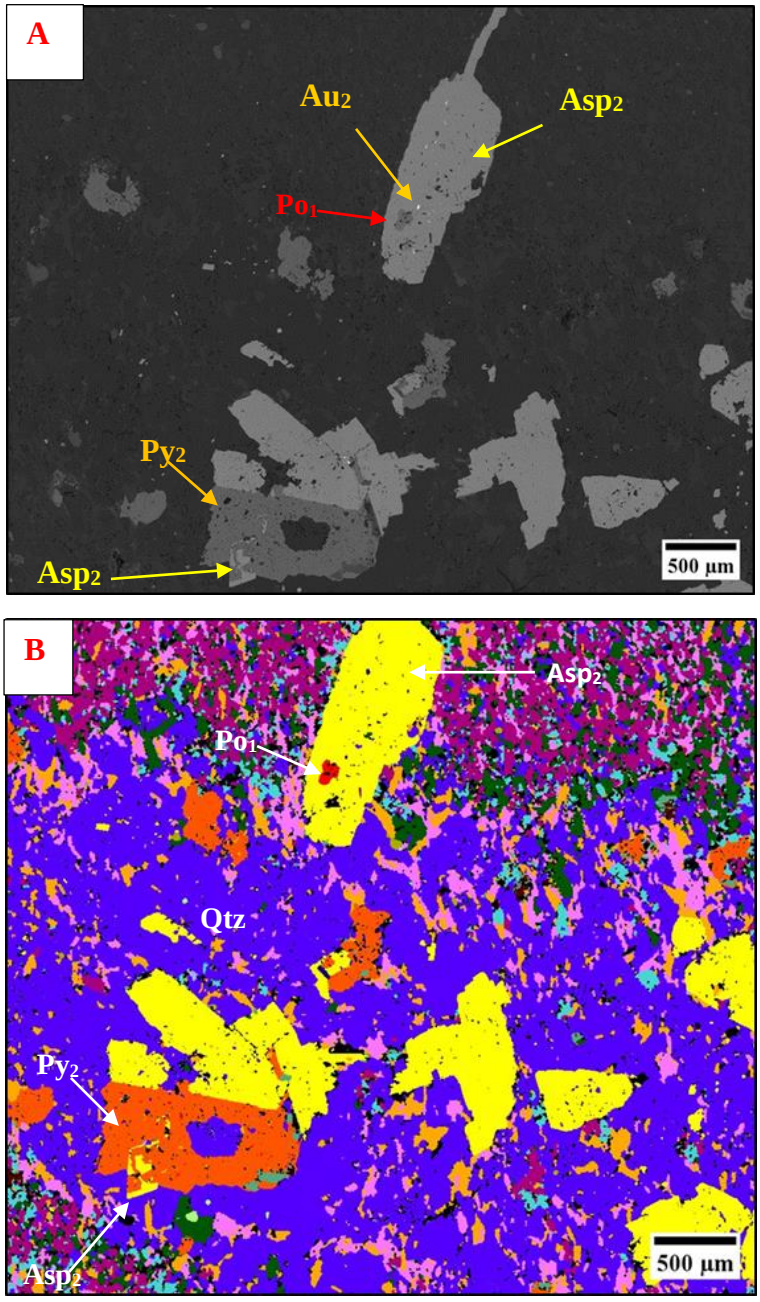

Figure 33 Backscattered electron (BSE) image and mineral phase map of a quartz sulphide vein showing A) Bright phases, gold grains included within coarse arsenopyrite. B) Fine-grained pyrrhotite included within pyrite and arsenopyrite. Pyrite overgrowing arsenopyrite. Euhedral Pyrite and arsenopyrite within a quartz vein. (SampleJS07 – OKD142 @218.75m; Clouds East section of the Twin Hills Gold Deposit).

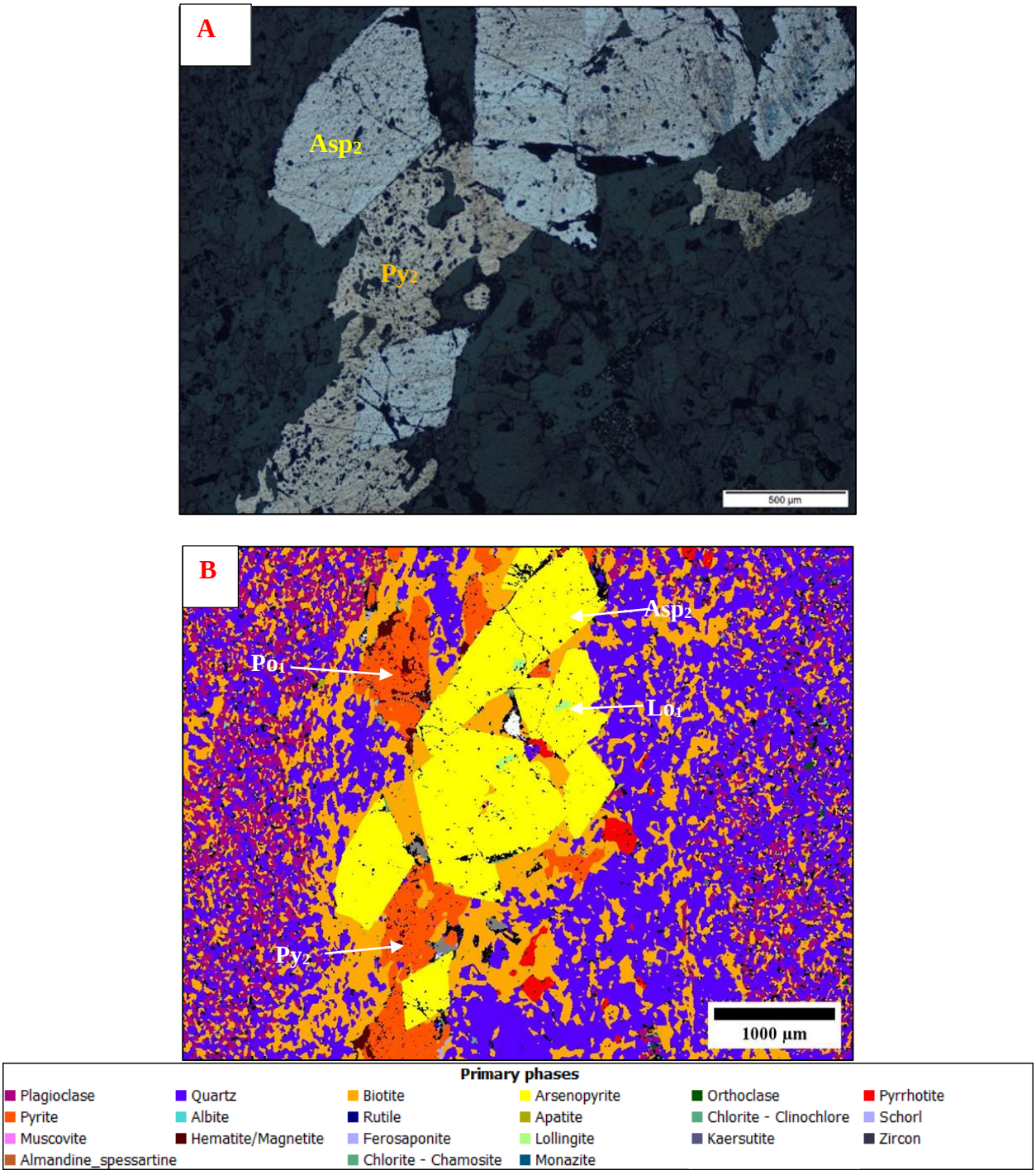

Figure 34 Photomicrograph and mineral phase map of a quartz sulphide vein showing A) Very coarse-grained, euhedral arsenopyrite and pyrite crystals within a quartz vein. Reflected light microscopy B) The mineral phase map. Shown are: fine grains of pyrrhotite included within pyrite; coarse-grained pyrrhotite within quartz vein. Fine-grained lollingite crystals included within very coarse arsenopyrite crystals. (SampleJS13 – OKD211 @111.85m; Clouds East section of the Twin Hills Gold Deposit).

4.3 Gold Deportment

A total of 24 polished thin-section samples were selected for transmitted and reflected light microscopy analysis. These samples were selected such that they are representative of all the lithological units, altered and unaltered zones as well as mineralized and un mineralized zones. In reflected light microscopy, gold grains were identified in three thin sections. A total of six polished thin sections were selected out of the 24 for automated scanning electron microscopy via the Tescan Integrated Mineral analyzer (TIMA). Gold grains were identified in all of the six polished thin sections. The location, grain size, and mode of occurrence of the gold grains are discussed below. This study has arbitrarily classified the gold grains as coarse-grained (> 50µm), medium-grained (5 – 50µm), and fine-grained (<5µm). The mode of occurrence of the gold grains is defined in terms of gold liberation, free surface area (exposure), and mineral associations according to the guidance in Coetzee, et al., (2011). Liberation can be defined as the area percentage of the mineral grain of interest in the particle. Free surface area can be defined as percentage of the grain of interest that has a free surface (Cropp, 2013). Liberation and free surface area are two textural classifications used in proccess mineralogy to predict the ease of recovery (Figure 35) (Cropp, 2013).

The results of this gold deportment study should be considered as an indication of the gold deportment and not definitive, due to the limited number of samples investigated.

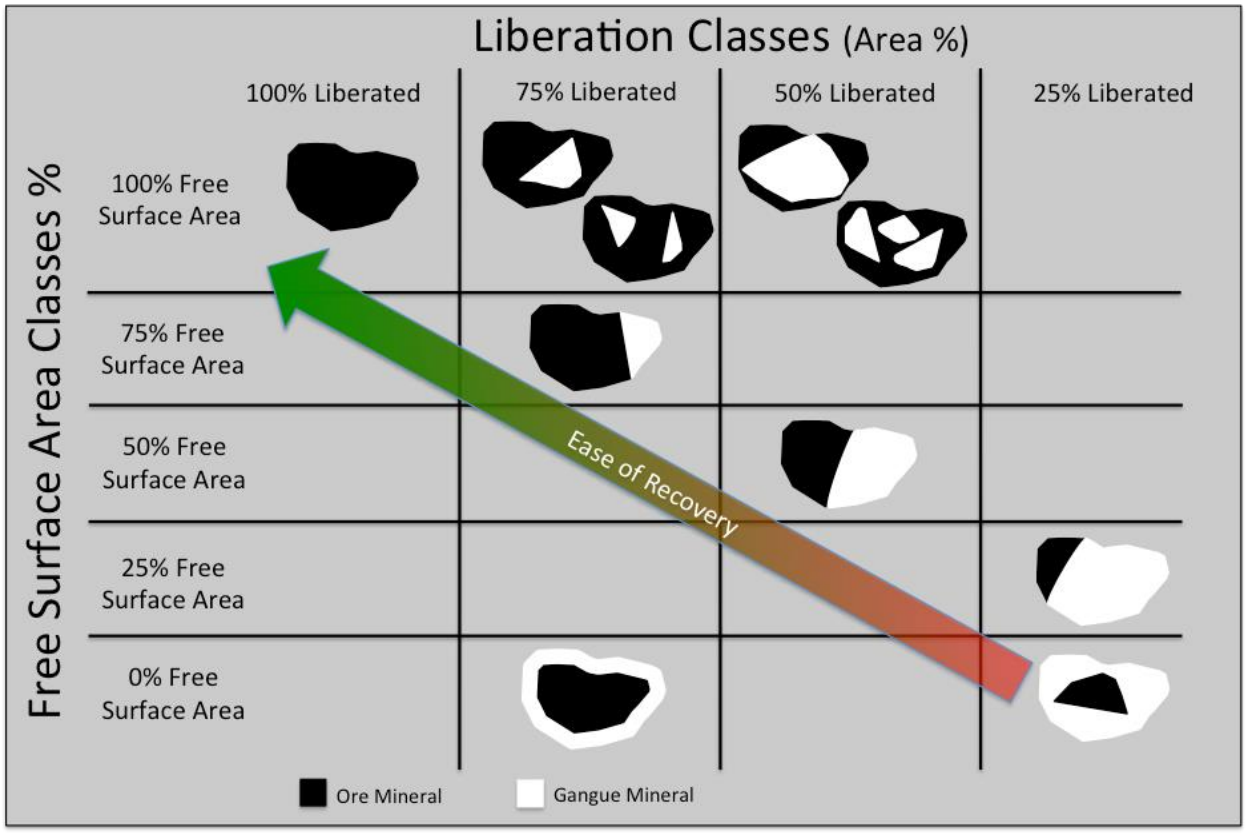

Figure 35 An illustration of particles classified by liberation and surface area (Cropp, 2013).

- **Gold grains within the groundmass of the metagreywacke**

Several visible gold (VG) grains have been identified in hand samples within the groundmass of the psammitic metagreywacke (Figure 36 and Figure 37). Gold grains in the groundmass have also been identified in reflected light microscopy and also by automated scanning electron microscopy using TIMA. The gold grains in the groundmass are closely associated with arsenopyrite crystals (Figure 38). Gold liberation analysis using TIMA mapped all gold grains within the groundmass (Figure 39). The sizes of the gold grains in the groundmass vary from medium grained (5 – 50µm) to coarse grained (up to 2mm in drill core as visible gold). The shapes of the gold grains in the groundmass are largely irregular, with some elongate grains (Figure 39 and Figure 40).

Figure 36 Light grey (bleached) fine-grained interbedded metagreywacke, silicified and potassic alteration mainly characterized by quartz veinlets with biotite selvages. VG within the groundmass. OKD189 @ 186.92m, Clouds East section of the Twin Hills Gold Deposit.

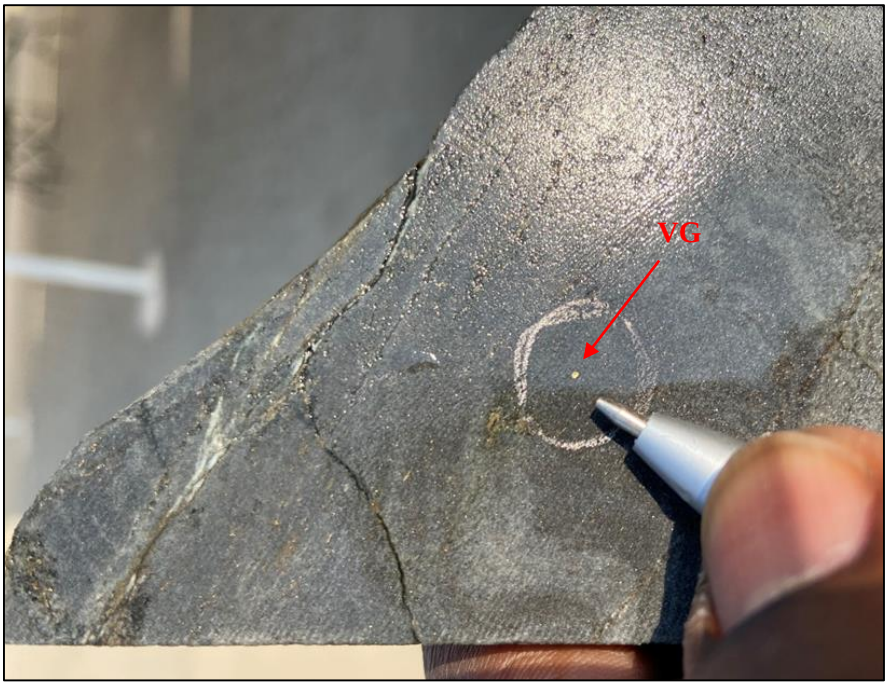

Figure 37 Visible gold nugget (VG) within the groundmass of the light grey (bleached), interbedded metagreywacke. OKD096 @ 67.63m Clouds East section of the Twin Hills Gold Deposit.

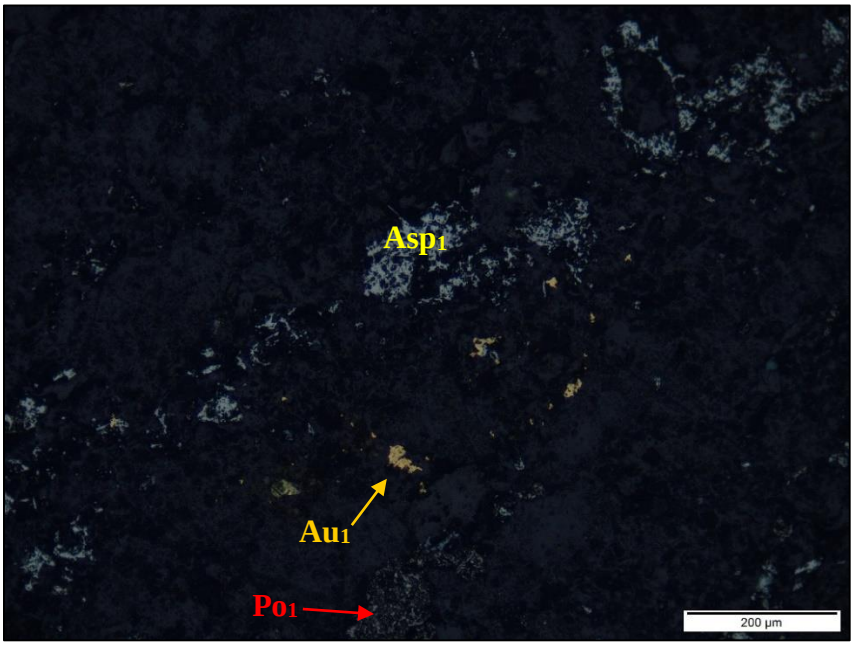

Figure 38 Reflected-light photomicrograph showing gold grains disseminated within the groundmass adjacent to arsenopyrite and pyrrhotite. (Magnification: 10 X). (SampleJS02 – OKD079 @ 200.17m; 4.9 g/t Au, The Bulge section of the Twin Hills Gold Deposit).

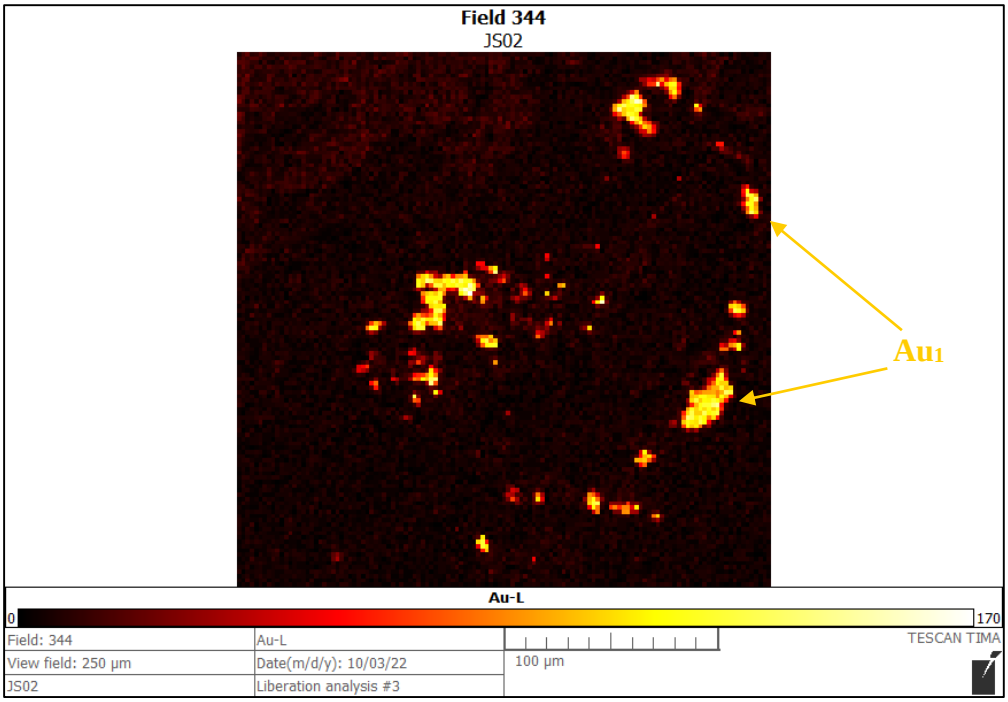

Figure 39 Element map, phase liberation image of gold grains disseminated within the groundmass of the metagreywacke in sample JS02. (SampleJS02 – OKD079 @ 200.17m; 4.9 Au, g/t, The Bulge section of the Twin Hills Gold Deposit).

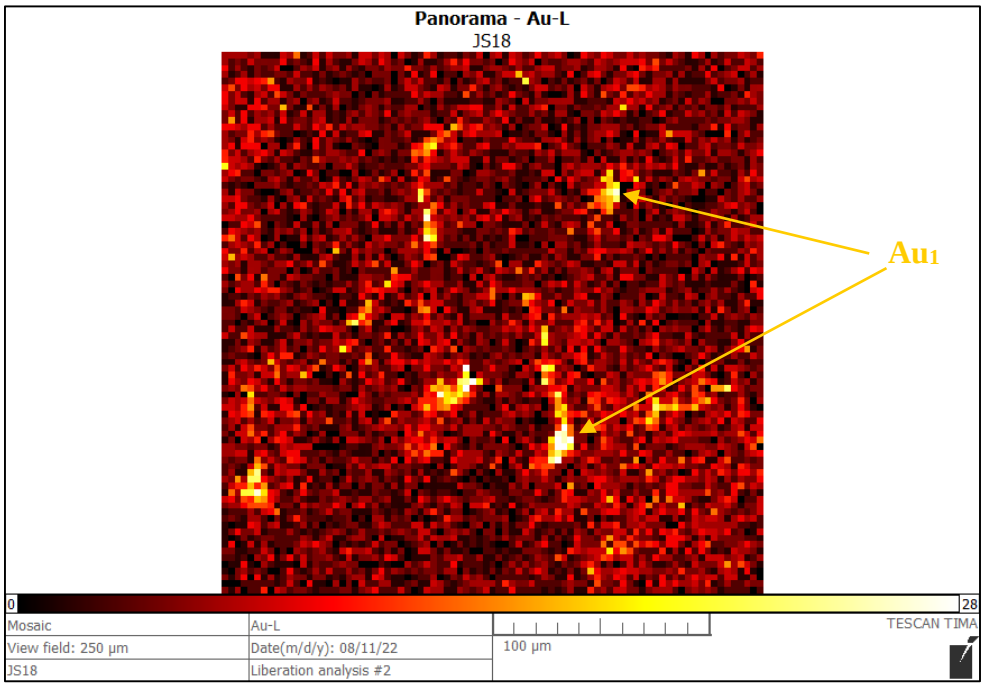

Figure 40 Element map, Gold (Au) map, showing gold grains disseminated within the groundmass of the metagreywacke in sample JS18. (SampleJS18 – OKD211 @ 120.67m; 3.3 g/t au, The Bulge section of the Twin Hills Gold Deposit).

- **Gold grains within biotite selvages associated with quartz veinlets.**

Visible gold grains have been located within the biotite selvages adjacent to quartz veinlets (Figure 41). Gold grains have also been found within biotite selvages to quartz-Sulphide veins in TIMA images using the phase liberation of gold grains (Figure 42 and Figure 43). Some of the gold grains in the biotite selvages are closely associated with arsenopyrite crystals.

Figure 41 . Quartz veinlets with biotite selvages contain pyrrhotite, arsenopyrite, and visible gold (VG) grains. The bottom left arrow shows a VG grain surrounded by arsenopyrite crystals. The host rock is light grey (bleached), fine-grained metagreywacke with fine-grained acicular arsenopyrite disseminated within the groundmass OKD274@ 201.34m, The Bulge section of the Twin Hills Gold Deposit).

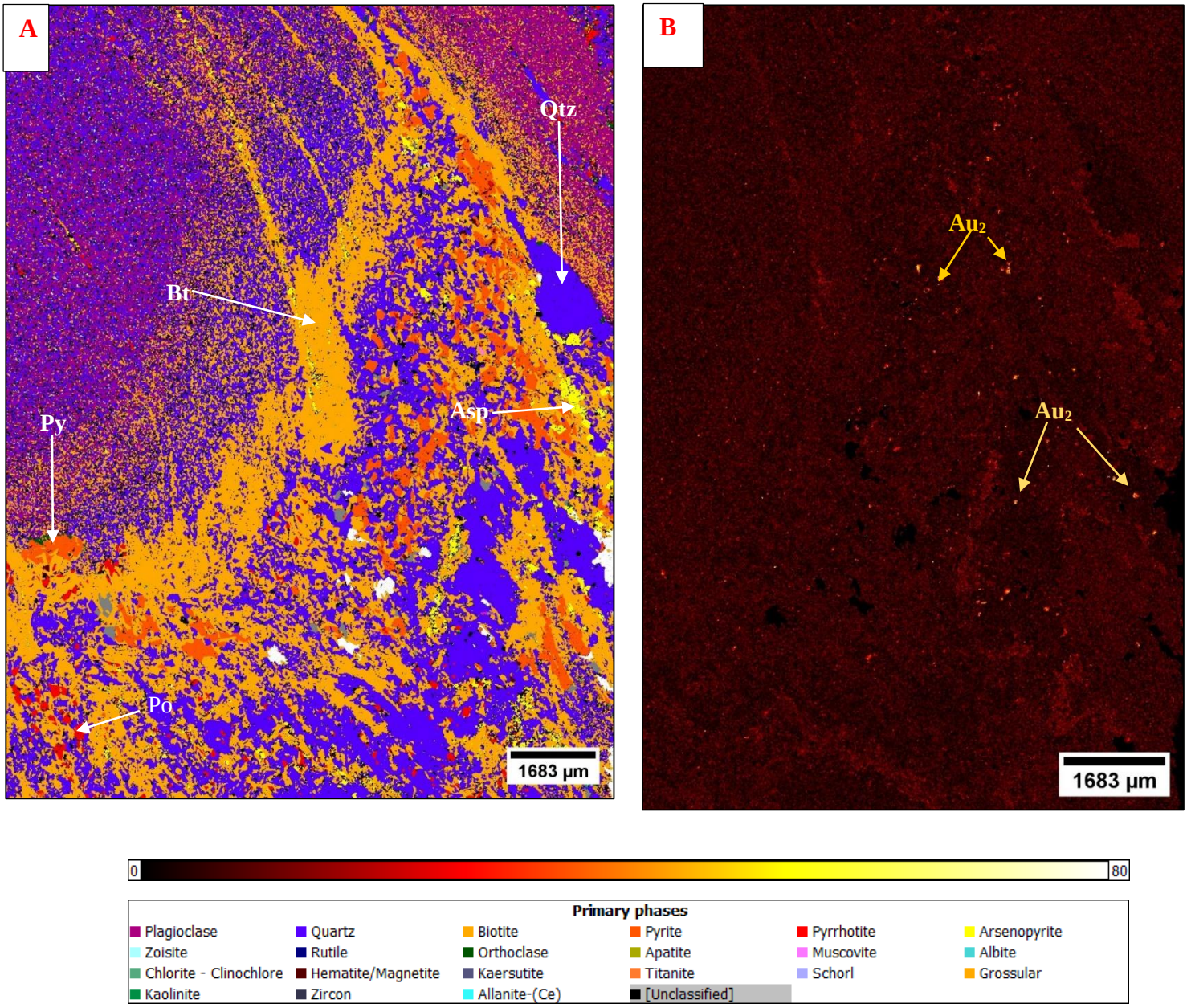

Figure 42 SEM images of quartz veinlets with biotite selvages showing A) Mineral phases within quartz veinlets with biotite selvages. B) Fine gold grains disseminated within biotite selvages. (SampleJS23 – OKD038 @104.89m; 1.9 g/t Au, The Bulge section of the Twin Hills Gold Deposit).

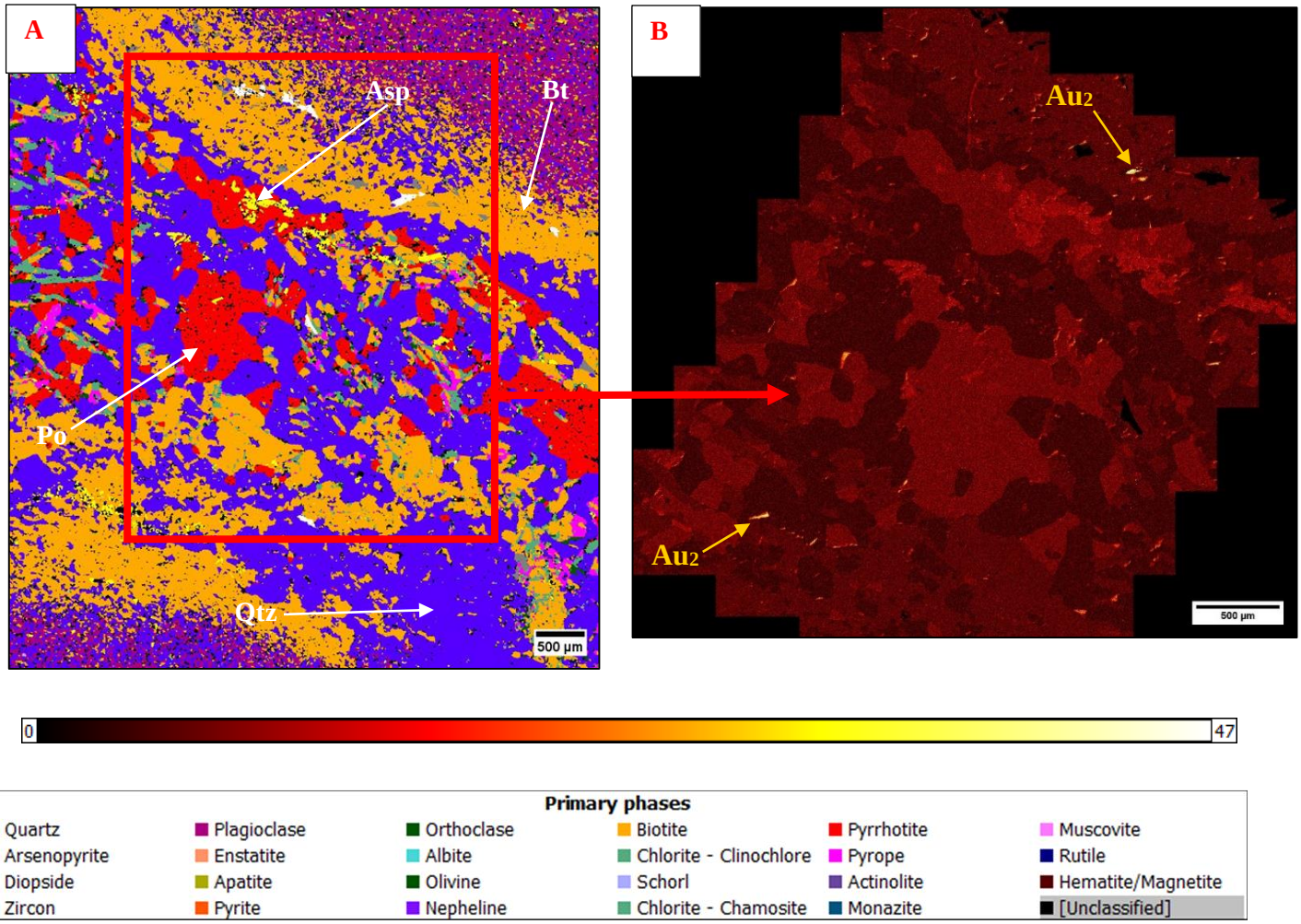

Figure 43 SEM images of quartz veinlets with biotite selvages showing A) Mineral phases within quartz veinlets with biotite selvages. B) Gold grains disseminated within biotite selvages associated with the quartz vein. Gold grains attached to arsenopyrite and pyrrhotite crystals. (SampleJS08 – OKD079 @204.49m; 1.3 g/t Au, The Bulge section of the Twin Hills Gold Deposit).

- **Gold grains included within arsenopyrite**

Several fine gold grains have been identified as included within very coarse-grained, euhedral arsenopyrite crystals. These coarse-grained, gold-bearing arsenopyrite crystals are mainly associated with quartz veins (Figure 44). Up to 18 very fine-grained (<<10 µm) gold grains have been identified to be included within one euhedral, coarse-grained (1500 µm) arsenopyrite crystal (Figure 45). The gold-bearing arsenopyrite crystals have thus far only been identified from rocks within the Clouds section of the Twin Hills Gold Deposit. Figure 46 shows gold grains included within coarse-grained, euhedral arsenopyrite crystals in reflected light microscopy.

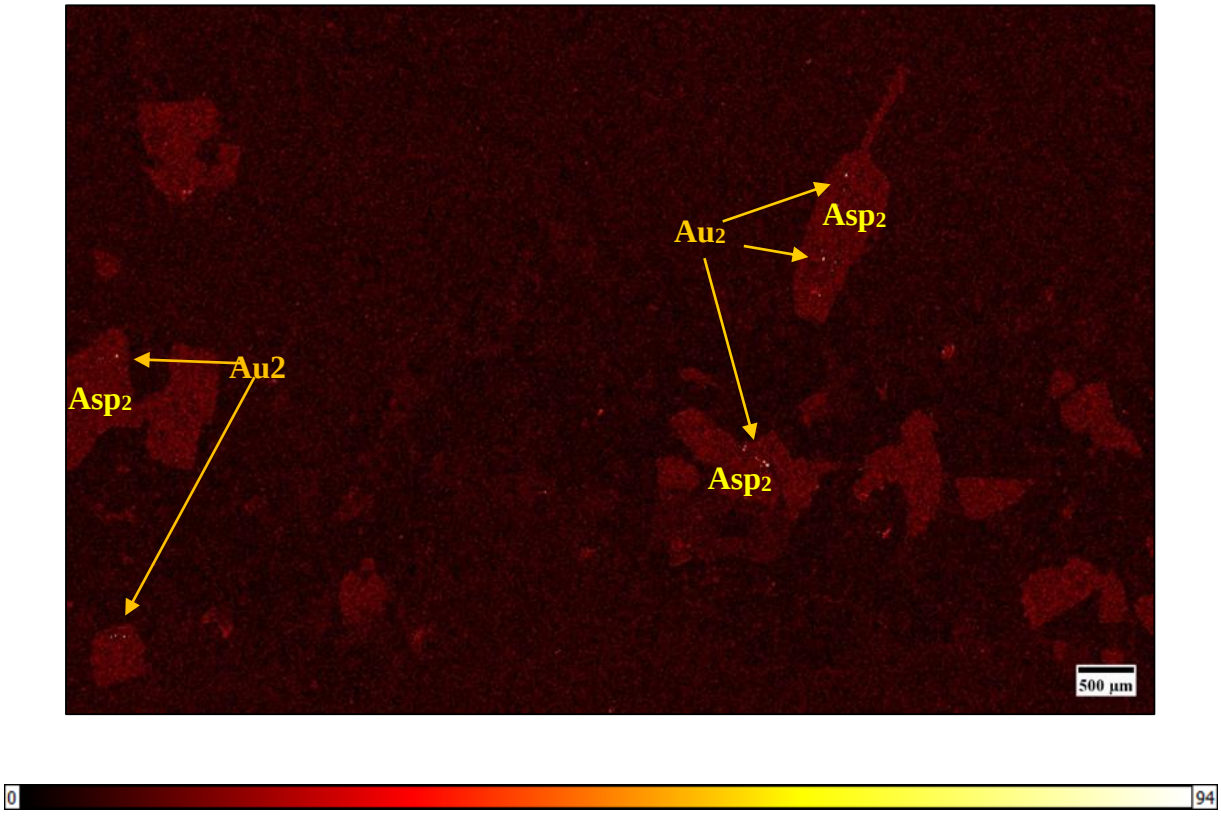

Figure 44 SEM image, phase liberation image of several fine-grained gold grains included within coarse-grained, euhedral arsenopyrite crystals. (SampleJS07 – OKD142 @218.75m; Clouds East section of the Twin Hills Gold Deposit).

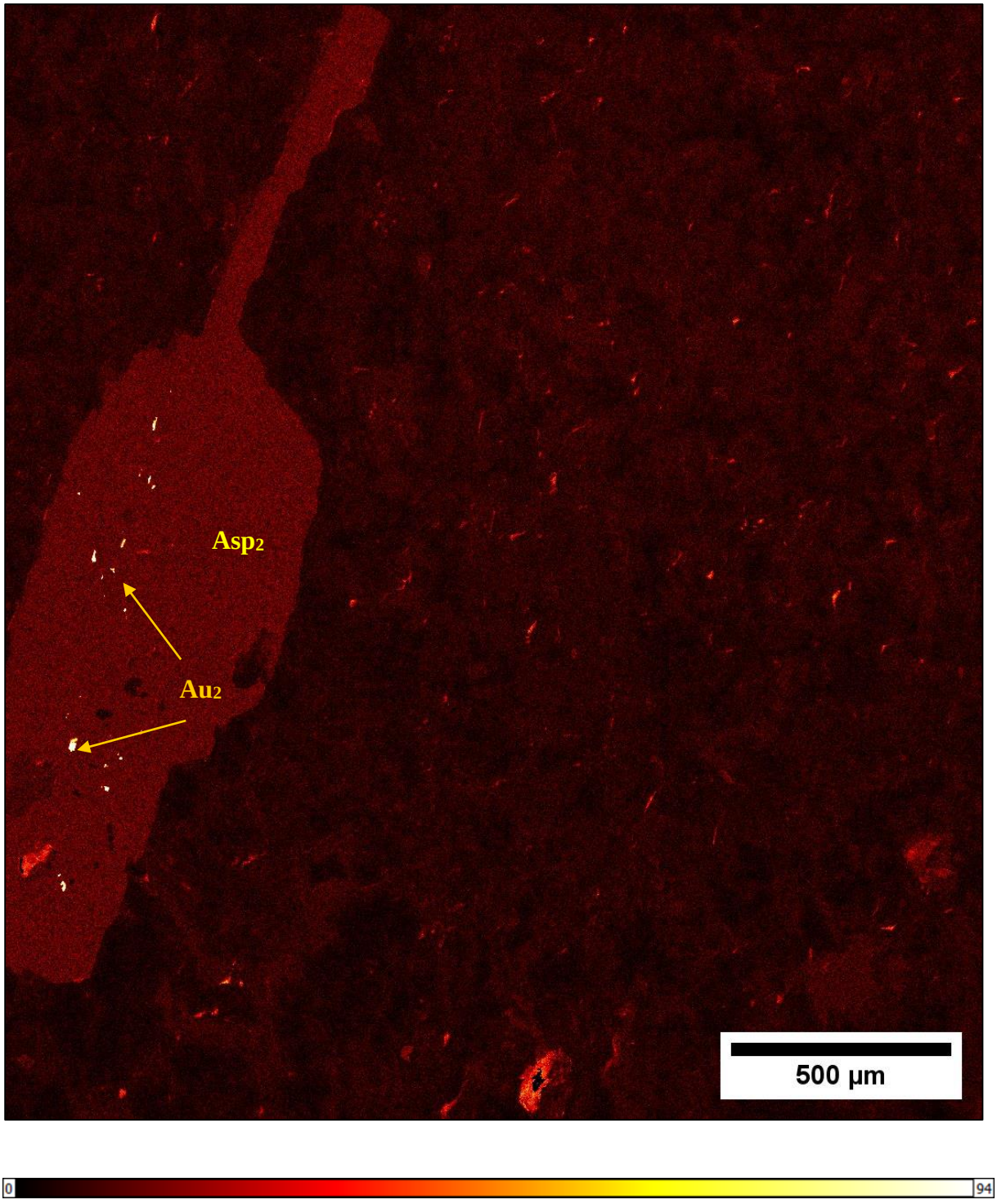

Figure 45 SEM image, phase liberation image of eighteen medium- coarse grained gold grains (5 – 70 µm) included within coarse-grained, euhedral arsenopyrite crystal. (SampleJS07 – OKD142 @218.75m; Clouds East section of the Twin Hills Gold Deposit).

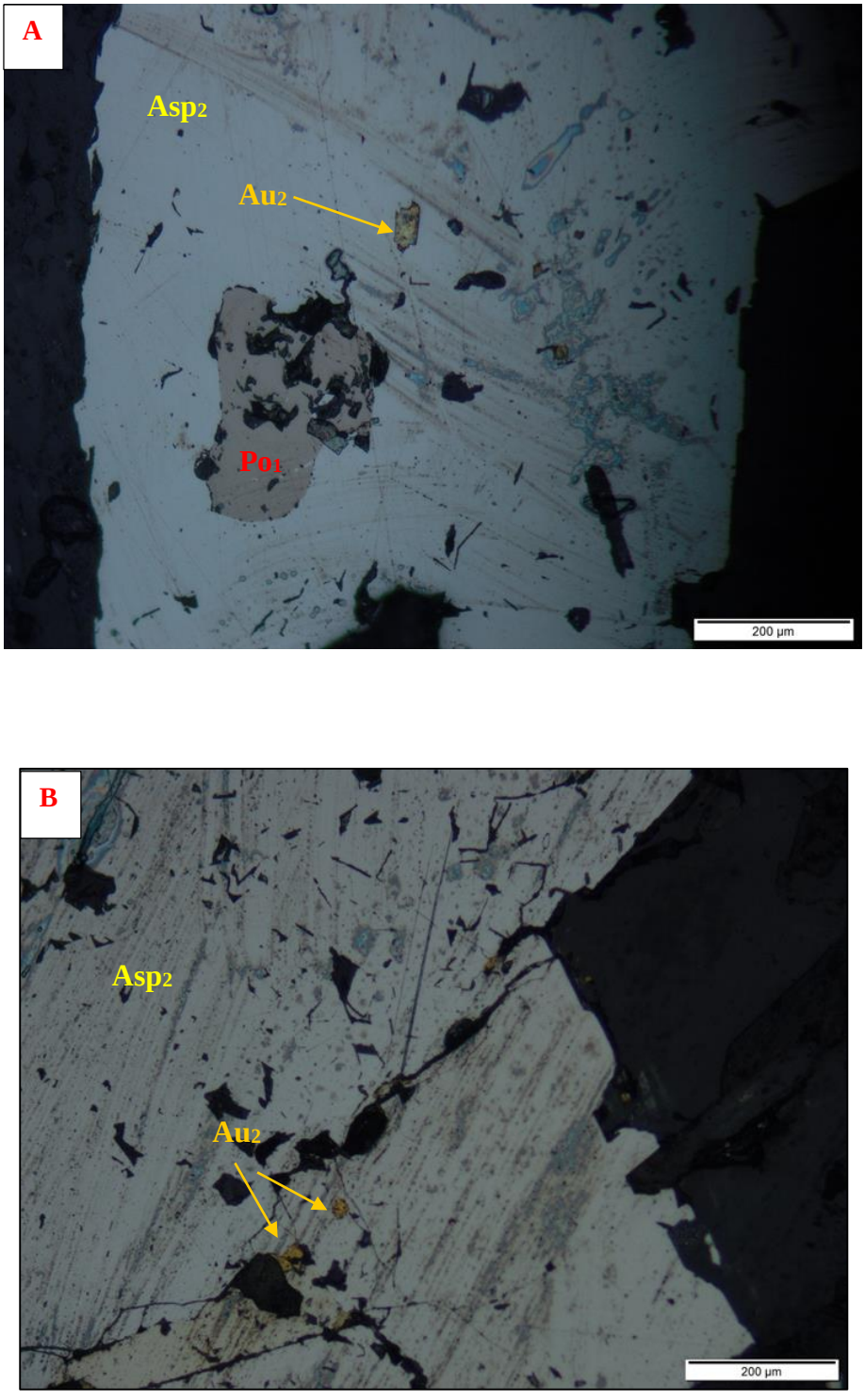

Figure 46 Photomicrographs of very coarse, euhedral arsenopyrite crystals showing A) One gold grain included within a very coarse arsenopyrite crystal. Reflected light microscopy. B) Two gold grains included within a very coarse arsenopyrite crystal. (Magnification: 20 X). (SampleJS07 – OKD142 @ 218.75m; 6.1 g/t; Clouds section of the Twin Hills Gold Deposit).

4.3 Alteration

Two main alteration types can be identified within the host lithologies of the Twin Hills Gold Deposit, namely, potassic alteration and silicification and they mainly occur within the metagreywacke unit.

4.3.1 Potassic Alteration

Potassic alteration is the dominant type of alteration in the project area. It is characterized by a pervasive, light to dark brown coloration of the metagreywacke due to the presence of secondary, recrystallized biotite (Figure 47). The potassic alteration also occurs on the edges of the quartz veinlets as biotite selvages. In transmitted light, potassic alteration is characterized by very coarse biotite laths (up to 2mm) in contrast to the fine-grained biotite (~100µm) in the groundmass of the unaltered parts of the metagreywacke (Figure 48 and Figure 49). The quartz veinlets with biotite selvages are mainly parallel to bedding but become discordant to bedding in some sheared interbeds. A characteristic crackled texture occurs in the interbeds where these quartz veinlets occur discordant to bedding/foliation. Quartz veinlets with biotite selvages are often associated with pyrrhotite and arsenopyrite veinlets and stringers.

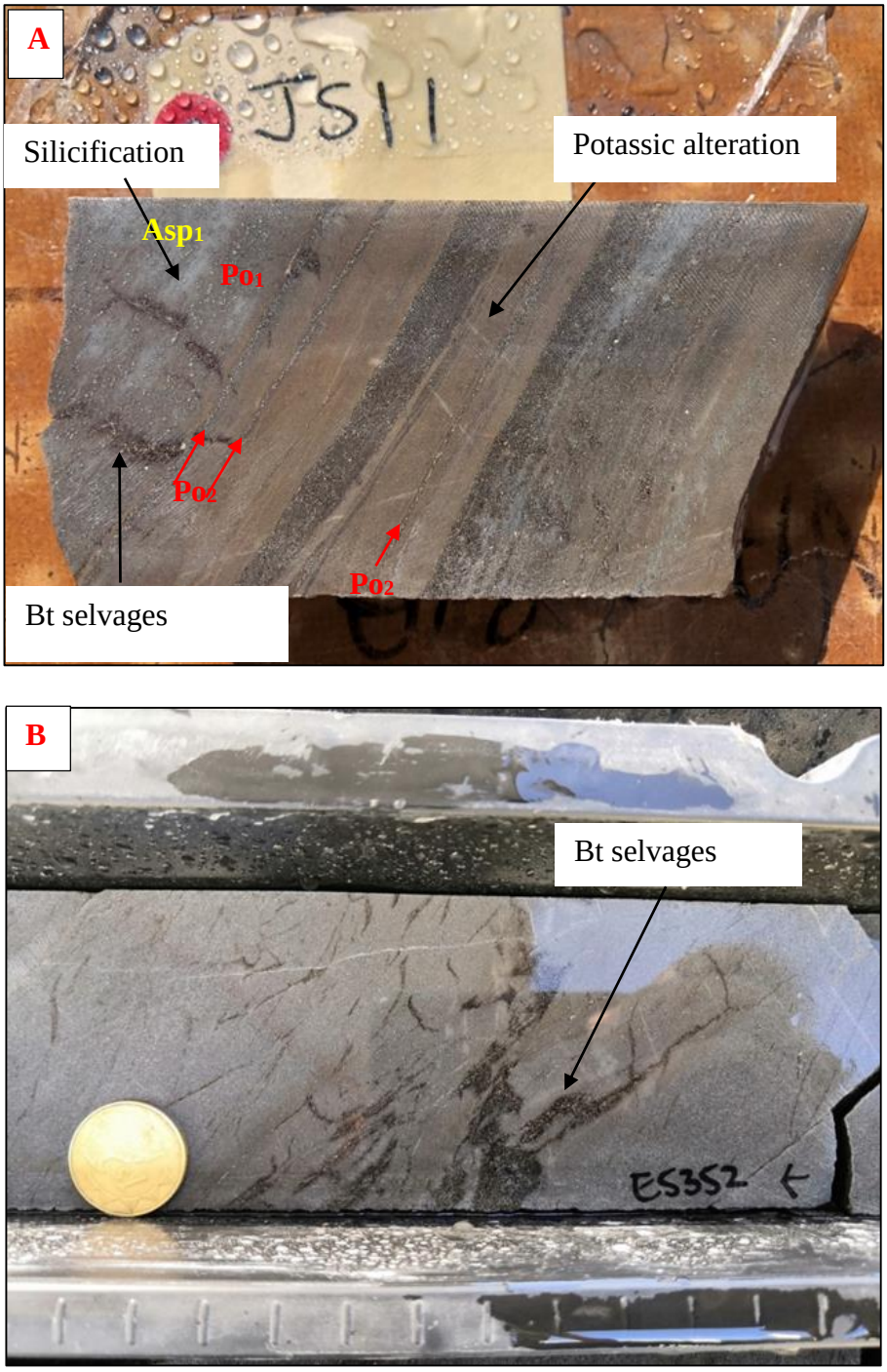

Figure 47 Photographs of borehole core showing A) Potassic alteration characterized by the brown coloration and the discordant quartz veinlets with biotite selvages within the Interbedded metagreywacke. The biotite selvages contain pyrrhotite and pyrite. Pyrrhotite stringers and veinlets are also seen in this sample. Minor silicification can also be seen in these samples as the lighter grey discoloration. B)Potassic alteration characterized by a brown coloration and highly discordant quartz veinlets with biotite selvages exhibiting a characteristic crackled texture in a shear zone. Pyrrhotite and arsenopyrite occur as disseminations within the matrix and as stringers.

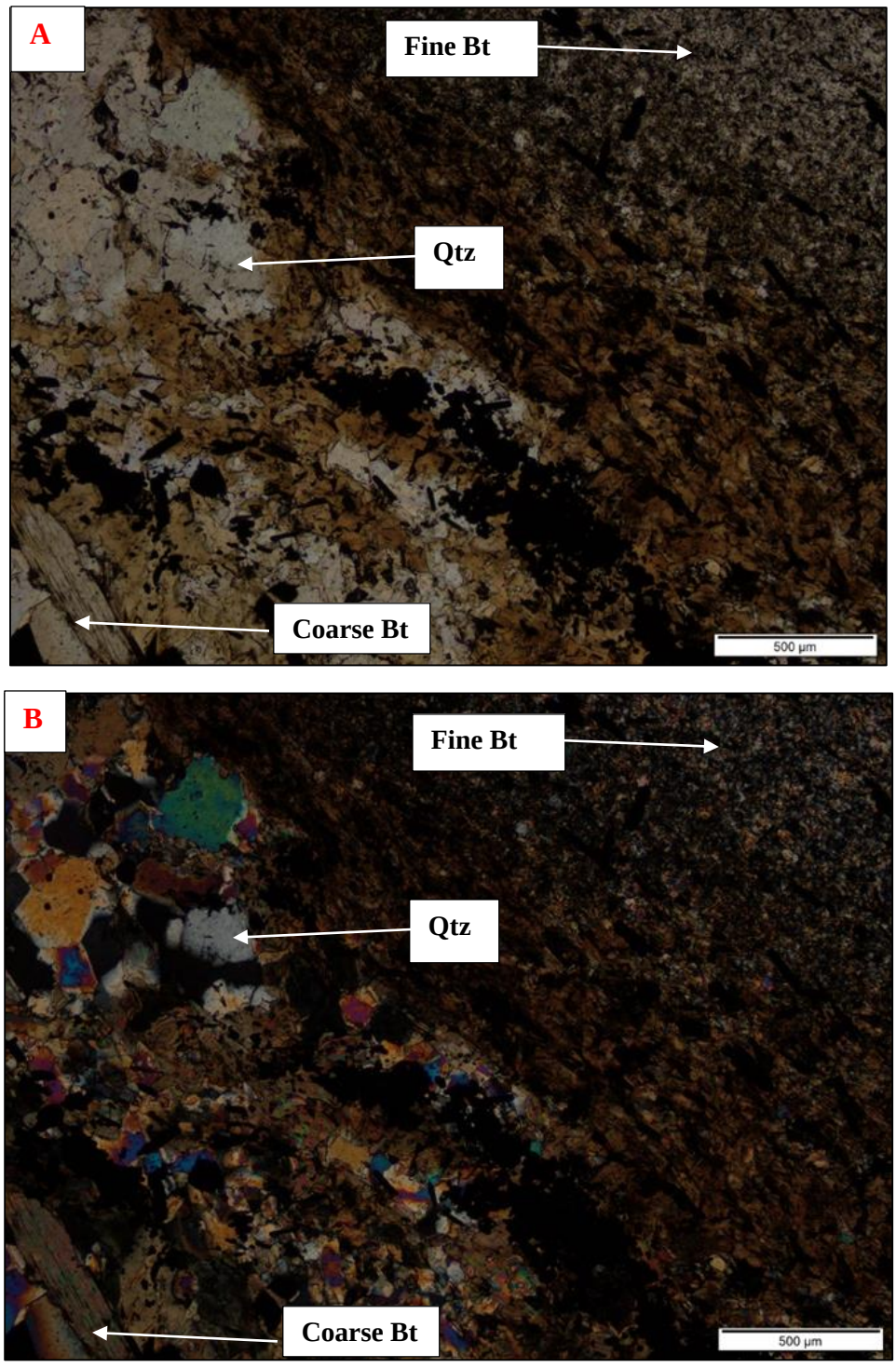

Figure 48 Photomicrographs of interbedded metagreywacke showing A) Quartz veinlets with biotite selvages characterized by coarser biotite laths and quartz grains versus the fine-grained biotite and quartz grains in the groundmass. Opaque minerals within the core of the vein. PPL. (Magnification: 4X). (SampleJS08 – OKD079@ 204.49m; Twin Hills Central Twin Hills Central section of the Twin Hills Gold Deposit).B) Crossed polarized light (XPL) view of A). B) Crossed polarized light (XPL) view of A.

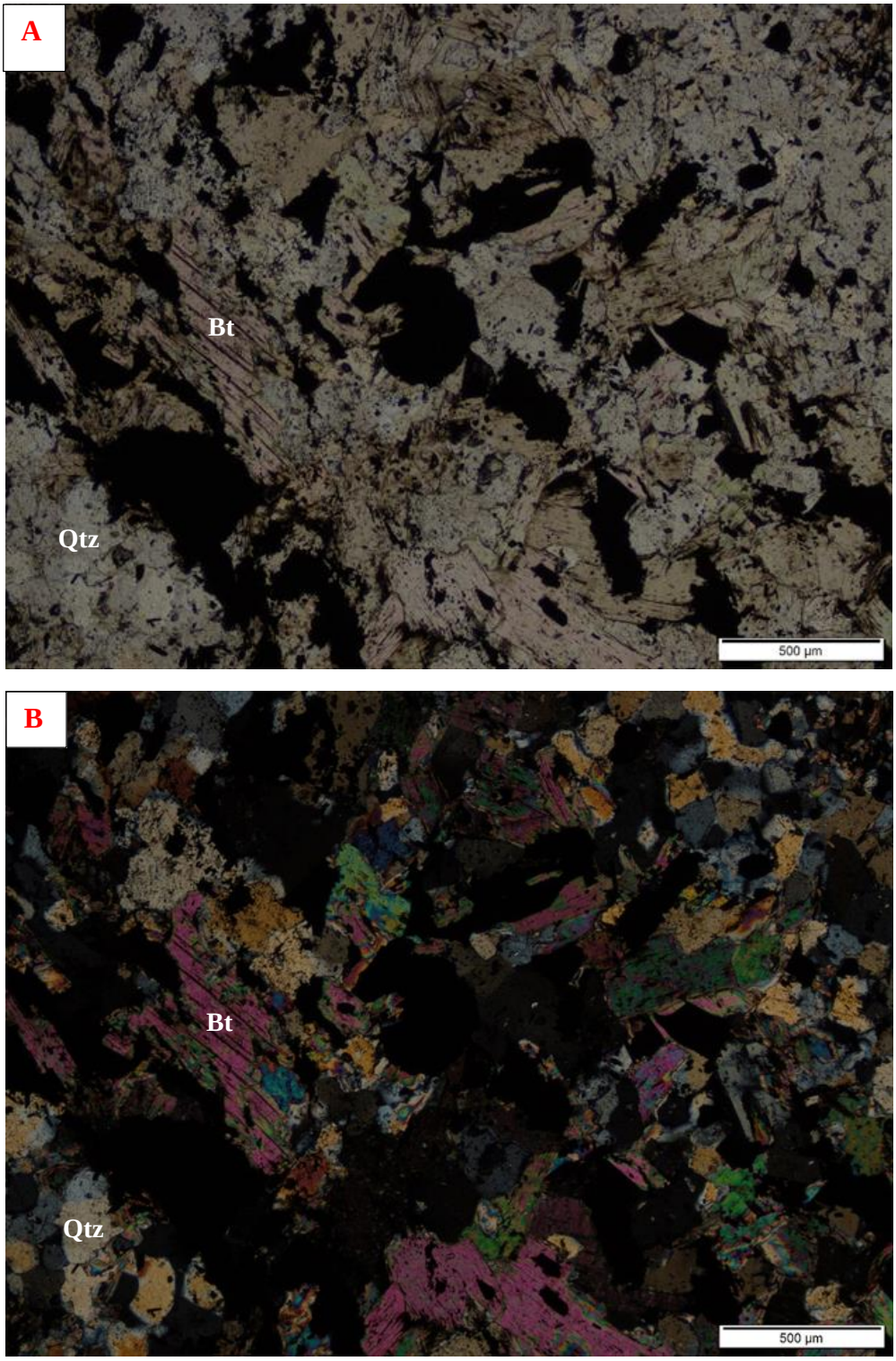

Figure 49 Photomicrographs of interbedded metagreywacke showing A) Transmitted light photomicrograph showing very coarse biotite laths with opaque minerals (Sulphides). PPL. (Magnification: 4 X). (SampleJS01 – OKD079 @ 191.96m; Twin Hills Central section of the Twin Hills Gold Deposit).B) Crossed polarized light (XPL) view of A.

4.3.2 Silicification

Silicification is the second most dominant alteration type in the Twin Hills Deposit. Silicified interbeds are characterized by a bleached white appearance and a complex, often vitreous texture (Figure 50, Figure 51 and Figure 52). The degree of silicification ranges from minor to strong silicification. Silicification often occurs in association with potassic alteration. Areas with both silicification and potassic alteration are characterized by fine-grained, acicular arsenopyrite and pyrrhotite disseminated within the matrix and often forming Sulphide veinlets and stringers (Figure 47 and Figure 52). The interbeds with high gold grades are usually characterized by the presence of both silicification and potassic alteration. In transmitted light microscopy analysis, silicification is characterized by coarse, recrystallized quartz grains (~500µm) overprinting fine quartz grains (<50µm) in the groundmass (Figure 53 and Figure 54). Silicified interbeds are often spatially associated with large (>1m wide) quartz veins. These quartz veins are often devoid of sulphides, with the sulphides only occurring within cracks in the quartz veins (Figure 50).

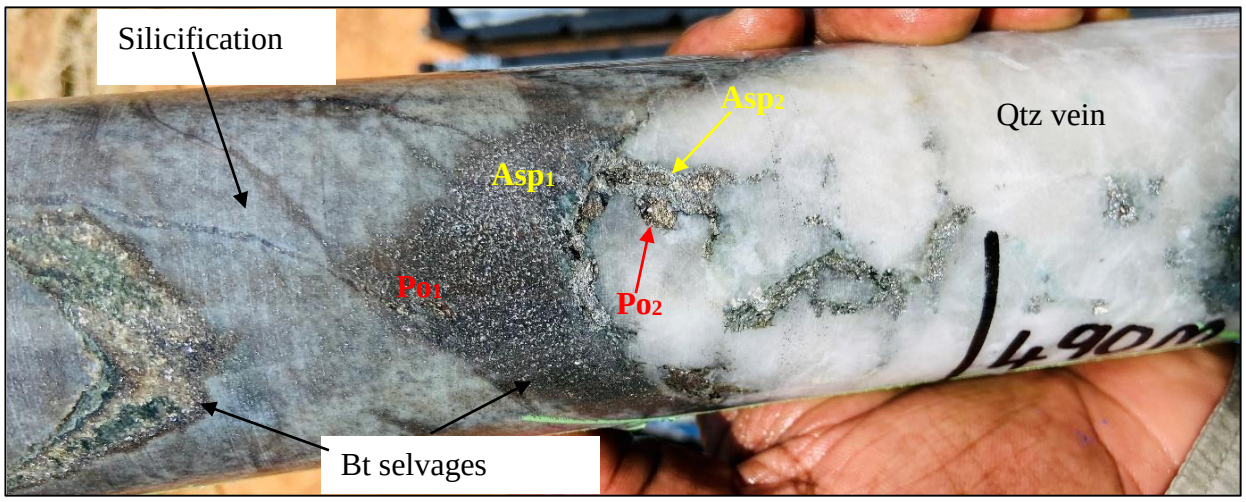

Figure 50 Silicification and potassic alteration with fine-grained disseminated arsenopyrite and pyrrhotite. Coarse arsenopyrite and pyrrhotite form veinlets and stringers. Quartz vein with arsenopyrite and pyrrhotite veinlets within fractures.

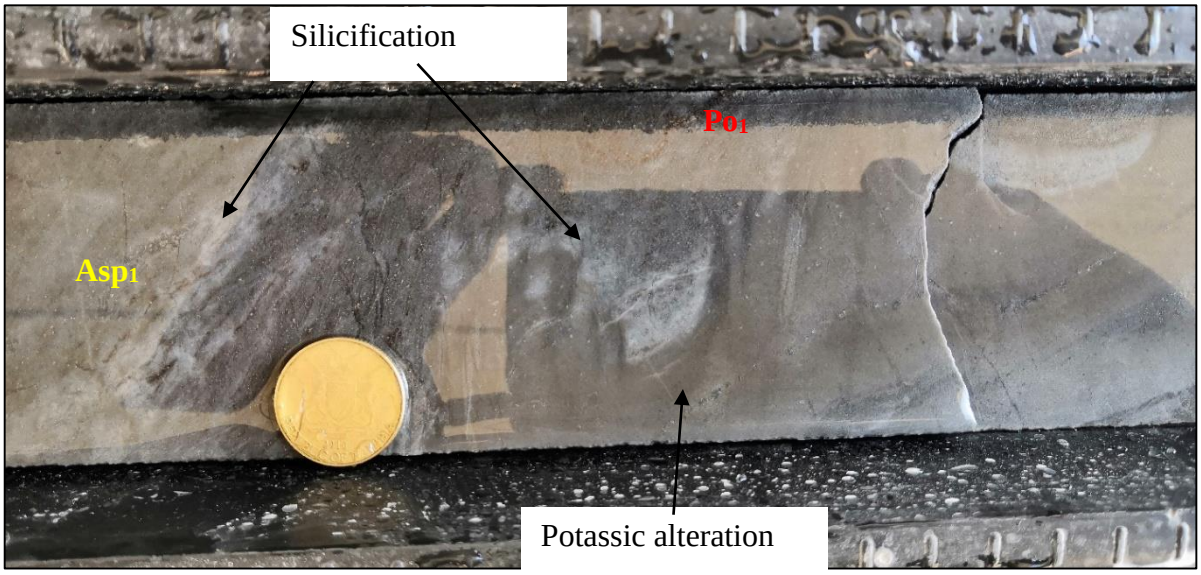

Figure 51 Intense silicification characterized by the white discoloration and a vitreous texture. Potassic alteration is also observed, characterized by the brown discoloration. Fine-grained arsenopyrite and pyrrhotite are disseminated within the groundmass.

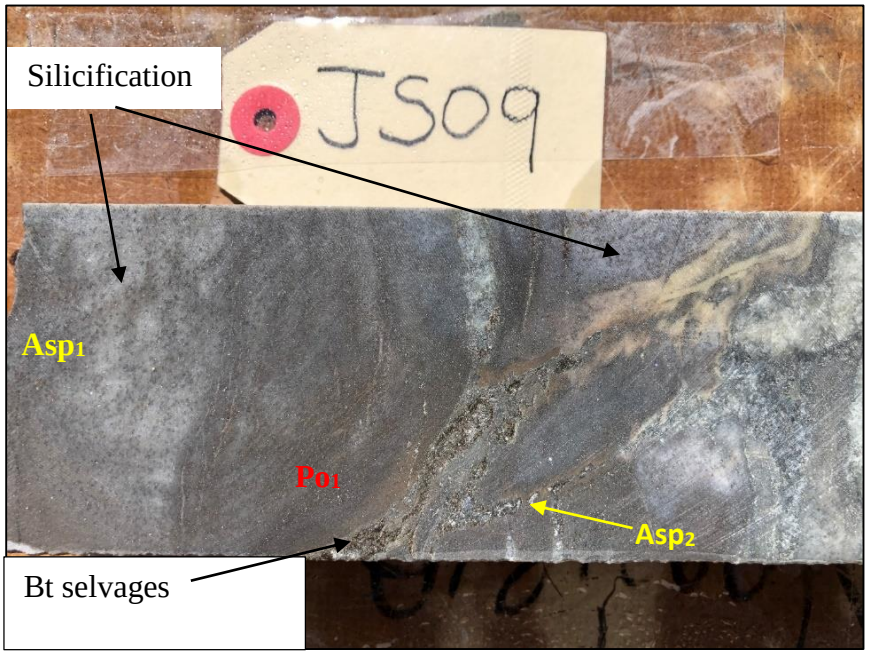

Figure 52 Silicification is characterized by the white discoloration. Potassic alteration is characterized by the brown discoloration and discordant quartz veinlets with biotite selvages. Arsenopyrite occurs as fine-grained acicular crystals (Asp_1) and coarse arsenopyrite aggregate crystals (Asp_2). The finer acicular arsenopyrite, pyrrhotite, and pyrite crystals are disseminated within the groundmass. The coarser arsenopyrite aggregate crystals (Asp_2) are marginally attached to the quartz veinlets with biotite selvages.

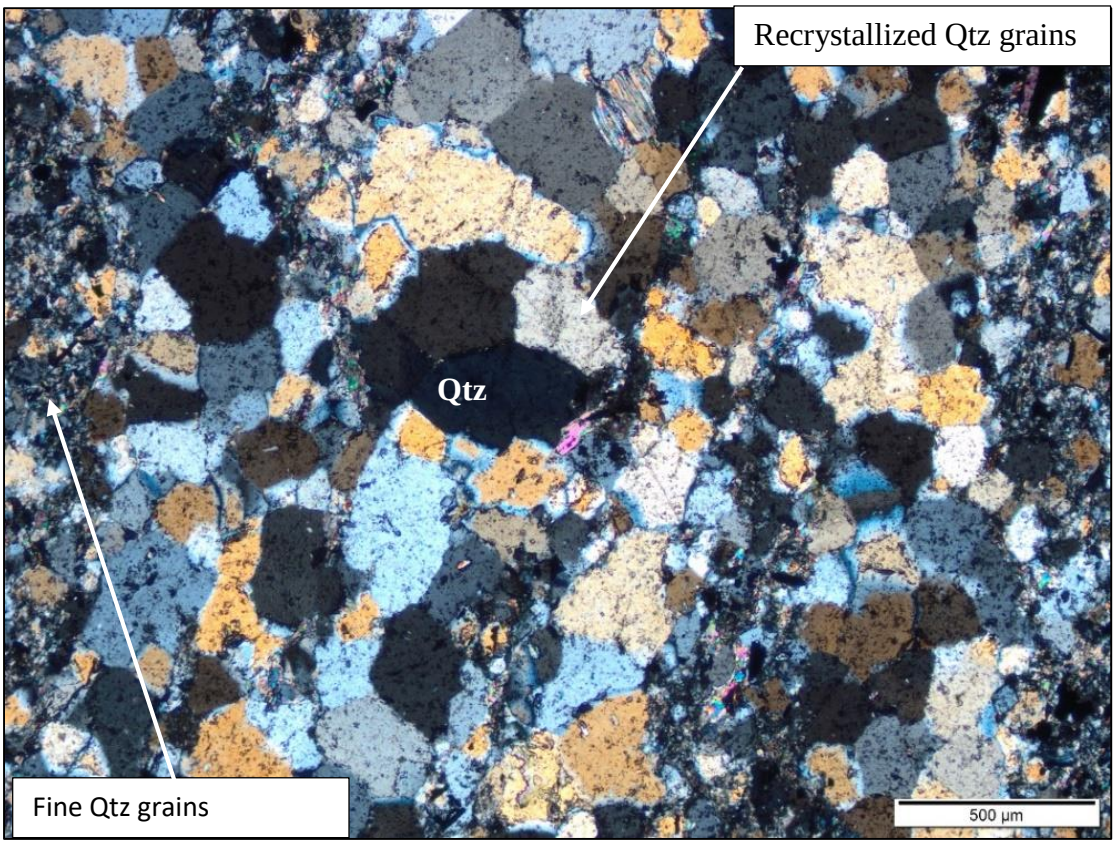

Figure 53Transmitted light photomicrograph showing very coarse quartz grains overprinting fine grains of quartz in the groundmass. XPL. (Magnification: 4 X). (SampleJS02 – OKD079 @ 200.17m; Twin Hills Central section of the Twin Hills Gold Deposit).

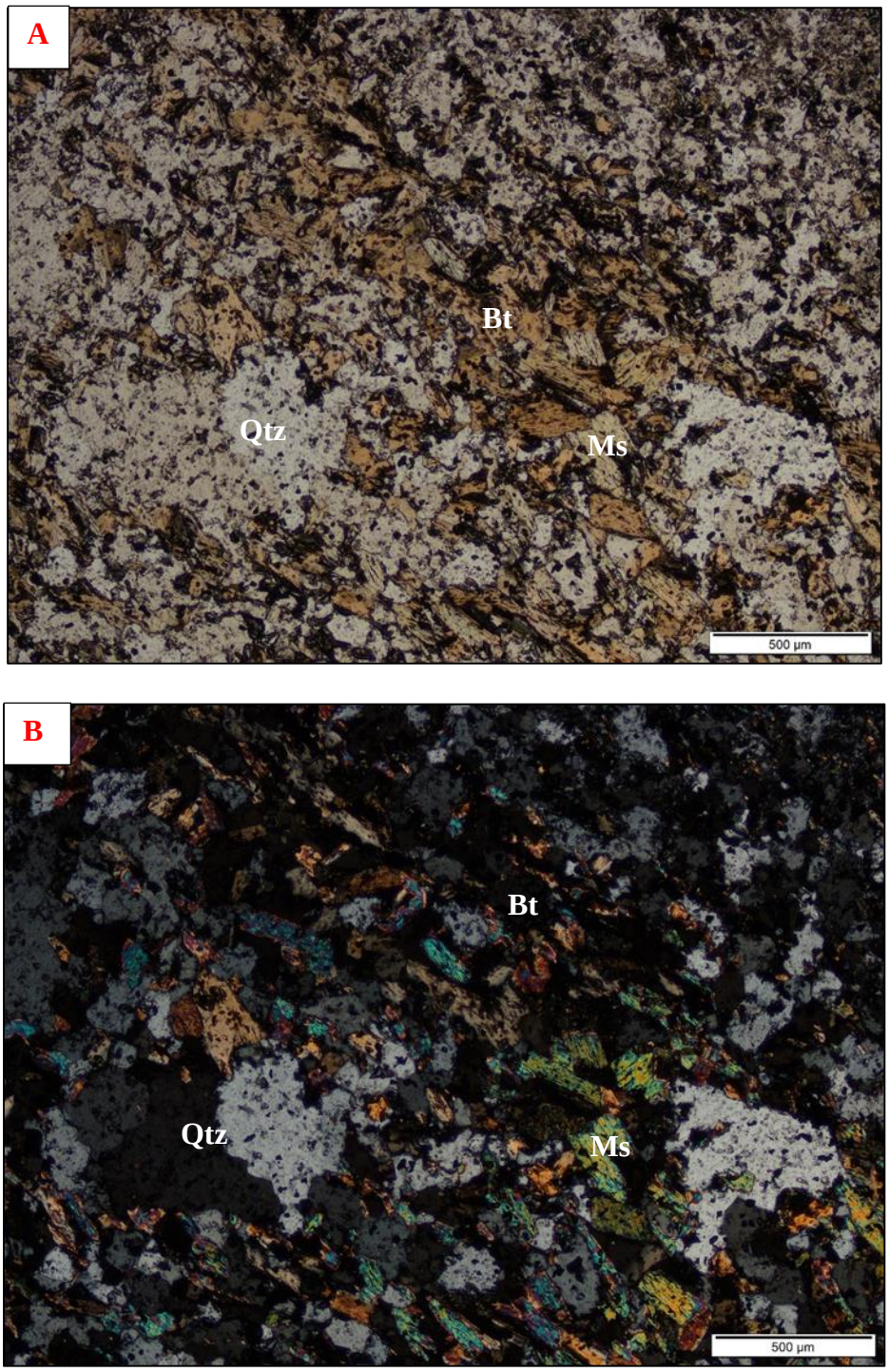

Figure 54 Photomicrographs of interbedded metagreywacke showing A) Very coarse biotite laths and quartz grains (recrystallized), potassic alteration and silicification, Plane polarized light (PPL). (Magnification: 4X). (SampleJS05 – OKD080 @ 230.95 m; Prospect: Twin Hills Central). B). Crossed polarized light (XPL) view of A.

Chapter 5: Discussion

5.1 Petrography

The Twin Hills gold mineralization is essentially hosted within the metaturbidite package of the Kuiseb Formation of the Swakop Group, Damara Supergroup. The composition of the host units ranges from pelitic, mica-rich, and schistose interbeds to psammitic, quartz-rich interbeds of the metagreywacke. The metagreywacke is characterized by graded bedding, often composed of white, medium grained, quartz-rich bases and dark grey, fine-grained, mica-rich (mainly biotite) tops (Figure 12).

These fining sequences within the metagreywacke often define the way up in the sedimentary package. Determining the younging direction within the metagreywacke package at Twin Hills is not always straightforward since the graded bedding is not always visible owing to metamorphism and deformation during the Damara orogeny.

The thickness of the individual beds varies from a few millimeters, essentially laminated, to centimeter-scale beds. The massive, psammitic interbeds of the metagreywacke, which can be several meters thick, can be interpreted to be the thick, more sandy units within the turbiditic sequence. The mica-rich beds are highly schistose with a lepidoblastic texture, while the quartz-dominated beds are massive, exhibiting a granoblastic texture in hand specimen samples. Examination of the quartz dominated massive interbeds of the metagreywacke under transmitted light microscopy however revealed a schistose texture within these massive interbeds (Figure 13). These observations confirm that the schistose nature is indeed present throughout the metagreywacke. The identification of a significant concentration of feldspar minerals (~50%),

including plagioclase and orthoclase, also confirm these host units being classified as metagreywacke (Figure 14).

5.1.1 Lithologic control on mineralization

Petrographic descriptions indicate that the psammitic interbeds of the metagreywacke are better mineralized than the pelitic interbeds (Figure 23 and Figure 24). This is indicated by the higher quantity and multiple modes of occurrence of sulphides in the psammitic interbeds. The significantly higher gold grades are located in the psammitic interbeds which are often characterized higher concentration of sulphides and greater potassic alteration and silicification.

- **The alignment of pyrrhotite and arsenopyrite in the groundmass of the metagreywacke**

The orientation of the sulphides in the groundmass, particularly pyrrhotite and arsenopyrite, depends on the composition and texture of the host rock. Pyrrhotite and arsenopyrite crystals are aligned parallel to foliation in the groundmass of the more pelitic interbeds of the metagreywacke. On the contrary, the sulphides mentioned above are dominantly randomly oriented within the more psammitic interbeds of the metagreywacke (Figure 23 and Figure 24).

The direction of growth of the Sulphides precipitating in the more micaceous (pelitic) interbeds is limited owing to the alignment of the micaceous minerals in response to the regional stress field during deformation and metamorphism. This meant that the sulphides precipitated during deformation were aligned parallel to the foliation developed at that time. The pelitic interbeds also have a very low permeability due to the high micaceous mineral composition. Low permeability in the groundmass meant only limited mineralized fluid flow through the pelitic interbeds. This

consequently led to the low concentration of sulphides and gold precipitating in the pelitic interbeds of the metagreywacke and the more pelitic units such as the biotite and cordierite schists.

Conversely, the psammitic interbeds are characterized by a significant concentration of sulphides, notably arsenopyrite and higher gold grades (including vissible gold) (Figure 36 to Figure 40). This can be explained as a result of increased permeability within the psammitic interbeds owing to the high porosity created by the quartz grain boundaries. The competence contrast between the quartz grains and the mica laths could also contribute to the high permeability within the psammitic units.

The sulphide minerals that formed in the groundmass of the psammitic interbeds of the metagreywacke were also significantly controlled by the angular quartz grain boundaries. The coarser nature of the quartz grains maintained their permeability despite the deformation, therefore almost buffering against the deformation. This meant the arsenopyrite and pyrrhotite crystals that precipitated within the psammitic interbeds of the metagreywacke could grow in different directions resulting in the random orientation of the sulphides, mainly arsenopyrite and pyrrhotite.

- **Why the psammitic interbeds of the metagreywacke are better mineralized than the pelitic interbeds**

The psammitic interbeds of the metagreywacke are much more competent and thus deform in a brittle manner, increasing the permeability. The higher permeability created by these brittle fractures increased the capacity of the metagreywacke to hold more metal-laden fluid, which precipitated as quartz veinlets with biotite selvages via fracture and seal, crackle breccia and sheared interbeds. The pelitic interbeds of the metagreywacke behaved more ductile, resulting in very little space being created and minor sulphides precipitating within the groundmass.

5.2 Metamorphism

Pelitic and psammitic sediments deposited within the Khomas sea are the protolith for the meta-sedimentary units at Twin Hills. The mineral assemblage of the metagreywacke can be described as cordierite-biotite-quartz-plagioclase-muscovite. The cordierite porphyroblasts can be used as the index mineral to determine the metamorphic grade at Twin Hills. Several studies have classified cordierite in metapelite assemblages as a low-pressure, high-temperature mineral (Winter, 2001; Winter, 2013; Bucher & Grapes, 2011; Mapani, 2011). Cordierite is formed at low pressure and high temperature by the reaction of phlogopite and muscovite to form cordierite and K-feldspar. This reaction is displayed by the equation:

phlogopite + muscovite ↔ cordierite + K-feldspar + H_2O (Mapani, 2011).

Mapani (2011) classified cordierite as the low-pressure, high alumina equivalent of staurolite. Staurolite is an index mineral for the staurolite zone of the amphibolite facies in the metamorphism of pelitic rocks (Figure 55 and Figure 56). It is unstable under low-pressure, high aluminium environment and therefore cordierite forms in these environments. This suggests that the metamorphic grade of the Twin Hills area falls within the staurolite zone, low to middle amphibolite facies (Figure 56). This is in agreement with other studies on Twin Hills and the surrounding areas (Steven, 1992; Kisters, 2005; Wulff, 2008; Wicker, 2019; Shilunga & Kisters, 2022).

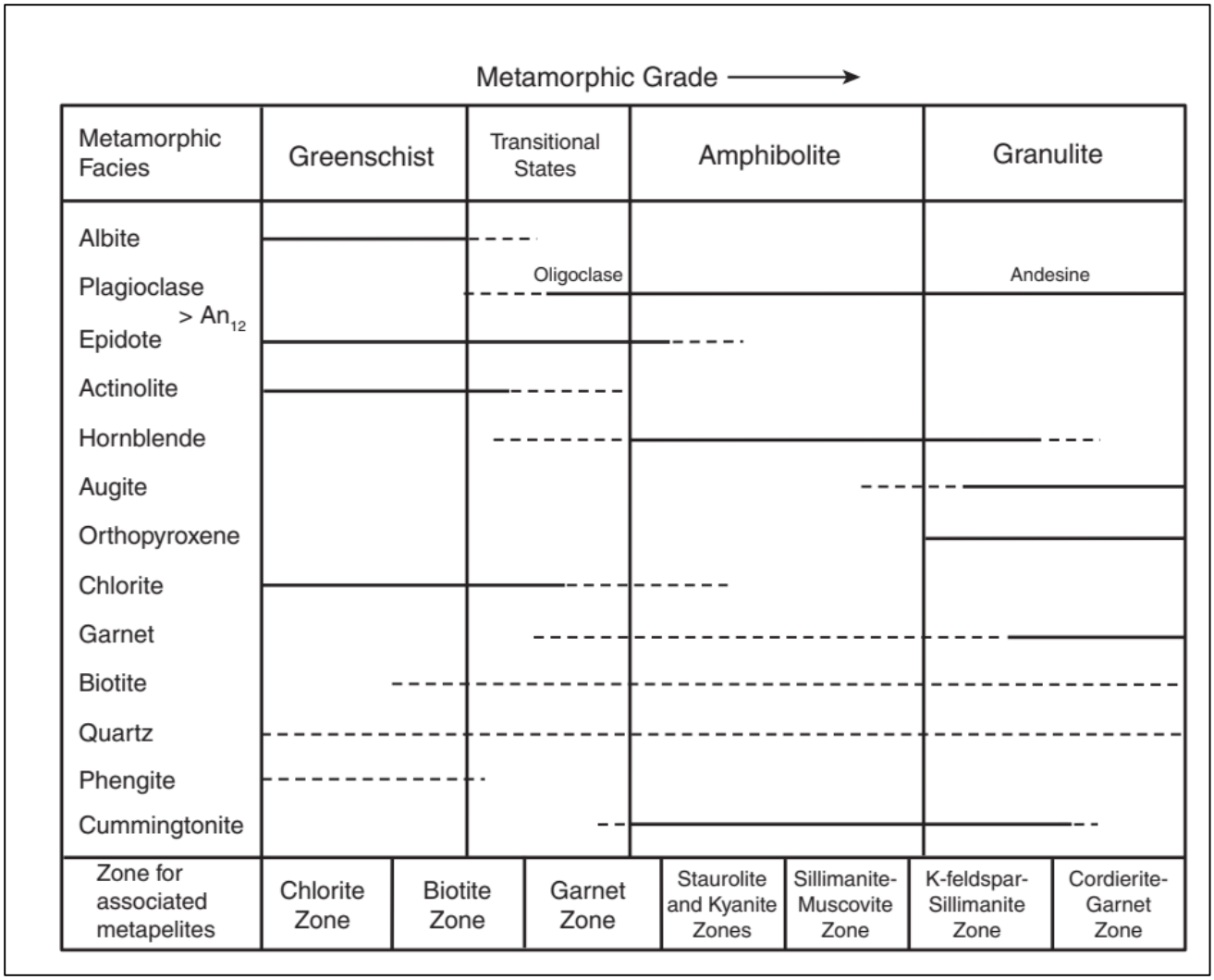

Figure 55 Typical mineral changes that take place during progressive metamorphism in metabasic rocks and pelitic rocks in medium P/T facies series (Winter, 2013).

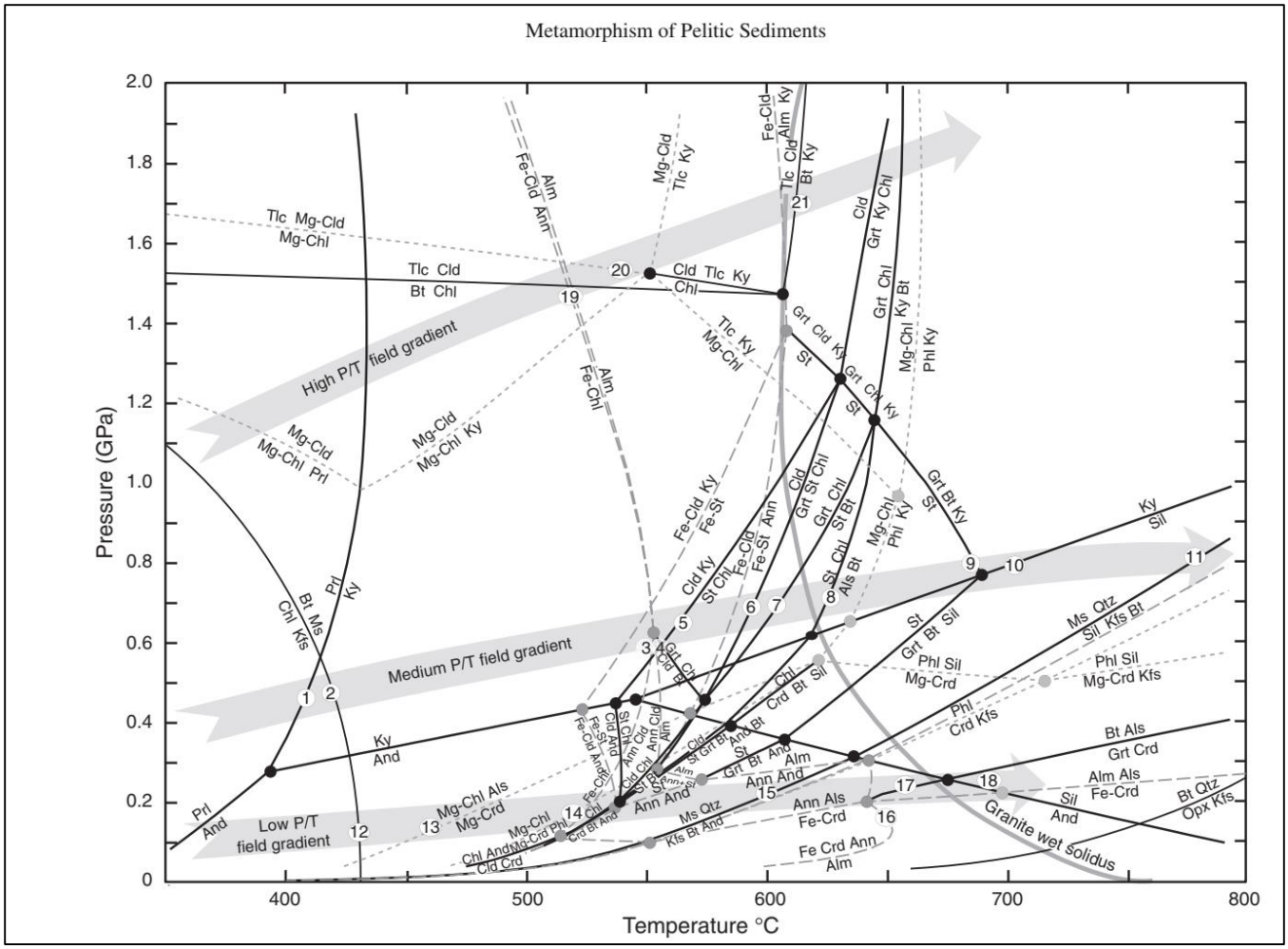

Figure 56 Petrogenetic grid for the system KFMASH at grey dashed curves represent the system KFASH and grey small-dashed curves represent the system KMASH. Reactions are not balanced and commonly leave out the quartz, muscovite, which are considered to be present in excess. Typical high, medium, and low P/T metamorphic field gradients are represented by broad-shaded arrows (Winter, 2013).

Puhan, (1983) proposed the peak metamorphic conditions in the Navachab area to be amphibolite facies grade with temperatures and pressures between 550 - 645˚C, and 2 – 3kbar, respectively. This correlates well with the proposed low to middle amphibolite facies grade of metamorphism at Twin Hills about 30 km to the northeast.

5.3 Ore Mineral Paragenesis

The evolution of sulphides with prograde metamorphism in orogenic gold deposits is well documented (Pitcairn, et al., 2010; Large, et al., 2007; Large, et al., 2011; Li, et al., 2014; Finch & Tomkins, 2017; Zhong, et al., 2015). This study has adapted the models from literature to explain the mineral paragenesis of the Twin Hills Gold Deposit.

5.3.1 Diagenetic Stage

Diagenetic pyrite has not been identified within the metagreywacke at Twin Hills, but is inferred from the wide occurrence of hydrothermal arsenopyrite and its association with gold in the metagreywacke. All the areas with significant gold grades within the metagreywacke (>0.4 g/t) have arsenopyrite crystals. It is proposed that the diagenetic stage involved diagenetic pyrite (Py_0), likely arsenian pyrite, which was initially enriched in As, Au, and other trace elements (Table 2).

The diagenetic arsenian pyrite evolved during prograde metamorphism. Studies on the evolution of sulphides with prograde metamorphism in orogenic gold deposits show that diagenetic pyrite initially has higher concentrations of arsenic, gold and other trace elements that were locked up in the crystal lattice of the arsenian pyrite (Pitcairn, et al., 2010; Large, et al., 2007; Finch & Tomkins, 2017; Zhong, et al., 2015). The absence of diagenetic pyrite in the metagreywacke at Twin Hills could be attributed to the high metamorphic grade (low to middle amphibolite facies). Most of the diagenetic arsenian pyrite would have been converted to pyrrhotite at circa 400˚C in the greenschist facies (Pitcairn, et al., 2010: Finch & Tomkins).

5.3.2 Pre-Quartz Veining Stage

Metamorphic fluids were produced with progressive metamorphism and deformation from the devolitization of the hydrous, clay minerals, which were the precursors to the micaceous minerals (Pitcairn, et al., 2010; Large, et al., 2007). Arsenian pyrite (Py_0) recrystallized to pyrrhotite (Po_1),

and the trace elements that were initially locked up within the pyrite crystal lattice, including arsenic and gold, were expelled into the metamorphic fluids. Arsenic then reacted with iron (Fe) in the groundmass (most likely from biotite) to precipitate arsenopyrite (FeAsS), (Asp_1) (Pitcairn, et al., 2010). Free gold (Au_1) precipitated from the gold bearing metamorphic fluids via phase separation in areas where a drop in fluid pressure occurred resulting in disseminated gold grains (Shilunga & Kisters, 2022). This can be observed at Twin Hills, where economic gold grades are often found in hinge zones of parasitical folds within the metagreywacke. The recently formed pyrrhotite (Po_1) and arsenopyrite (Asp_1) crystals were then exposed to deformation that accompanied the progressive metamorphism. This led to the elongation of pyrrhotite and arsenopyrite crystals which are best observed within the pelitic interbeds of the metagreywacke. The sizes of the arsenopyrite and pyrrhotite crystals increased with increasing temperature and probably longer crystallization time during progressive metamorphism. This led to the formation of the coarse grained, often aggregates of pyrrhotite (Po_1) and arsenopyrite (Asp_1) crystals within the groundmass.

5.3.3 Quartz Veining Stage

Progressive metamorphism and deformation led to increased permeability and advanced fluid flow within the host rocks. These fluids cooled and crystallized to form quartz veins. The quartz veining stage is characterized by quartz veins associated with much coarser, euhedral arsenopyrite (Asp_2), pyrite (Py_2), and pyrrhotite (Po_2) crystals. The relative abundance of pyrite in the quartz veins and the co-existence of coarse-grained, euhedral pyrite (Py_2) and pyrrhotite (Po_2) in these quartz veins implies that the stability fields within the quartz veins were favorable for the co-existence of both pyrite and pyrrhotite. Fine gold (Au_2) grains have been identified to be mainly included within the larger, coarse-grained arsenopyrite (Asp_2) crystals within quartz veinlets. Individual gold grains

were not identified within the quartz veins, except where located within fractures. The quartz veining stage is interpreted as a remobilization event characterized by the remobilization of fine gold grains disseminated within the biotite selvages and coarse arsenopyrite crystals with fine gold grains included within the arsenopyrite crystal lattice. The fine gold (Au_2) grains included within the arsenopyrite crystals could have formed via the exsolution of gold from the arsenopyrite crystal lattice as a result of an increase in temperatutre and pressure conditions with progressive metamorphism.

5.3.4 Calcite Veining Stage

The calcite veining stage is interpreted as a later, post-peak deformation episode. The calcite veinlets, often form breccias, suggesting post-peak deformation at low temperatures. The pyrite veinlets and stringers associated with the calcite also point to much cooler post–peak deformation temperatures.

Table 2 Ore mineral paragenetic sequence of the Twin Hills Gold Deposit interpreted from the textural relationships of ore minerals and rock-forming minerals. The bold lines indicate high mineral abundance; the thin lines minor mineral abundance; the discontinuous lines indicate uncertainty in the determination of the paragenetic sequence as these minerals where not observed in the study.

Minerals	**Sedimentation - Diagenetic stage**	**Deformation - metamorphism** **Pre-quartz veining Stage**	**Deformation - metamorphism** **Quartz veining stage**	**Post- deformation** **Calcite veining stage**
Pyrite	Py_0	Py_1	Py_2	Py_3
Pyrrhotite		Po_1	Po_2	
Arsenopyrite		Asp_1	Asp_2	
Gold	Au_0	Au_1	Au_2	
Lollingite			Lo_1	
Quartz				
Biotite				
Muscovite				
Plagioclase				

5.4 Genetic Model and Timing of Mineralization

The genesis and evolution of gold in the Twin Hills Gold Deposit can be explained in terms of a sediment-hosted orogenic gold deposit model (Kribek, 1991; Wood & Large, 2007; Pitcairn, et al., 2010; Finch & Tomkins, 2017; Large, et al., 2011).

Gold in the Twin Hills Deposit is interpreted to have been introduced into the regional sedimentary basin as early as the diagenetic stage, during the sedimentation of the turbiditic sediments of the Kuiseb Formation into the Khomas sea (first order basin). It is proposed that during this stage, reduced, deep-seated H_2S-rich basinal brines carrying gold and arsenic were exhaled along synsedimentary rift faults onto the sea floor. The gold, arsenic and other trace elements were trapped, partitioned, and concentrated onto the diagenetic arsenian pyrite (Py_0) in the ocean-floor/pelagic sediments (Figure 57). This process led to the enrichment of gold and other trace elements in the arsenian pyrite which formed within the deep-sea, turbiditic sediments of the Kuiseb Formation.

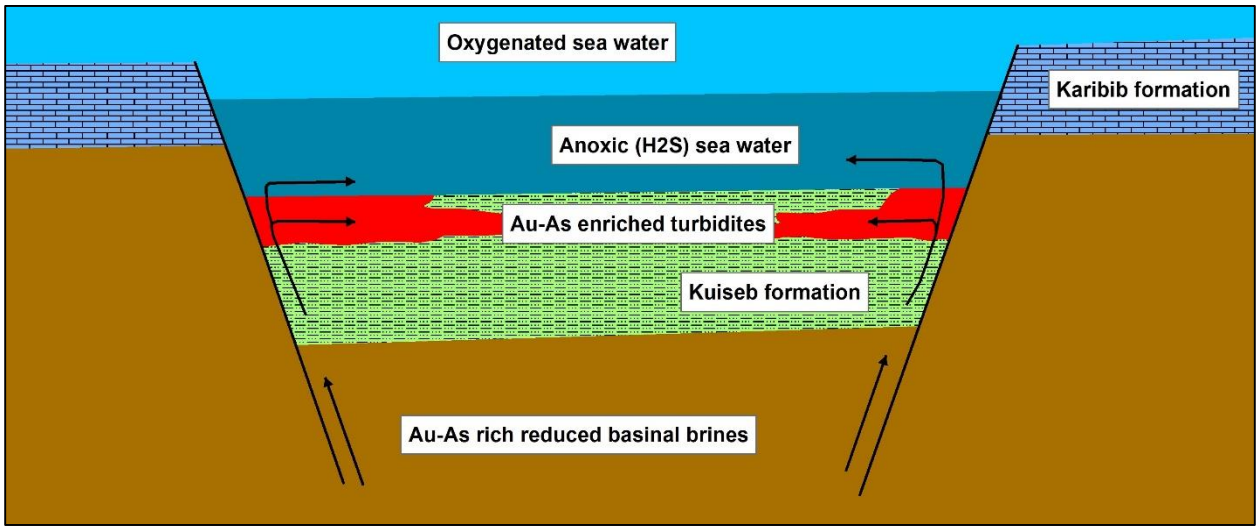

Figure 57 Generalized pre-orogenic cross section across the Karibib basin. The model shows the exhalation of Au-As rich basinal brines which led to the enrichment of the diagenetic arsenian pyrite (Py_0) with gold and other trace elements(Stage 1). Modified after (Large, et al., 2007).

The deformation and metamorphism that accompanied the closure of the Khomas sea following the collision between the Congo and Kalahari cratons led to the start of the Damara orogeny. The turbiditic sediments of the Kuiseb Formation deposited in the Karibib basin of the Khomas sea at Twin Hills were folded into a syncline (Figure 58). The original normal faults which formed the margins to the Karibib Basin were reactivated as thrust faults during basin closure and the onset of deformation. Osino Resources Corp. interpreted this thrust fault as the Karibib Fault Zone (KFZ) in (Figure 58).

Metamorphic fluids were produced with progressive devolatilization of the turbiditic sediments. Gold, locked initially within the crystal lattice of arsenian pyrite (Py_0), was released into the metamorphic fluid at ~400˚C during the pyrite-pyrrhotite transition.

Metal-laden metamorphic fluids migrated along the Karibib Fault and related second order structures and splays. Changes in the physiochemical properties such as temperature, pressure, pH, led to the precipitation of free gold from the gold bearing fluids in the groundmass of the metagreywacke (Figure 58). The quartz veining stage is characterized by the crystallization of the metamorphic fluid, forming quartz veinlets that are dominantly parallel to the dominant S2 foliation and are characterized by biotite selvages. A second (later) set of quartz veins without biotite selvages have been identified within the deposit. These veins were probably emplaced when the metamorphic fluids got much cooler and could not form a reaction rim. These veins cross-cut foliation, and could probably imply that they were emplaced post-peak metamorphism and deformation. These second set of quartz veins are characterized by very coarse, euhedral arsenopyrite crystals with gold inclusions, coarse subhedral pyrite crystals and minor pyrrhotite. (Figure 32).

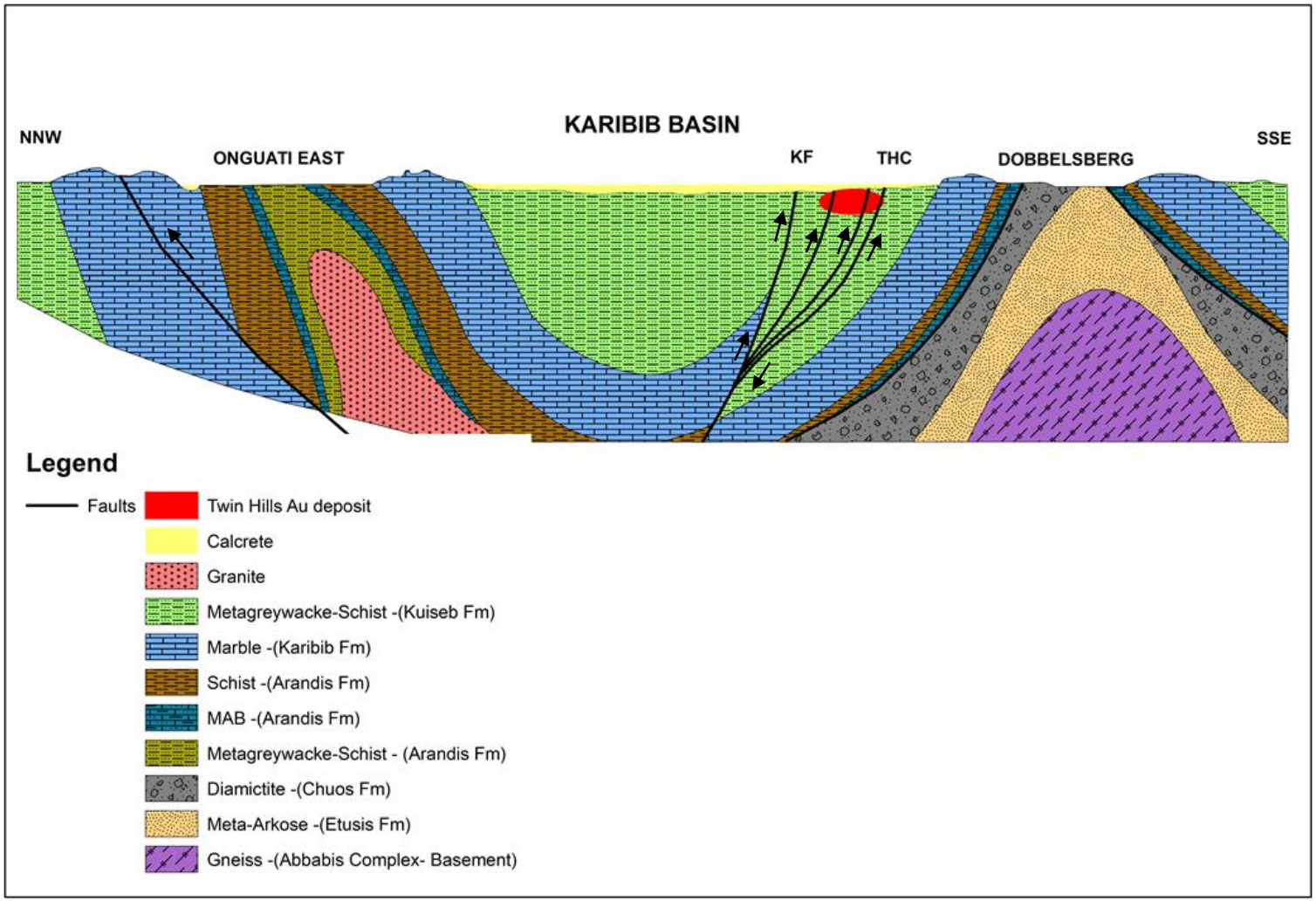

Figure 58 Generalized post-orogenic cross section across the Karibib basin. The Karibib syncline is cored by the metagreywacke and schists of the Kuiseb Formation. The Karibib Fault (KF) and splays from the KF with Twin hills deposit located within the splays from the Karibib fault (Modified after Osino Resources, 2021)

The presence of pyrite in these veins could potentially mean that these veins formed post-peak metamorphism. This is when temperatures were cooler and were in the stability field of pyrite (below 400°C). The metamorphic fluids remobilized some of the earlier formed gold, arsenopyrite, and pyrite to form quartz-arsenopyrite-pyrite-pyrrhotite veins with much coarser euhedral arsenopyrite (Asp_2) with gold (Au_2) inclusions. Indications of post-peak gold mineralization have been identified at the Navachab gold deposit, where the timing of the gold mineralization is interpreted as being slightly retrograde, amphibolite to greenschist facies conditions (500-550°C, ~ 2 kbar) (Wulff, 2008).

5.5 Gold Deportment

5.5.1 Gold grains disseminated within the groundmass of the metagreywacke

This study has arbitrarily classified the grains of the gold as follows: coarse-grained (> 50µm), medium-grained (5 – 50µm), and fine-grained (<5µm). The grain sizes of the gold grains mapped in the groundmass range from medium-grained (5 – 50µm) to very coarse-grained (up to 2mm in drill core as visible gold).

Most of the gold grains occur as free gold and are attached to arsenopyrite crystals but not included within the arsenopyrite crystals. The free gold grains will therefore be characterized by liberation and free surface area values of 100%. The gold grains partially attached to arsenopyrite will be described by liberation and free surface area values of > 70%.

5.5.2 Gold grains disseminated within biotite selvages associated with quartz veinlets.

The gold grains within biotite selvages to quartz veinlets were only identified via automated scanning electron microscopy. These gold grains were identified in three of the six thin sections. The size of the gold grains in the biotite selvages ranges from fine-grained (<5µm) to medium-

grained (5 – 50µm). Most of these gold grains occur as free gold, while a few grains were identified to be partially attached to arsenopyrite and less frequently, pyrrhotite crystals. The free gold grains can be described with liberation and free surface area values of 100%. The gold grains attached to the sulphides can be characterized by average liberation and free surface area values of > 70%.

5.5.3 Gold grains included within arsenopyrite crystals

The gold grains included within arsenopyrite crystals were identified in reflected light microscopy and automated scanning electron microscopy. The gold grains were identified in two polished thin sections produced from two boreholes. These included polished thin section JS07 from borehole OKD142 and thin section JS13 from borehole OKD211. The boreholes mentioned above were drilled at the Clouds section of the Twin Hills Deposit. The sizes of the gold grains included within the arsenopyrite crystals range from fine-grained (<5µm) to medium-grained (5 – 50µm). These gold grains can be described in terms of an average liberation values of 25% and free surface area of 0%.

Osino Resources Corp. have reported slightly lower recoveries from the Clouds section of the Twin Hills Deposit (88% as opposed to the >91% recovery in other sections of the Twin Hills Deposit) in the pre-feasibility studies (Osino Resources, 2022). The inclusion of gold grains within arsenopyrite crystals could explain the lower recoveries from the Clouds section.

According to (Mitchell et al., 1997), gold grains that are <50 µm can only be effectively recovered by chemical methods. This means that all the coarse-grained gold (>50µm) will be easily recovered via gravity separation methods, while the medium and fine-grained (<50 µm) gold grains can be recovered by the cyanide leach process.

5.6 Implications for Exploration

The Kuiseb Formation metasediments in the Damara Belt have been significantly under-explored for sediment-hosted gold deposits. This is despite the intermittent small scale exploitation of the Ondundu gold deposit for over a century which is also located within the Kuiseb Formation meta-turbidites. The discovery of the Twin Hills Gold Deposit in 2019 by Osino Resources Corp has highlighted the fertility of the Kuiseb Formation metasediments. The recent discovery of significant gold mineralization at Kokoseb by Wia Gold Limited in 2022 has further highlighted the fertility of the Kuiseb Formation.

The outcomes of this research reiterate the importance of the Kuiseb Formation meta-turbidites as a significant fertile source for gold and mineralizing fluids in sediment-hosted gold deposits. A sediment-hosted gold deposit model should be adopted in conjunction with a mineral systems approach. This approach will narrow the targeting vectors of exploration programs and highlight the pathways and traps of the mineralizing fluids (Wyborn, et al., 1994; Lewis & Downes, 2008; McCuaig, et al., 2010). Pathways for the mineralized fluids will include basin margins, faults, shear zones and major lineaments. The traps will include jogs/bends in stratigraphy, splays from faults and fold closures (Figure 59).

A sediment-hosted gold deposit model and mineral systems approach should also be applied to other meta-sediment hosting stratigraphic sequences within the Damara Belt such as the Arandis Formation in the Central Zone and its equivalent, Okonguarri Formation in the Northen Zone. These stratigraphic horizons have proven gold fertility as they host the only two currently producing gold mines in Namibia. The Arandis Formation hosts the Navachab gold mine whilst the Okonguarri Formation hosts the Otjikoto gold mine.

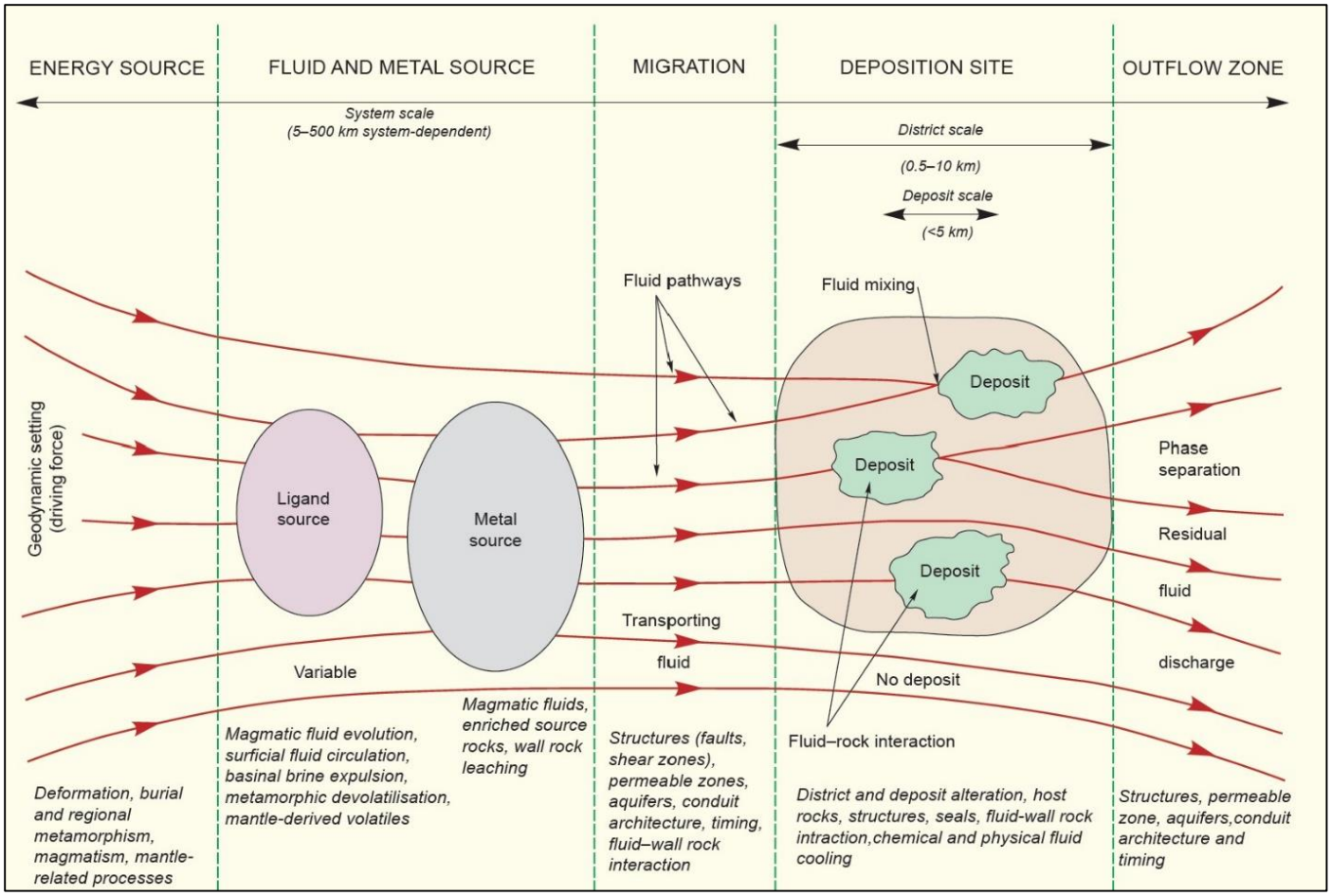

Figure 59 The mineral system concept of hydrothermal orebody formation (Lewis & Downes, 2008).

Chapter 6

Conclusions

This study aimed to understand the petrography of the host rocks, the formation of the ore minerals and carry out a comprehensive gold deportment study of the Twin Hills gold mineralization. These findings were then used to adopt a genetic model that best describes the genesis of the Twin Hills Gold Deposit. This study achieved its aims by a combining data acquired through drill core description, transmitted and reflected light microscopy, scanning electron microscopy (SEM) based TIMA analysis and correlation with existing literature.

Mineralogical studies revealed the classic turbiditic nature of the host rocks characterized by graded bedding with gradations ranging from pelitic, mica-rich interbeds to psammitic, quartz-rich interbeds of the metagreywacke. TIMA analysis showed the significant concentration of feldspar minerals, namely plagioclase and orthoclase (~50%) within the metagreywacke unit. Additional rock forming minerals include quartz, biotite, muscovite and cordierite. It is on this basis that the wall rocks are classified as metagreywacke.

Cordierite as the low-pressure, high alumina equivalent of staurolite has been used as the index mineral to determine the metamorphic grade at Twin Hills. The metamorphic grade of the Twin Hills area was consequently determined to be low to middle amphibolite facies. This is in agreement with other metamorphic grade studies the vicinity of Twin Hills.

The widespread occurrence of arsenopyrite and association with significant gold concentrations within the metagreywacke, suggests that arsenian pyrite was the precursor to the arsenopyrite prior to orogenesis. It is proposed that the low to middle amphibolite facies metamorphism caused the

prevalence of pyrrhotite over pyrite in the groundmass of the host rocks. Most of the pyrite was converted to pyrrhotite at circa 400ºC during prograde metamorphism.

This research proposes at least three stages of mineralization within the Twin Hills Gold Deposit. The first stage is the diagenetic stage, which involved the enrichment of the diagenetic arsenian pyrite (Py_0) in the turbiditic sediments with gold and other trace elements via the exhalation of reduced, deep-seated Au-As enriched H_2S-rich basinal brines onto the sea floor. The second stage is the pre-quartz veining stage during prograde metamorphism and deformation. During this stage, the arsenian pyrite (Py_0) recrystallized to pyrrhotite (Po_1), and the trace elements that were initially locked up within the pyrite crystal lattice, including arsenic and gold, were expelled into the metamorphic fluids. Free gold (Au_1) precipitated from the gold bearing metamorphic fluids via phase separation in areas where a drop in fluid pressure occurred. This resulted in the formation and concentration of disseminated gold to economic grades.

The third stage is the quartz veining stage, which was characterized by increased permeability and advanced fluid flow due to progressive metamorphism and deformation. This stage was responsible for the remobilization of fine gold grains (Au_1) that were disseminated within the groundmass of the metagreywacke and concentrating them into the biotite selvages. Gold grains included within coarse arsenopyrite crystals (Asp_2) as fine gold grains (Au_2) in the quartz veinlets could have been as a result of the exsolution of gold from the arsenopyrite crystal lattice. The metamorphic fluid crystallized to form quartz veins. Pyrite (Py_2) co-exists with pyrrhotite (Po_2) in these quartz veins which probably means that these quartz veins formed post-peak metamorphism. This is supported by textural evidence of these veins cross cutting the dominant foliation. This stage can be classified as a remobilization event, which led to further upgrading of the gold grades to economic levels.

The last stage is a calcite veining stage, which the study proposes to be a much later, post-deformation event characterized by calcite veins with pyrite. This stage is not associated with gold mineralization.

The gold deportment study has classified three main modes of occurrences of gold within the Twin Hills Deposit. The first occurrence is characterized by gold grains disseminated within the groundmass of the metagreywacke. The other modes of occurrence of gold include gold grains disseminated within biotite selvages associated with quartz veinlets and gold grains included within arsenopyrite crystals. Coarse-grained gold (> 50µm) includes most of the gold grains disseminated within the groundmass, such as the free visible gold grains (up to 2mm in drill core) and most of the gold grains that are attached to arsenopyrite crystals.

The medium-grained (5 – 50µm) gold includes all the grains in the groundmass associated with arsenopyrite crystals. A small amount of the fine(<5µm) gold grains are included within arsenopyrite crystals. The gold grains included within arsenopyrite crystals could explain the slightly lower recoveries reported from the Clouds section of the Twin Hills Gold Deposit.

A two stage gold recovery procedure in the form of a gravity separation method followed by a cyanide leach process will be ideal to ensure optimum gold recovery. All the coarse-grained gold (>50µm) will be recovered via gravity separation methods, while the medium and fine-grained (<50 µm) gold grains can be recovered by the cyanide leach process.

6.1 Limitations of the Study

This study could not incorporate a geochemistry component due to constraints on time. The study would have benefited from a Laser Ablation Inductively Coupled Plasma Mass Spectrometry (LA-ICPMS) analysis or Electron Microprobe Analysis (EPMA) on the sulphide minerals to determine the minor and trace element concentration in the different generations of the sulphides. This could aid the definition of the geochemical evolution of the sulphide minerals and the mineral paragenesis by grouping different generations of sulphides based on minor and trace element patterns.

The study could not identify diagenetic pyrite within the host rock and has attributed its absence to the high metamorphic grade (low to mid amphibolite facies). LA-ICPMS analysis on diagenetic pyrite would confirm whether there was enrichment of gold within the diagenetic pyrite.

The number of polished thin section samples selected for TIMA analysis were limited to six samples due to budget constraints. Consequently, the gold deportment results should be used as a guide only at this stage.

The time spent on the TIMA processing computer was also limited. Detailed information such as mineral locking data, number of gold grains in the slide and geochemistry data could not be obtained.

6.2 Recommendations for Future Work

Further work is recommended:

a) A detailed geochemistry study of the Twin Hills Deposit which should include LA-ICPMS analysis and/or EPMA study on the sulphide minerals. This will determine the minor and trace element concentration in the different generations of the sulphides.
b) A stable isotope and fluid inclusion study to better constrain the genetic model of the Twin Hills Gold Deposit.
c) A follow up petrographic analysis aimed at identifying the diagenetic pyrite within the host rocks.
d) A follow up gold deportment study using high resolution TIMA analysis or QEMSCAN on a large number of samples that are representative of the deposit.
e) Thermodynamic modelling to better constrain the pressure and temperature conditions and the metamorphic grade in the Twin Hills Deposit.

References

Brandt, R. (1985). Preliminary report on the stratigraphy of the Damara sequence and the geology and geochemistry of the Damaran granites in the area between Walvisbay and Karibib. Communs Geol. Surv. S.W. Afr./Namibia, 1, 31-44.

Bucher, K., & Grapes, R. (2011). Petrogenesis of Metamorphic Rocks. Springer-Verlag Berlin Heidelberg.

Coetzee, L. L., Theron, S. J., Martin, G. J., Van der Merwe, J. D., & Stanek, T. A. (2011). Modern gold deportment and its application to industry. SGS Mineral services- Technical Paper.

Creus, P. K. (2011). Geology and structural controls of lode-gold mineralization around the Navachab Gold Mine in the Pan-African Damara Belt of Namibia. MSc thesis. University of Stellenbosch. pp162

Cropp, A. (2013). Liberation and Free Surface Area in the Float Feed-MinAssist. Retrieved from MinAssist:https://minassist.com.au/liberation-and-free-surface-area-in-the-float-feed/

Finch, E. G., & Tomkins, A. G. (2017). Pyrite-Pyrrhotite Stability in a Metamorphic Aureole: Implications for Orogenic Gold Genesis. Economic Geology, v. 112, 661–674.

Geldenhuys, A., & Hetherington, G. (2021). Twin Hills Gold Project, Namibia NI 43-101 Technical Report. CSA Global.

Gloyn-Jones, J. (2018). Structural controls of auriferous reefs at Fairview Mine, Barberton. MSc thesis. University of Stellenbosch. pp123

Goldfarb, R. J., & Groves, D. I. (2015). Orogenic gold: Common or evolving fluid and metal sources through time. Lithos, 2–26.

Goldfarb, R. J., Groves, D. I., & Gardoll, S. (2001). Orogenic gold and geologic time: A global synthesis. Ore Geology Reviews 18, 1–75.

Goldfarb, R. J., Phillips, G. N., & Nokleberg, W. J. (1998). Tectonic setting of synorogenic gold deposits of the Pacific Rim. Ore Geology Reviews 13, 185–218.

Gray, D. R., Foster, D. A., Goscombe, B., Passchier, C. W., & Trouw, R. A. (2006). 40Ar-39Ar thermochronology of the Pan-African Damara Orogen, Namibia, with implications for tectonothermal and geodynamic evolution. . Precambrian research, 150, 49-72.

Gray, D. R., Foster, D. A., Meert, J. G., Goscombe, B. D., Armstrong, R., Trouw, R. A., & Passchier, C. W. (2007). A Damara Orogen perspective on the assembly of southwestern Gondwana.

Groves, D. I., Goldfarb, R. J., Gebre-Mariam, M., Hagemann, S. G., & Robert, F. (1998). Orogenic gold deposits: A proposed classification in the context of their crustal distribution and relationship to other gold deposit types. Ore Geology Reviews, 7–27.

Jacob, R. E., Kroner, A., & Burger, A. J. (1978). Areal extent and first U-Pb age of the pre-Damaran Abbabis complex in the central Damara belt of South West Africa. . Geologische Rundschau, 67(2) , 706-718.

Kasch, K. W. (1983). Continental collision, suture progradation and thermal relaxation: A plate tectonic model for the Damara Orogen in central Namibia. Geol. Soc. S. Afr. Special Publication, vol.11, 423-429.

Kisters, A. (2005). Controls of gold-quartz vein formation during regional folding in amphibolite-facies, marble-dominated metasediments of the Navachab Gold Mine in the Pan-African Damara Belt, Namibia. South African Journal of Geology. Volume 108, 365-380.

Kribek, B. (1991). Metallogeny, structural, lithological and time controls of ore deposition in anoxic environments. Mineralium Deposita, v. 26, 122–131.

Large, R. R., Bull, S. W., & Maslennikov, V. V. (2011). A Carbonaceous Sedimentary Source-Rock Model for Carlin-Type and Orogenic Gold Deposits. Economic Geology, v. 106, 331–358.

Large, R. R., Maslennikov, V. V., & Robbert, F. (2007). Multistage Sedimentary and metamorphic origin of pyrite and gold in the Giant Sukhoi Log Deposit, Lena Gold province, Russia. Economic Geology v.102, 1233 - 1267.

Lewis, P., & Downes, P. M. (2008). Mineral Systems and Processes in New South Wales: a project to enhance understanding and assist exploration. Quarterly Notes, Geological Survey of New South Wales.

Li, N., Deng, J., Yang, L.-Q., Goldfarb, R. J., Zhang, C., Marsh, E., . . . Lowers, H. (2014). Paragenesis and geochemistry of ore minerals in the epizonal gold deposits of the Yangshan gold belt, West Qinling, China. Mineral Deposita, 427 - 449.

Mapani, B. S. (2011). Introductory notes in metamorphic petrology. University of Namibia.

McCuaig, C. T., Beresford, S., & Hronsky, J. (2010). Translating the mineral systems approach into an effective exploration targeting system. Ore Geology Reviews 38, 128-138.

Miller, R. M. (1983). The Pan-African Damara orogen of South West Africa/Namibia. Geol. Soc. S. Afr. Special Publication, vol.11, 431-515.

Miller, R. M. (2008). The Geology of Namibia, Vol 2. Neoproteroiz to Lower Paleozoic. Minestry of Mines and Energy, Geological Survey.

Mitchell, C. D., Evans, E. J., & Styles, M. T. (1997). A review of gold particle-size and recovery methods. BGS Technical Report WC/97/14.

Oliver, G. J. (1995). The Central Zone of the Damara Orogen, Namibia, as a deep metamorphic core complex. Communs geol. Surv. Namibia, 10,, 33-42.

Oliver, J. L. (2014). NI 43 – 101 Technical Report on the Gold Kop - Damara Gold Project Central.

Osino Resources Corp. (2021) Twin Hills Gold Project, Namibia. Preliminary Economic Assessment. National Instrument 43-101 Technical Report.

Osino Resources Corp. (2022) Osino Announces Pre-feasibility Study Results for the Twin Hills Gold Project, Namibia. Press Release.

Osino Resources Corp. (2022) Namibia’s Next Gold Mining Champion. Corporate Presentation.

Petzel, V. F. (1988). Progress Report on Geological Exploration Conducted on The Farms Spes Bona 105 and Daheim 106 Grant M46/3/1631.

Pitcairn, I. K., Olivo, G. R., Teagle, D. A., & Craw, D. (2010). Sulphide evolution during prograge metamorphism of the Otago and Alpine schists, New Zealand. The Canadian Mineralogist. Vol 48, , 1267 - 1295.

Puhan, D. (1983). Temperature and pressure of metamorphism in the central Damara orogen. . Geol. Soc. S. Afr. Special Publ. 11.

Shilunga, J., & Kisters, A. (2022 In Press) Lithological and structural controls of disseminated-type orogenic gold mineralization in high-grade metamorphic turbidites from the Central Zone of the Damara Belt, Namibia. Ore Geology Reviews.

Steven, N. M. (1993). A study of epigenetic mineralisation in the Central Zone of the Damara Orogen, Namibia, with special reference to gold, tungsten, tin and rare earth elements. PhD Thesis, University of Cape Town pp221.

Underwood, D. (2020). Technical Report for the Karibib Gold Project in Namibia, Update of Exploration Activities.

Vollgger, S. A., Cruden, A. R., Ailleres, L., & Cowan, E. J. (2015). Regional dome evolution and its control on ore-grade distribution: Insights from 3D implicit modelling of the Navachab gold deposit, Namibia. Ore Geology Reviews, 268–284.

Wicker, V. (2019). Twin Hills East metaturbidite hosted gold mineralisation, Damara Belt, Southern Central Zone – Namibia: New constraints from structural, mineralogical and geophysical investigations. MSc. Thesis. Camborne School of Mines, UK. pp92.

Winter, J. D. (2001). An introduction to Igneous and Metamotphic Petrology. Prentice Hall.

Winter, J. D. (2013). Principles of Igneous and Metamorphic Petrology. Prentice Hall.

Wood, B. L., & Large, R. R. (2007). Syngenetic gold in western Victoria: occurrence, age and dimensions. Australian Journal of Earth Science, 54, 711-732.

Wulff, K. (2008). Petrography, geochemistry and stable isotope characteristics of the Navachab gold deposit, Namibia. PhD thesis, RWTH Aachen. pp205

Wulff, K., Dziggel, A., Kolb, J., Vennemann, T., Böttcher, M. E., & Meyer, M. F. (2010). Origin of Mineralizing Fluids of the Sediment-Hosted Navachab Gold Mine, Namibia:

Constraints from Stable (O, H, C, S) Isotopes. Society of Economic Geologists, Inc. Economic Geology, v. 105, 285–302.

Wyborn, L. A., Heirich, A. C., & Jaques, A. L. (1994). Australian Proterozoic Mineral Systems: Essential Ingredients and Mappable Criteria. Astralian Institute of Mining and Metallurgy Annual Conference, Melbourne, Proceedings, 109-115.

Zhong, R., Brugger, J., Tomkins, A. G., Chen, Y., & Li, W. (2015). Fate of gold and base metals during metamorphic devolatilization of a pelite. Geochimica et Cosmochimica Acta 171, 338–352.

Appendices

Appendix A– Abbreviations

Asp- Arsenopyrite

Po- Pyrrhotite

Py- Pyrite

Lo- Lollingite

VG-Vissible gold

Hm- Hematite

Bt- Biotite

Ms- Muscovite

Qtz- Quartz

Cd- Cordierite

IMGK- Interbedded metagreywacke

MGWK- Metagreywacke (massive)

CGWK- Cordierite metagreywacke

CDSH- Cordierite schist

KFZ - Karibib fault zone

SEM - scanning electron microscopy

nCZ- Northern Central Zone

sCZ- Southern Central Zone

TIMA- TESCAN Integrated Mineral Analyzer

Appendix B– Description of drill core samples

Hole id	Sample Description	Photograph	Thin Section Photomicrograph
OKD 079	IMGK, light grey, fine grained, bedded, fine mica rich bands alternating with relatively coarser, quartz rich bands; mm scale quartz veinlets with biotite selvages highly discordant to bedding (cracked texture?; indicative of shearing ?) with po and asp vnlts; po and asp also disseminated within the groundmass; intense potassic alteration indicated by a darker brownish colouration		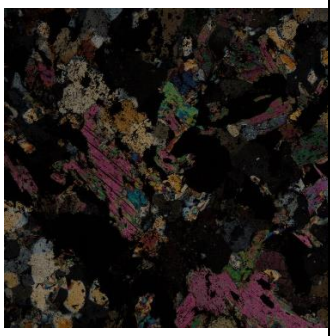
OKD 079	IMGK, light grey, fine grained, bedded, fine mica rich bands alternating with relatively coarser, quartz rich bands; strongly altered (with intesense silicification (white) and potasic alteration (brown)), minor mm scale quartz veinlets with biotite selvages highly discordant to bedding (cracked texture?; indicative of shearing ?) disseminated po within the groundmass; VG present.	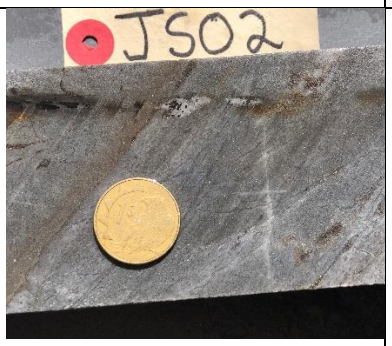	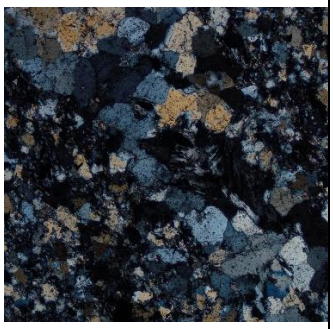
OKD 118	IMGK, light grey, fine grained, bedded, fine mica rich bands alternating with relatively coarser, quartz rich bands; strongly altered (with intesense potasic alteration (brown); crackled texture characterized by discontinous veinltes with bt selvages; po and asp veinlets		

OKD 118	MGWK, light grey, fine grained, massive, crackled texture? Characterized by discontinous bt selvage veinlets; intesne silicification; disseminated asp;		
OKD 080	MGWK, grey, fine grained, massive, sheared, crackled texture indicative of shearing characterized by discontinous, boudinaged quartz veinlets with biotite selvages; intense potassic alteration characterized by a brown coulouration and biotite selvages; very fine disseminated po and veinlets		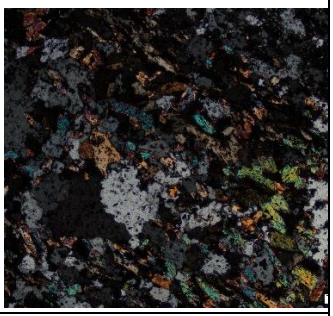
OKD 109	VNQ, white, coarse grained, in contact with MGWK, VG in VNQ in bt selvages; disseminated po, asp and minor py		
OKD 142	MGWK, grey, fine grained, massive, disseminated asp, po and minor py, minor pot alt		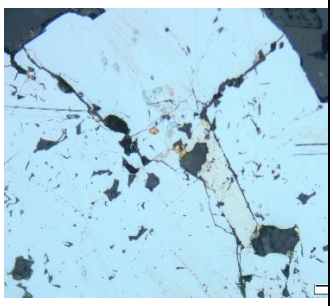
OKD 079	IMGK, grey, fine grained, bedded, boudinaged quartz vein with bt selvages, skarn alteration within the qaurtz vein, po and asp within quartz vein, po vnlts		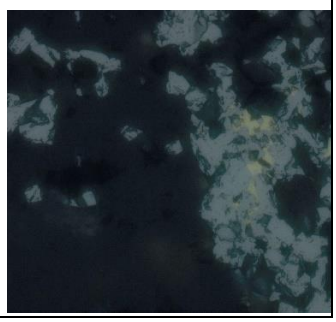

OKD 038	MGWK, grey, fine grained, massive, disseminated asp, po and minor py, pot alt and silicification, bt selvages with coarse asp , whilst very fine, acicular asp in groundmass		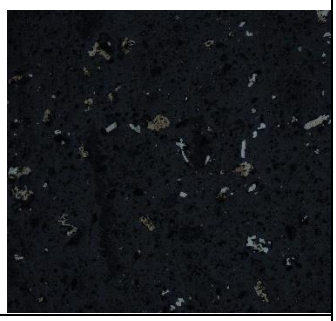
OKD 213	MGWK, light grey, fine grained, sheared, bt selvages with po and py		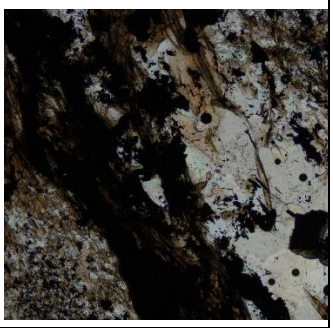
OKD 038	MGWK, light grey, fine grained, sheared, crackled texture with discontinous, boudinaged quartz veinlets with bt selvages, bt selvages with po and py		
OKD 213	IMGK, grey, fine grained, bedded, very minor pot alt, bt selvages, disseminated po		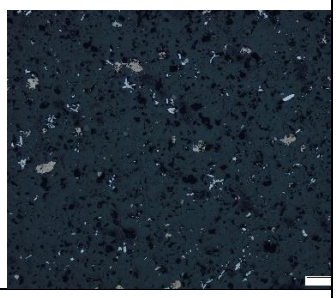
OKD 211	IMGK, brown, fine grained, intense pot alt, quart vnlts with bt selvages with asp, py and po; cracckled texure indicative of shearing?		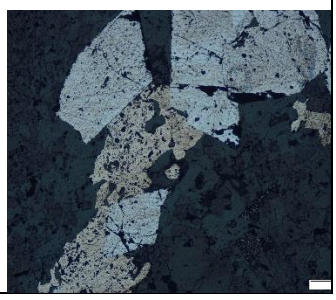

OKD 212	IMGK, brown, fine grained, strongly sheared, intense pot alt, quart vnlts with bt selvages with asp, py and po; cracckled texure indicative of shearing?, very fine grained asp, asp stringers		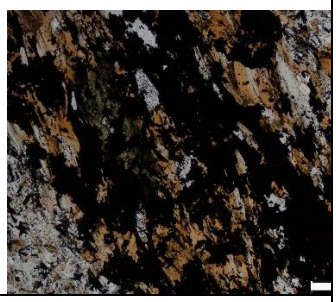
OKD 211	IMGK, brown, fine grained, strongly sheared, intense pot alt, quart vnlts with bt selvages with asp, py and po; cracckled texure indicative of shearing?, very fine grained asp, asp stringers		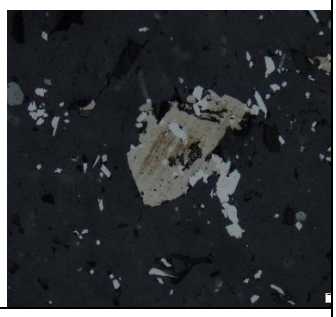
OKD 037	CDSH, grey, fine grained, finely laminated, highly schistose, quartz, biotite, no alteration, no mineralisation.		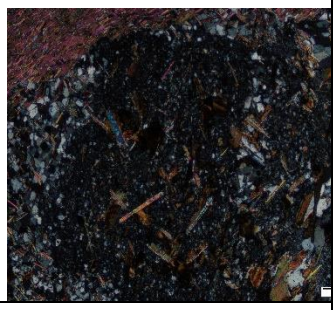
OKD 019	CGWK, grey, very fine grained, bedded, individual beds >1 cm wide, codierite porphyroblasts appear to be restricted to the darker, mica rich beds; Quartz and mica rich beds(biotite)		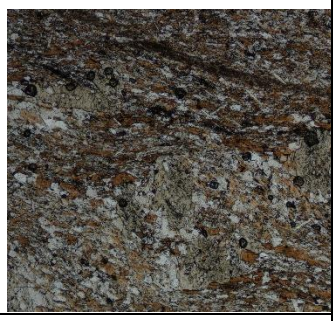
OKD 211	IMGK, grey, fine grained, beded, boudinaged quartz veins with biotite selvageswith pyrhotite, pyrite and arsenopyrite. Mineralogy includes Quartz and white micas (muscovite?)		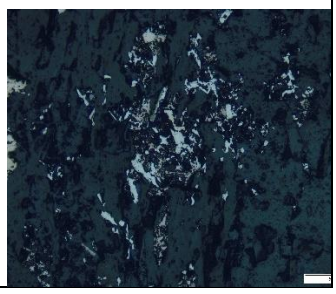

OKD 128	MGWK, grey, fine grained, massive, crackled texture characterized by quartz veinlets with biotite selvages in random directions; disseminated pyrhotite in the matrix.		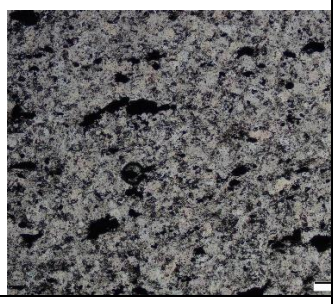
OKD 211	IMGK, grey, fine grained, bedded, light grey micas and dark grey micas (biotite?), very fine grained quartz , disseminated po in the groundmass, individual beds > 1cm .		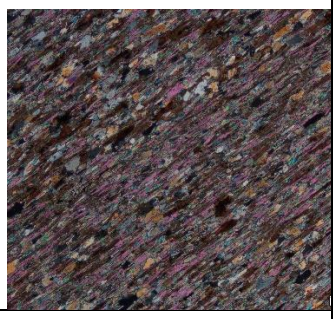
OKD 143	CSU, green, fine grained, massive, clinopyroxene (cpx) and tremolite crystalls, disseminated pryhotite.		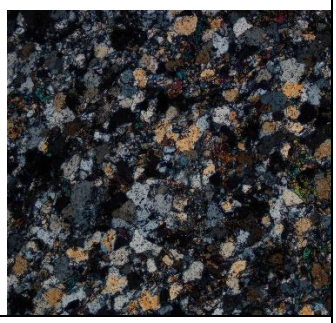
OKD 038	MGWK, brown, fine grained, massive, intense potassic alteration, biotite selvages around quartz veinlets; biotite selvages with arsenopyrite stringers+ pyrite+ disseminated pyrhotite		
OKD 038	MGWK, brown, fine grained, massive, intense potassic alteration, biotite selvages around quartz veinlets; biotite selvages with arsenopyrite stringers+ pyrite+ disseminated pyrhotite		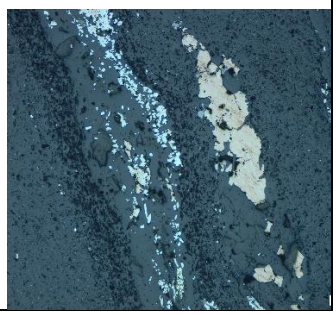

OKD 034	BISH, grey, very fine grained, laminated, highly schistose		

Appendix C– Thin section scans versus TIMA

Sample JS02- OKD079 @ 200.17 Bulge Prospect

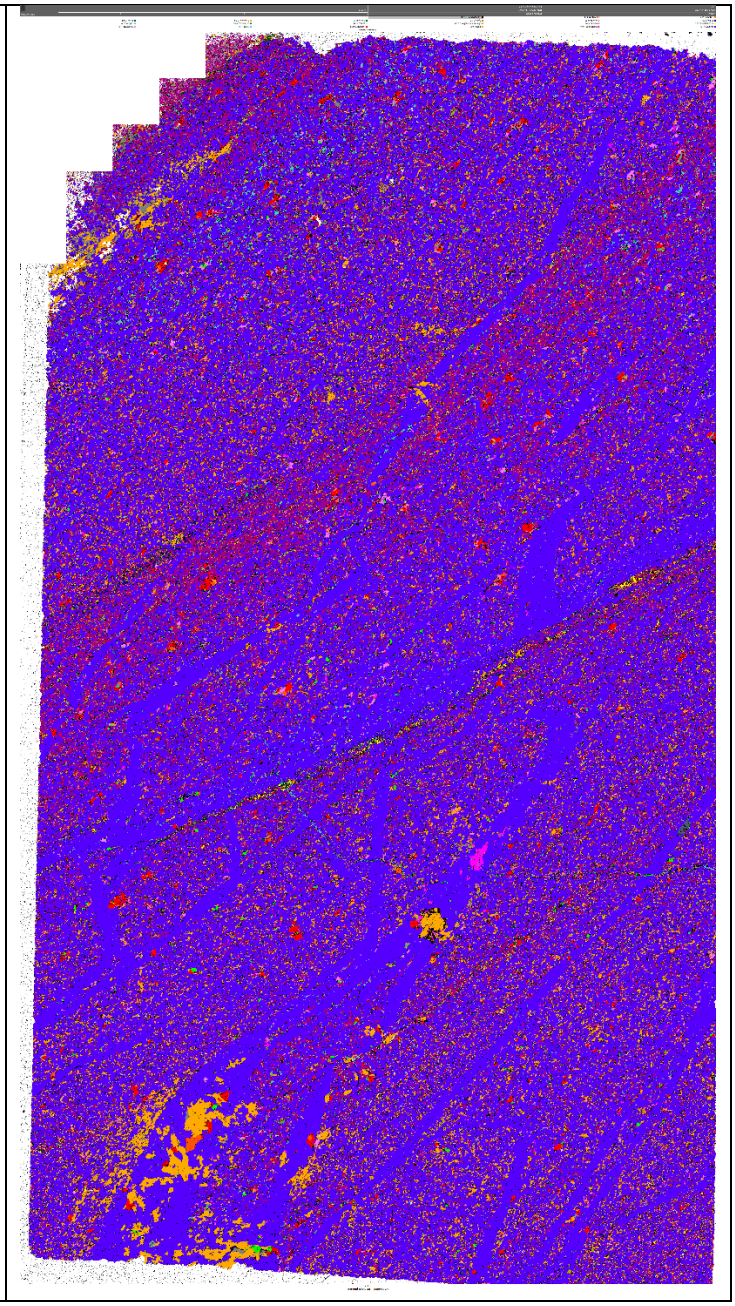

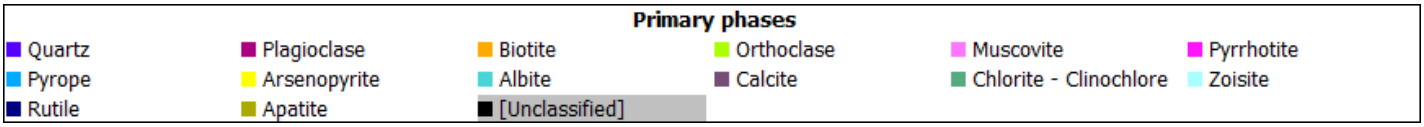

Sample JS07- OKD142 @ 218.75 Clouds Prospect

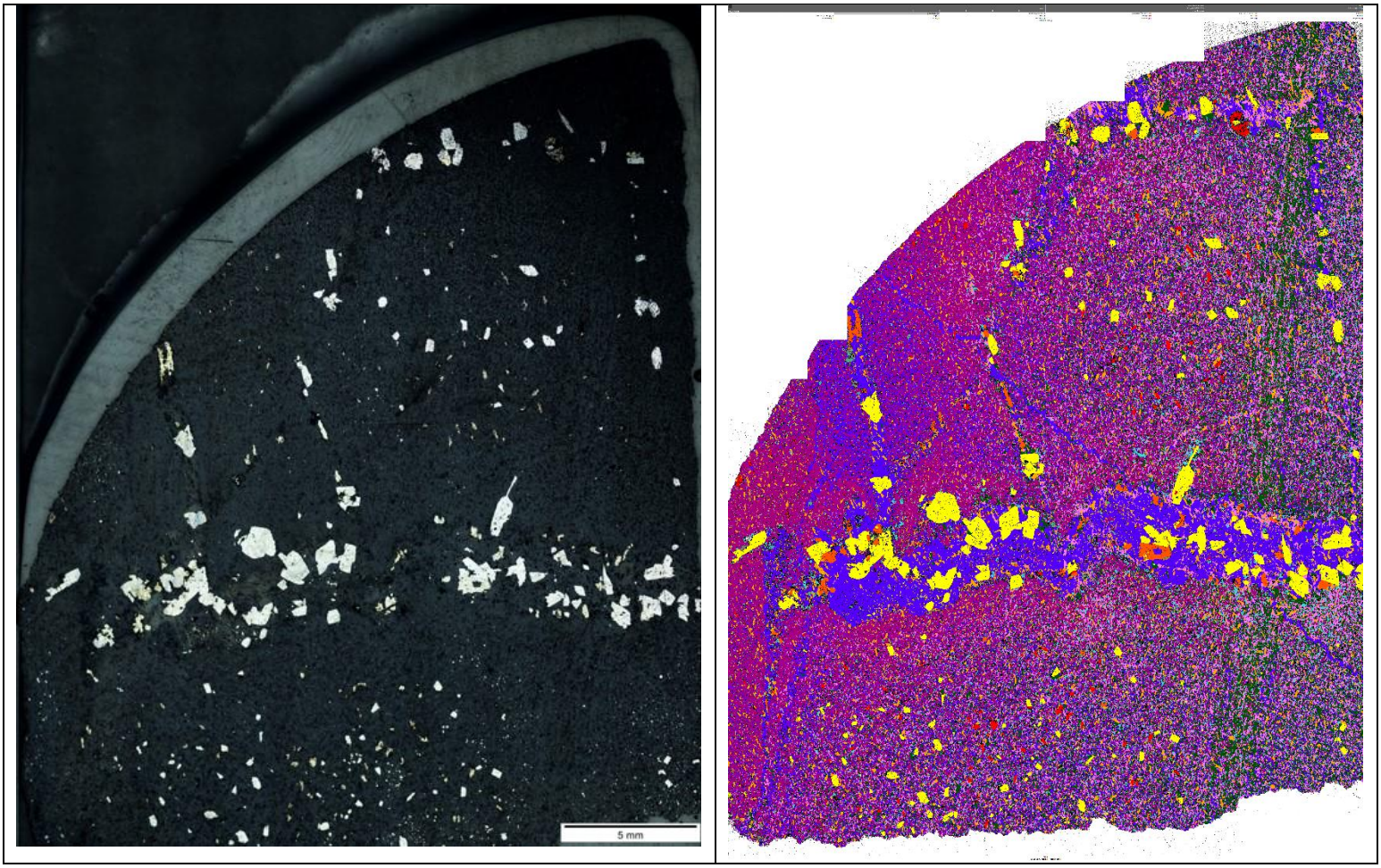

Primary phases

Plagioclase	Quartz	Muscovite	Orthoclase	Biotite	Arsenopyrite
Albite	Pyrite	Pyrrhotite	Rutile	Schorl	Chlorite - Chamosite
Apatite	Chlorite - Clinochlore	Almandine_spessartine		Hematite/Magnetite	[Unclassified]

Sample JS08- OKD079 @ 204.49 Bulge Prospect

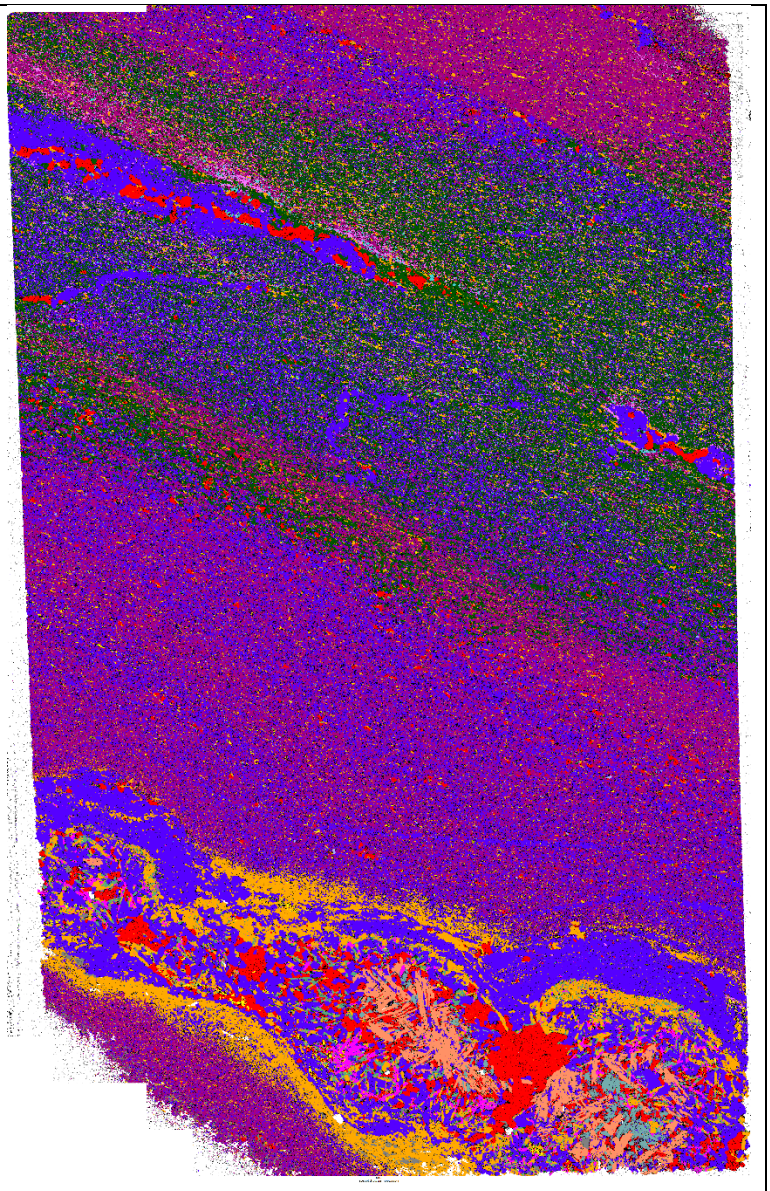

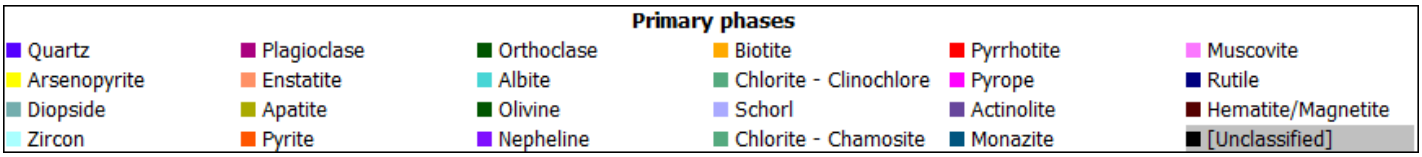

Sample JS13- OKD211 @ 111.85m Clouds East Prospect

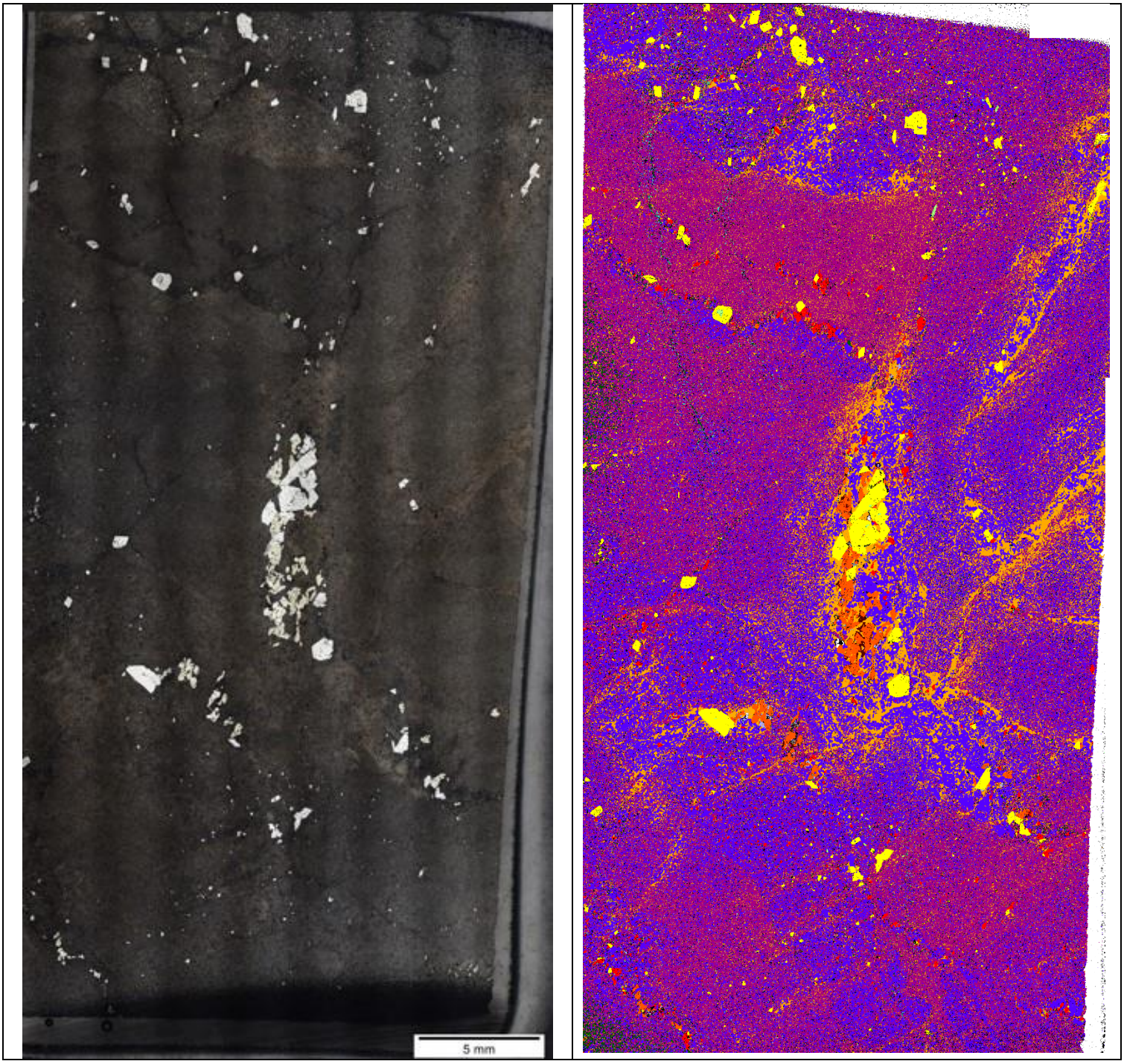

Primary phases

Plagioclase	Quartz	Biotite	Arsenopyrite	Orthoclase	Pyrrhotite
Pyrite	Albite	Rutile	Apatite	Chlorite - Clinochlore	Schorl
Muscovite	Hematite/Magnetite	Ferosaponite	Lollingite	Kaersutite	Zircon
Almandine_spessartine		Chlorite - Chamosite	Monazite	[Unclassified]	

Sample JS18- OKD211 @ 120.67 m Clouds East Prospect

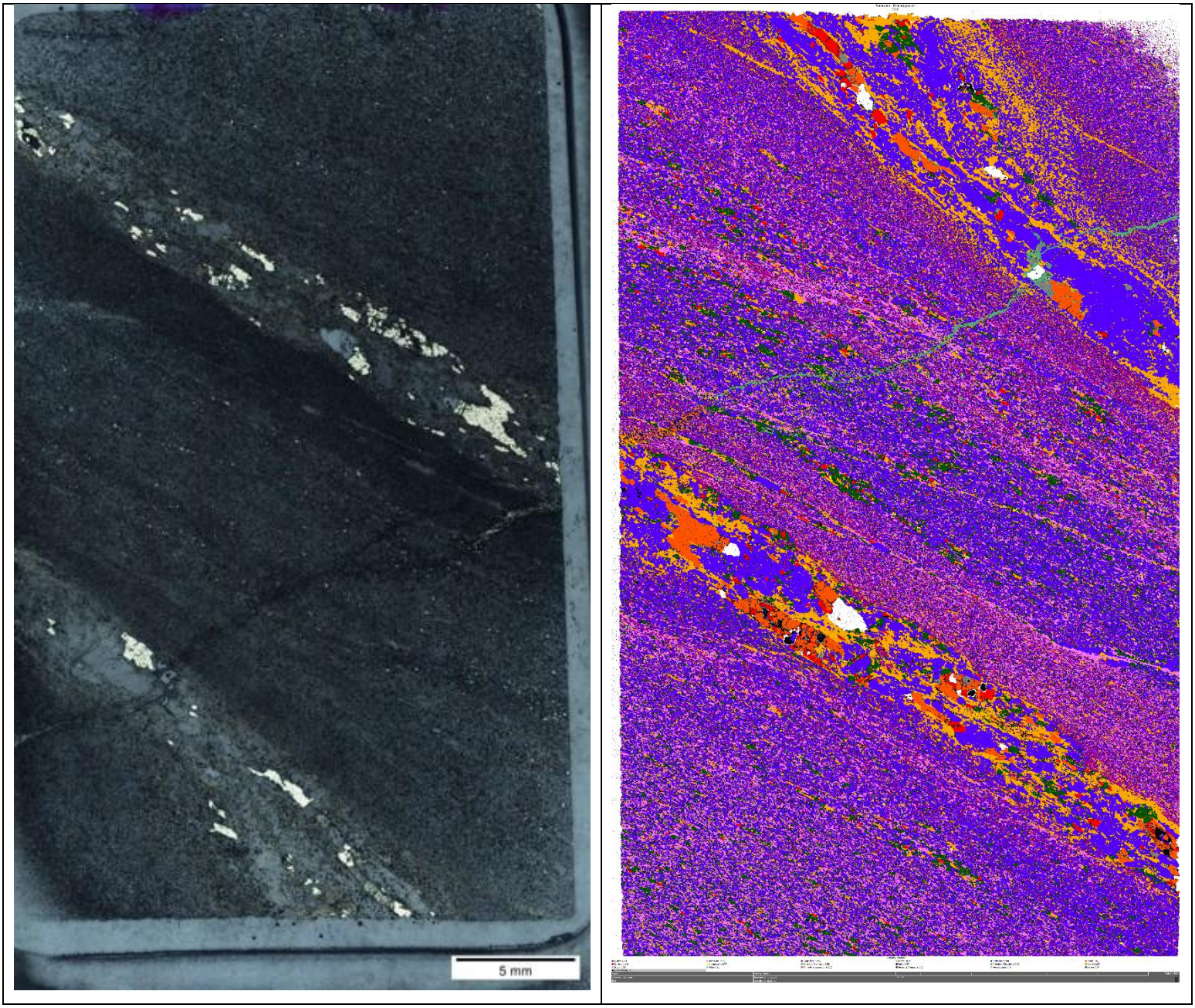

Primary phases

Quartz	Muscovite	Plagioclase	Biotite	Orthoclase	Pyrite
Pyrrhotite	Arsenopyrite	Chlorite - Chamosite	Rutile	Chlorite - Clinochlore	Apatite
Schorl	Albite	Almandine_spessartine		Hematite/Magnetite	Ferosaponite
Zircon	[Unclassified]				

Sample JS23- OKD038 @ 104.89m Bulge Prospect

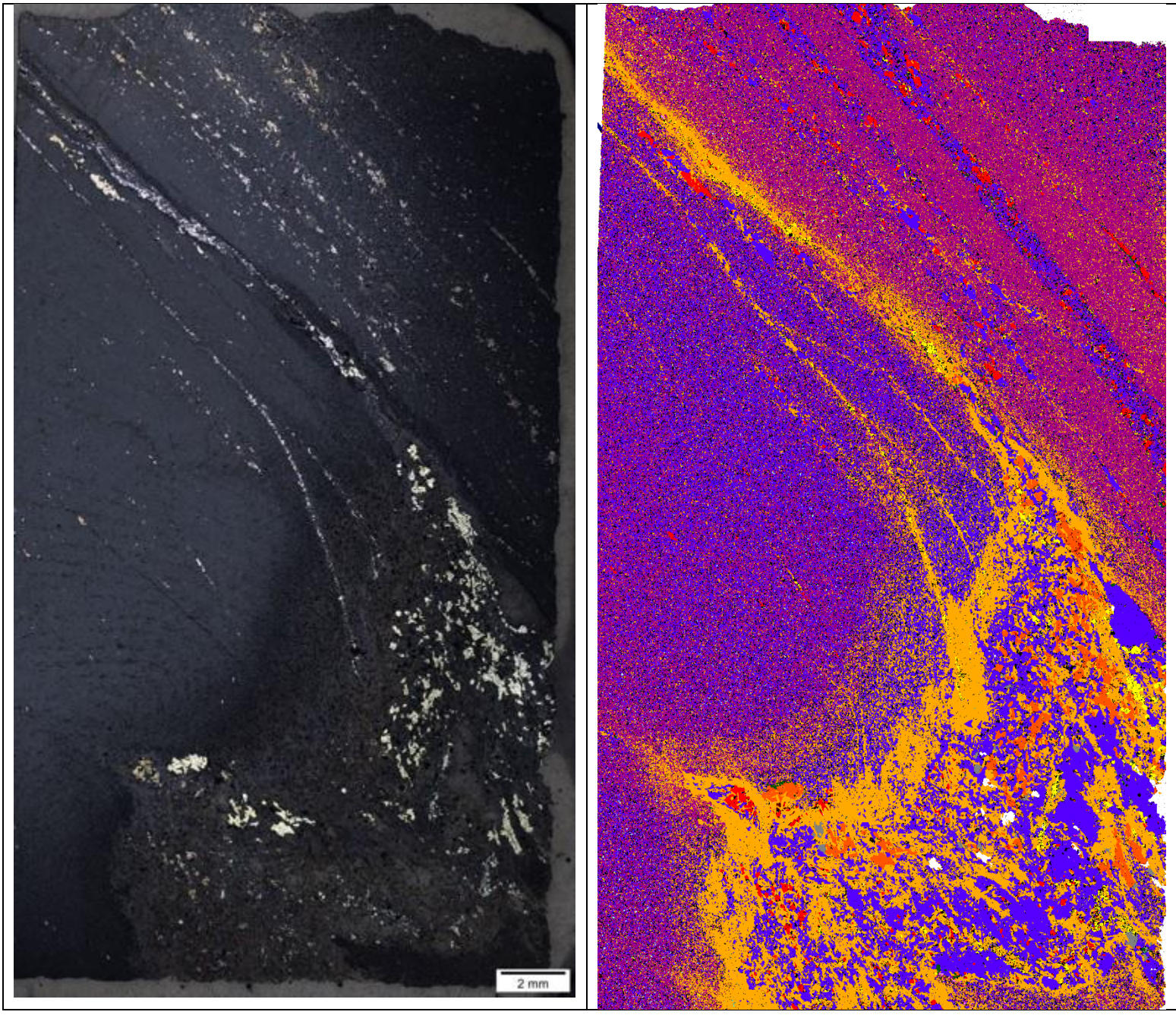

Primary phases

Plagioclase	Quartz	Biotite	Pyrite	Pyrrhotite	Arsenopyrite
Zoisite	Rutile	Orthoclase	Apatite	Muscovite	Albite
Chlorite - Clinochlore	Hematite/Magnetite	Kaersutite	Titanite	Schorl	Grossular
Kaolinite	Zircon	Allanite-(Ce)	[Unclassified]		

Appendix D– Cross sections

OKD038-Bulge prospect, thin section samples JS11 and JS22

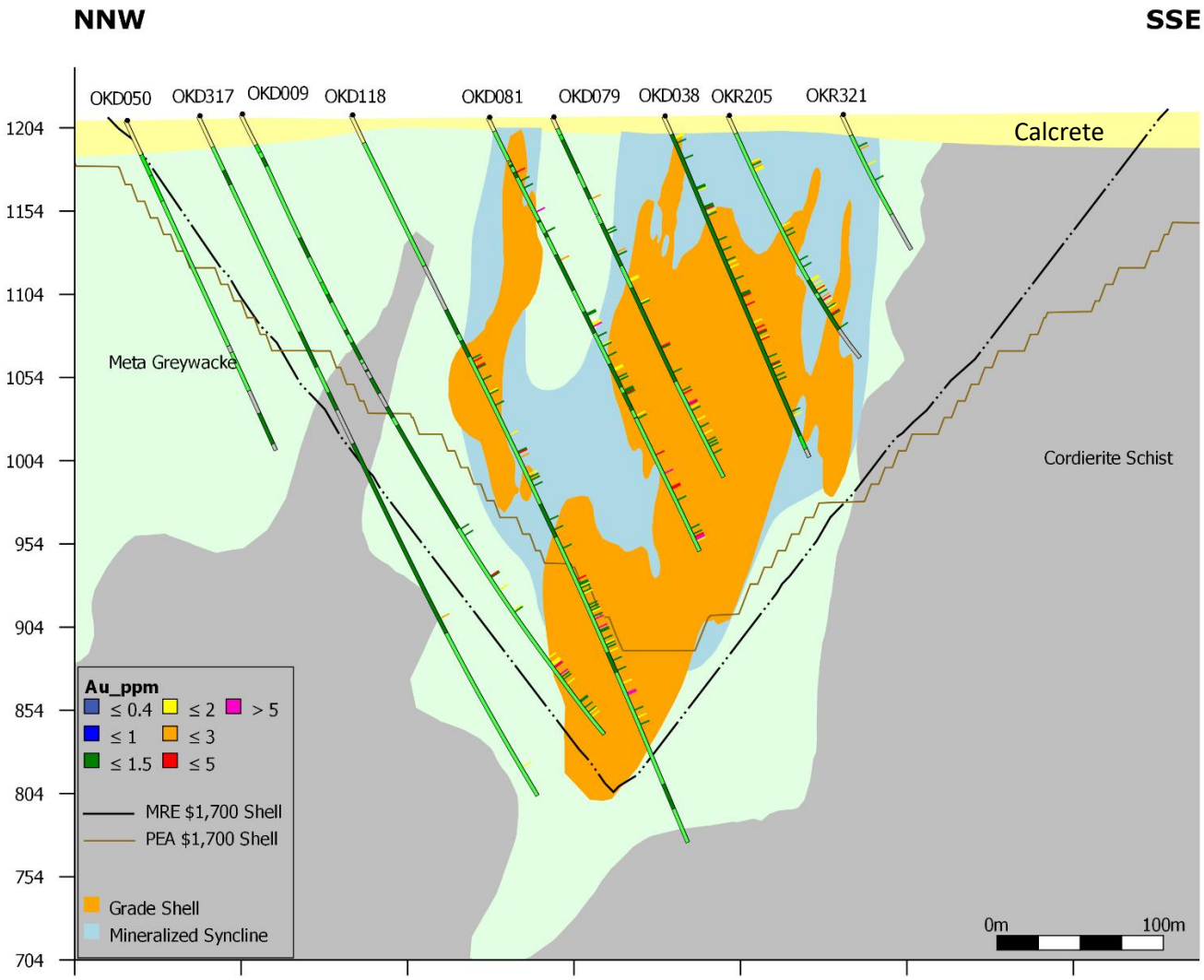

OKD109- Twin Hills Central prospect, thin section sample JS06

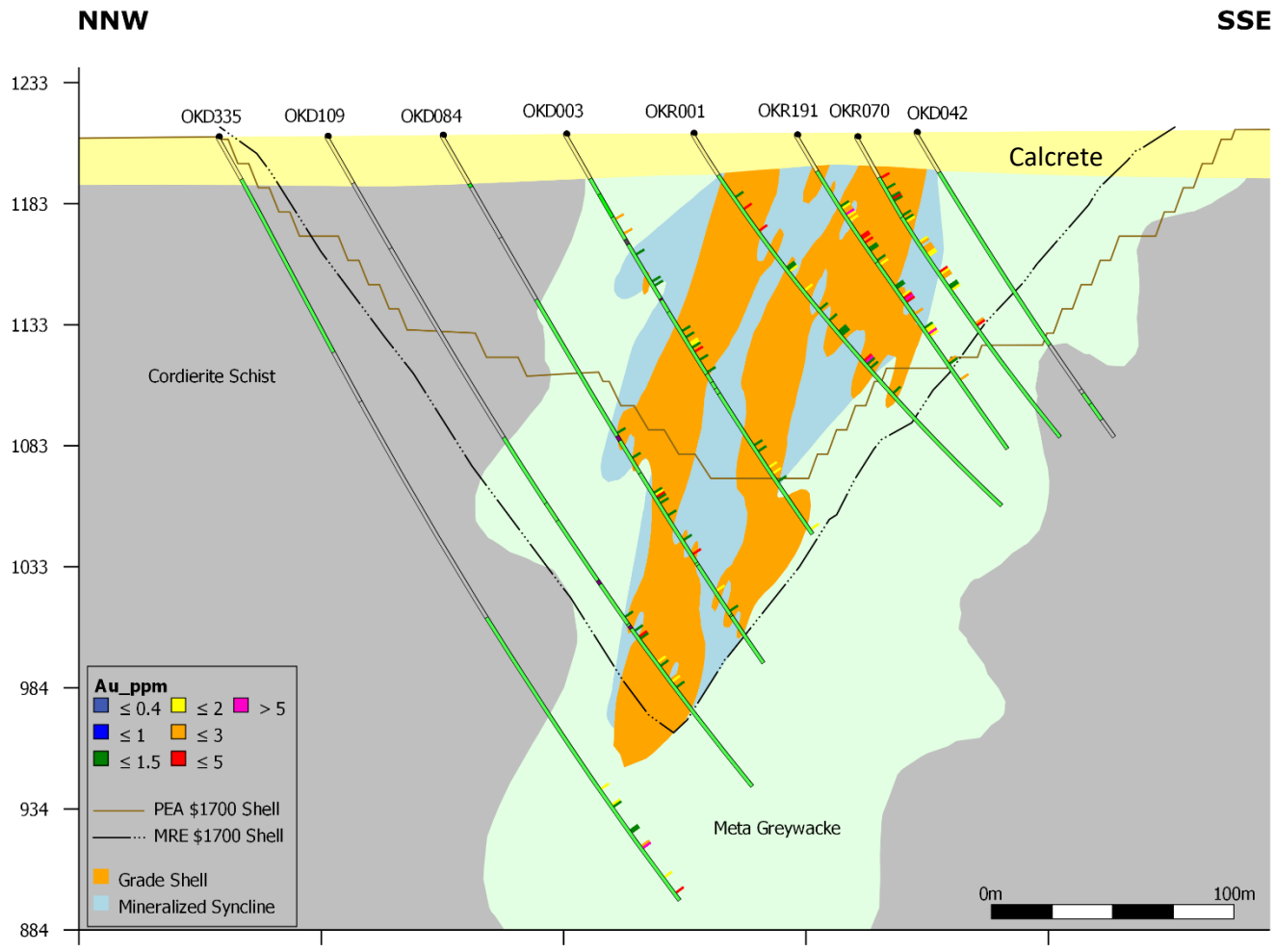

OKD128- Twin Hills Central prospect, thin section sample JS19

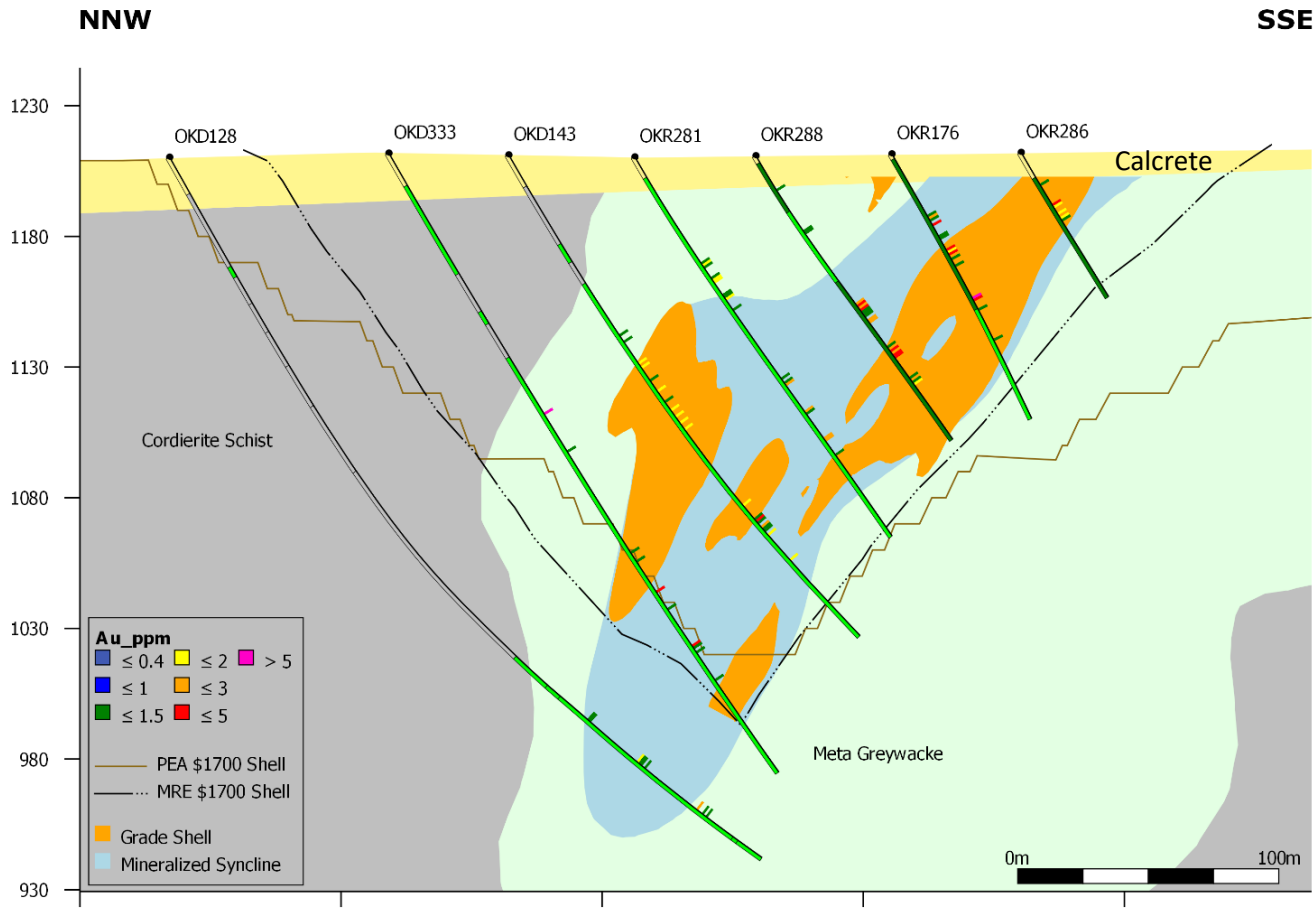

OKD212-Clouds East prospect, thin section sample JS14

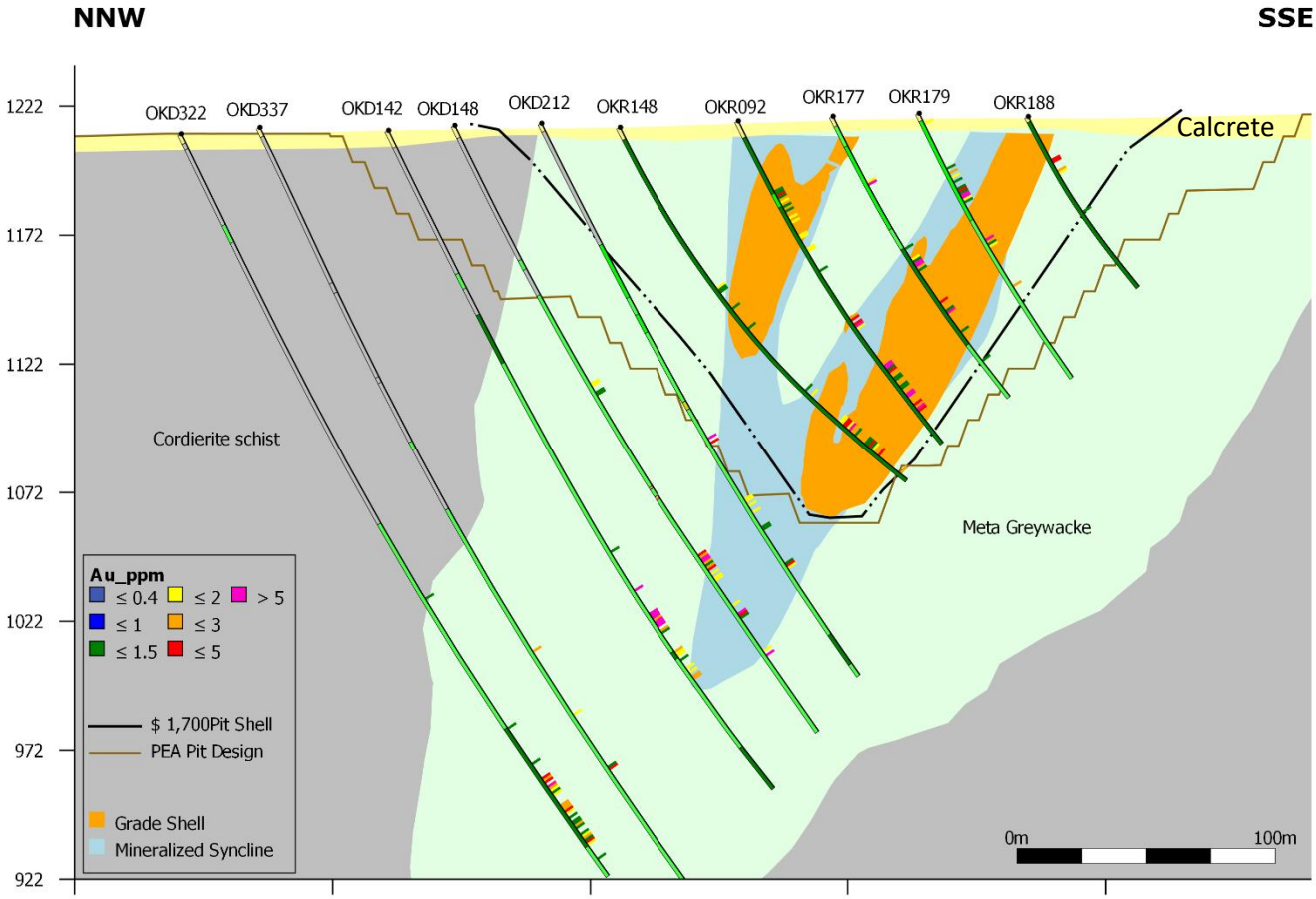

OKD213- Twin Hills Central prospect, thin section sample JS12

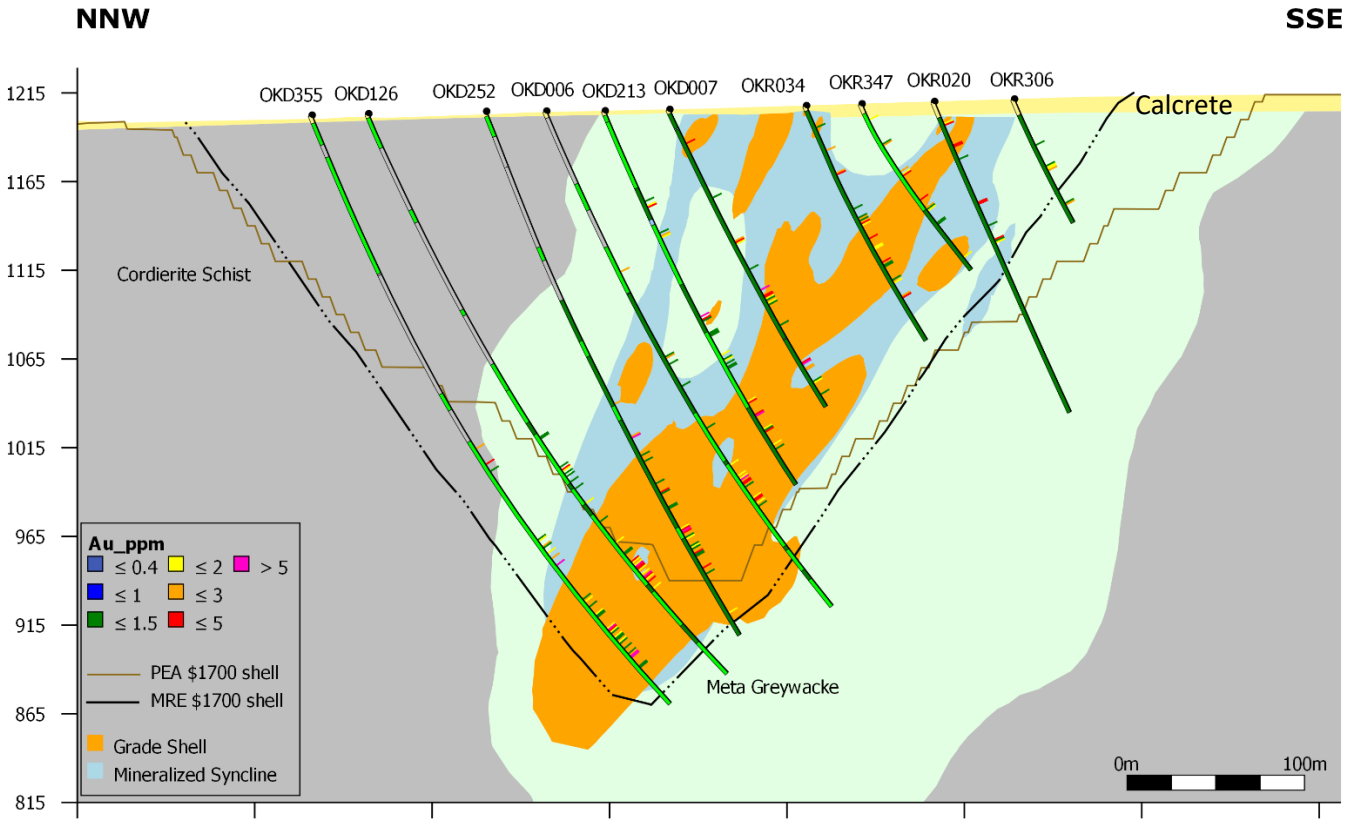

Appendix E– Borehole logs

OKD038 – Lithology

Hole_ID	Depth From (m)	Depth To (m)	Lithology	Texture	GrainSize	Oxidation	Colour	Comments
OKD038	0	12.34	Calcrete	Conglomeratic	Medium grained	Fresh	cream	QTZ GTE MGWK fragments
OKD038	12.34	20.44	Massive metagreywacke	Brecciated	Fine grained	Highly Oxidised	grey	CALC filling fractures
OKD038	20.44	26	Massive metagreywacke	Fractured	Fine grained	Moderately Oxidised	grey	CALC filling fractures
OKD038	26	26.35	Massive metagreywacke	Bedded	Fine grained	Slightly Oxidised	grey	

OKD038	26.35	28.3	Massive metagreywacke	Bedded	Fine grained	Highly Oxidised	grey	
OKD038	28.3	36.71	Massive metagreywacke	Massive	Fine grained	Moderately Oxidised	grey	Fractured
OKD038	36.71	54.18	Massive metagreywacke	Bedded	Fine grained	Slightly Oxidised	grey	
OKD038	54.18	57.85	Massive metagreywacke	Massive	Fine grained	Fresh	grey	
OKD038	57.85	58.72	Massive metagreywacke	Bedded	Fine grained	Fresh	grey	
OKD038	58.72	60.98	Massive metagreywacke	Massive	Fine grained	Fresh	grey	

OKD038	60.98	63.26	Massive metagreywacke	Bedded	Fine grained	Fresh	grey	
OKD038	63.26	64.26	Massive metagreywacke	Massive	Fine grained	Fresh	grey	
OKD038	64.26	71.2	Massive metagreywacke	Bedded	Fine grained	Fresh	grey	
OKD038	71.2	72.94	Massive metagreywacke	Massive	Fine grained	Fresh	grey	
OKD038	72.94	82.33	Massive metagreywacke	Bedded	Fine grained	Fresh	grey	Breccia @ 81.39 m
OKD038	82.33	83.19	Massive metagreywacke	Brecciated	Fine grained	Fresh	grey	

OKD038	83.19	84.82	Massive metagreywacke	Bedded	Fine grained	Fresh	grey	Massive MGWK beds
OKD038	84.82	87.84	Massive metagreywacke	Massive	Fine grained	Fresh	grey	
OKD038	87.84	98.28	Massive metagreywacke	Bedded	Fine grained	Fresh	grey	Breccia @ 92.5 - 92.94 m calcite vn with py @ 97.7
OKD038	98.28	100.55	Massive metagreywacke	Massive	Fine grained	Fresh	grey	bedded MGWK intervals fractured zone @ 102 - 102.36
OKD038	100.55	101.6	Massive metagreywacke	Bedded	Fine grained	Fresh	grey	
OKD038	101.6	111.15	Massive metagreywacke	Massive	Fine grained	Fresh	grey	bedded MGWK intervals

OKD038	111.15	220.9	Massive metagreywacke	Bedded	Fine grained	Fresh	grey	CSU beds VNQ @ 192.7
OKD038	220.9	230.41	Biotite Schist	Schistose	Fine grained	Fresh	dark grey	
OKD038	230.41	236.12	Cordierite schist	Porphyroblastic	Fine grained	Fresh	dark grey	

OKD038 – Mineralogy

Hole_ID	Depth_From (m)	Depth_To (m)	Min1	Min1 (%)	Min2	Min2 (%)	Min3	Min3 (%)
OKD038	0	12.33	No Mineralization					
OKD038	12.33	21.11	Oxidized Sulphide	1				
OKD038	21.11	26.1	Oxidized Sulphide	2				
OKD038	26.1	34	Oxidized Sulphide	2	Pyrite	1		
OKD038	34	37.2	Oxidized Sulphide	1	Pyrite	1		
OKD038	37.2	38	Pyrite	2	Oxidized Sulphide	1		

OKD038	38	44	Oxidized Sulphide	1				
OKD038	44	45.81	Oxidized Sulphide	3	Pyrite	3		
OKD038	45.81	52	Pyrite	1	Oxidized Sulphide	1		
OKD038	52	57.8	Pyrrhotite	1	Pyrite	1		
OKD038	57.8	59	Pyrite	2	Pyrrhotite	1		
OKD038	59	63	Pyrite	2	Pyrrhotite	1		
OKD038	63	64.22	Pyrite	1	Pyrrhotite	1		
OKD038	64.22	66.65	Pyrite	2	Pyrrhotite	1		
OKD038	66.65	71	Pyrrhotite	1	Pyrite	1		
OKD038	71	72.14	Pyrrhotite	1				
OKD038	72.14	73.65	Pyrrhotite	1	Arsenopyrite	1		
OKD038	73.65	76.6	Pyrrhotite	1	Pyrite	1		
OKD038	76.6	77	Arsenopyrite	1	Pyrrhotite	1	Pyrite	1

OKD038	77	81.36	Pyrite	1	Pyrrhotite	1		
OKD038	81.36	85.41	Pyrite	2	Pyrrhotite	1	Arsenopyrite	1
OKD038	85.41	90.1	Pyrrhotite	1	Pyrite	1		
OKD038	90.1	95	Pyrite	2	Pyrrhotite	1	Arsenopyrite	1
OKD038	95	98.6	Pyrite	2	Pyrrhotite	1		
OKD038	98.6	103.9	Pyrrhotite	1	Pyrite	1		
OKD038	103.9	106	Pyrrhotite	2	Pyrite	2		
OKD038	106	114.25	Pyrrhotite	1	Pyrite	1		
OKD038	114.25	116	Pyrrhotite	2	Pyrite	1		
OKD038	116	119.45	Pyrrhotite	1	Pyrite	1		
OKD038	119.45	122	Pyrrhotite	2	Arsenopyrite	2	Pyrite	1
OKD038	122	125	Pyrrhotite	2	Pyrite	2		
OKD038	125	127.2	Pyrrhotite	2	Pyrite	1		
OKD038	127.2	130	Pyrrhotite	2	Arsenopyrite	2	Pyrite	1
OKD038	130	136.37	Pyrrhotite	1	Arsenopyrite	1	Pyrite	1
OKD038	136.37	140	Arsenopyrite	2	Pyrrhotite	1		

OKD038	140	148	Pyrrhotite	2				
OKD038	148	157	Pyrrhotite	2	Arsenopyrite	1		
OKD038	157	158.9	Pyrrhotite	1	Arsenopyrite	1		
OKD038	158.9	161.15	Pyrrhotite	1				
OKD038	161.15	163	Pyrrhotite	2				
OKD038	163	165.81	Pyrrhotite	1				
OKD038	165.81	169	Pyrrhotite	2				
OKD038	169	172	Pyrrhotite	2	Arsenopyrite	2	Pyrite	1
OKD038	172	184	Pyrrhotite	1	Arsenopyrite	1	Pyrite	1
OKD038	184	186.7	Pyrrhotite	1				
OKD038	186.7	187.5	Pyrrhotite	1	Arsenopyrite	1		
OKD038	187.5	191.15	Pyrrhotite	1				
OKD038	191.15	193.71	Pyrrhotite	1	Arsenopyrite	1	Pyrite	1
OKD038	193.71	203.98	Pyrrhotite	1	Pyrite	1		
OKD038	203.98	207.85	Arsenopyrite	3	Pyrrhotite	2		
OKD038	207.85	211.45	Arsenopyrite	2	Pyrrhotite	1		

OKD038	211.45	222.56	Pyrrhotite	1				
OKD038	222.56	223	Arsenopyrite	2	Pyrrhotite	1		
OKD038	223	224.41	Pyrrhotite	1	Pyrite	1		
OKD038	224.41	228.72	No Mineralization					
OKD038	228.72	229	Pyrite	1				
OKD038	229	236.12	No Mineralization					

OKD038 – Alteration

Hole_ID	Depth From (m)	Depth To (m)	Alteration 1	Intensity	Alteration 2	Intensity
OKD038	0	12.34	No Alteration			
OKD038	12.34	20	FeOx	Strong	Silicification	Moderate
OKD038	20	26.4	FeOx	Moderate		
OKD038	26.4	28.3	FeOx	Strong		
OKD038	28.3	45.81	FeOx	Moderate	Silicification	Moderate
OKD038	45.81	50.28	Potassic	Weak		
OKD038	50.28	51.1	Potassic	Moderate	Silicification	Moderate
OKD038	51.1	55.3	Potassic	Weak		
OKD038	55.3	60.58	Potassic	Weak		
OKD038	60.58	70.17	Silicification	Weak	Potassic	Weak
OKD038	70.17	73	Potassic	Weak		
OKD038	73	81.36	Potassic	Weak		
OKD038	81.36	85.3	Potassic	Weak		

OKD038	85.3	90.2	Silicification	Strong	Potassic	Strong
OKD038	90.2	94.1	Silicification	Strong	Potassic	Strong
OKD038	94.1	98.55	Potassic	Moderate	Silicification	Moderate
OKD038	98.55	102	Silicification	Strong	Potassic	Strong
OKD038	102	105.55	Potassic	Moderate		
OKD038	105.55	112.19	Potassic	Weak		
OKD038	112.19	120	Potassic	Moderate	Silicification	Weak
OKD038	120	122	Potassic	Moderate	Silicification	Moderate
OKD038	122	127.4	Potassic	Moderate	Silicification	Moderate
OKD038	127.4	132.17	Potassic	Strong	Silicification	Strong
OKD038	132.17	136.5	Potassic	Moderate	Silicification	Weak
OKD038	136.5	139.8	Potassic	Strong	Silicification	Strong
OKD038	139.8	141.26	Potassic	Weak		
OKD038	141.26	157	Potassic	Strong	Silicification	Moderate
OKD038	157	161.15	Potassic	Weak		
OKD038	161.15	163.31	Potassic	Strong		

OKD038	163.31	165.87	Potassic	Weak		
OKD038	165.87	180.98	Potassic	Strong	Silicification	Strong
OKD038	180.98	184	Potassic	Strong	Silicification	Moderate
OKD038	184	187.1	No Alteration			
OKD038	187.1	187.5	Potassic	Moderate	Silicification	Weak
OKD038	187.5	192	No Alteration			
OKD038	192	193.7	Silicification	Weak	Potassic	Weak
OKD038	193.7	203.98	No Alteration			
OKD038	203.98	207.06	Potassic	Moderate	Silicification	Weak
OKD038	207.06	216.25	No Alteration			
OKD038	216.25	219.55	Potassic	Moderate	Silicification	Moderate
OKD038	219.55	222.56	No Alteration			
OKD038	222.56	224.65	Potassic	Moderate	Silicification	Weak
OKD038	224.65	236.12	No Alteration			

OKD079 – Lithology

Hole_ID	Depth From (m)	Depth To (m)	Lithology	Texture	GrainSize	Oxidation	Colour	Comments
OKD079	0	7.63	Calcrete	Gritty	Medium grained	Slightly Oxidised	cream	
OKD079	7.63	12	Interbedded metagreywacke	Bedded	Fine grained	Moderately Oxidised	grey	
OKD079	12	15.5	Biotite Schist	Schistose	Fine grained	Slightly Oxidised	grey	gritty like altered
OKD079	15.5	25.6	Massive metagreywacke	Massive	Fine grained	Moderately Oxidised	grey	folding
OKD079	25.6	29.2	Massive metagreywacke	Massive	Fine grained	Fresh	grey	feox plane folding
OKD079	29.2	38.2	Massive metagreywacke	Massive	Fine grained	Fresh	grey	

OKD079	38.2	48.46	Interbedded metagreywacke	Bedded	Fine grained	Fresh	grey	
OKD079	48.46	56	Massive metagreywacke	Massive	Fine grained	Fresh	grey	
OKD079	56	66.7	Interbedded metagreywacke	Bedded	Fine grained	Fresh	grey	
OKD079	66.7	67.66	Interbedded metagreywacke	Bedded	Fine grained	Fresh	grey	sinistral fault
OKD079	67.66	73.3	Interbedded metagreywacke	Bedded	Fine grained	Fresh	grey	
OKD079	73.3	73.56	Massive metagreywacke	Massive	Fine grained	Fresh	grey	
OKD079	73.56	83.68	Massive metagreywacke	Massive	Fine grained	Fresh	grey	
OKD079	83.68	86	Massive metagreywacke	Massive	Fine grained	Fresh	grey	
OKD079	86	86.83	Massive metagreywacke	Massive	Fine grained	Fresh	grey	

OKD079	86.83	88	Massive metagreywacke	Massive	Fine grained	Fresh	grey	
OKD079	88	91.45	Massive metagreywacke	Massive	Fine grained	Fresh	grey	
OKD079	91.45	102.51	Massive metagreywacke	Massive	Fine grained	Fresh	grey	VNCC
OKD079	102.51	117.91	Interbedded metagreywacke	Bedded	Fine grained	Fresh	light grey	
OKD079	117.91	147.32	Massive metagreywacke	Massive	Fine grained	Fresh	dark grey	folding VNCC
OKD079	147.32	147.7	Massive metagreywacke	Massive	Fine grained	Fresh	dark grey	VNCC
OKD079	147.7	179	Massive metagreywacke	Massive	Fine grained	Fresh	dark grey	shear @ 159.63m
OKD079	179	183.37	Massive metagreywacke	Massive	Fine grained	Fresh	dark grey	VNCC
OKD079	183.37	197.85	Interbedded metagreywacke	Bedded	Fine grained	Fresh	light grey	

OKD079	197.85	198.7	Interbedded metagreywacke	Bedded	Fine grained	Fresh	light grey	VNCC
OKD079	198.7	236.12	Interbedded metagreywacke	Bedded	Fine grained	Fresh	light grey	CSU folding. Garnets sinistral fault
OKD079	236.12	252.03	Interbedded metagreywacke	Bedded	Fine grained	Fresh	dark grey	folding

OKD079 – Mineralogy

Hole_ID	Depth_From (m)	Depth_To (m)	Min1	Min1 (%)	Min2	Min2 (%)	Min3	Min3 (%)
OKD079	0	7.63	No Mineralization					
OKD079	7.63	24.03	Oxidized Sulphide	1				
OKD079	24.03	32.52	Pyrite	1	Arsenopyrite	1		
OKD079	32.52	39.83	No Mineralization					
OKD079	39.83	48.46	Pyrite	1	Arsenopyrite	1	Pyrrhotite	1
OKD079	48.46	55.08	Pyrite	1	Pyrrhotite	1		
OKD079	55.08	68.9	Pyrite	2	Arsenopyrite	2	Pyrrhotite	1
OKD079	68.9	76.95	Pyrite	1				
OKD079	76.95	82.92	Pyrite	1	Arsenopyrite	1	Pyrrhotite	1
OKD079	82.92	86.83	Pyrite	1				

OKD079	86.83	102.51	Pyrite	3	Arsenopyrite	1	Pyrrhotite	1
OKD079	102.51	108.22	Pyrrhotite	1	Pyrite	1	Arsenopyrite	1
OKD079	108.22	111.84	Pyrite	1	Pyrrhotite	1		
OKD079	111.84	113.55	Pyrrhotite	2	Pyrite	1	Arsenopyrite	1
OKD079	113.55	136.32	Pyrrhotite	2	Pyrite	1		
OKD079	136.32	148	Pyrrhotite	2	Arsenopyrite	1	Pyrite	1
OKD079	148	157.86	Pyrrhotite	1	Pyrite	1		
OKD079	157.86	166.07	Pyrrhotite	2	Pyrite	1	Arsenopyrite	1
OKD079	166.07	179	Pyrite	1	Pyrrhotite	1		
OKD079	179	183.3	No Mineralization					
OKD079	183.3	187.12	Pyrrhotite	1				
OKD079	187.12	204.85	Pyrrhotite	1	Pyrite	1	Arsenopyrite	1
OKD079	204.85	209.86	No Mineralization					
OKD079	209.86	219.2	Pyrite	1	Pyrrhotite	1	Arsenopyrite	1

OKD079	219.2	221.89	No Mineralization					
OKD079	221.89	244.99	Pyrrhotite	2	Pyrite	2	Arsenopyrite	1
OKD079	244.99	248.59	Pyrrhotite	1				
OKD079	248.59	249.09	Pyrrhotite	1	Arsenopyrite	1		
OKD079	249.09	251.5	Pyrrhotite	1				
OKD079	251.5	252.03	Pyrrhotite	2	Arsenopyrite	1	Pyrite	1

OKD079 – Alteration

Hole_ID	Depth From (m)	Depth To (m)	Alteration 1	Intensity	Alteration 2	Intensity
OKD079	0	12	No Alteration			
OKD079	12	15.5	FeOx	Weak		
OKD079	15.5	25.6	FeOx	Weak		
OKD079	25.6	39.83	No Alteration			
OKD079	39.83	41	Potassic	Weak	Silicification	Moderate
OKD079	41	48.46	Potassic	Weak	Silicification	Weak
OKD079	48.46	56	Potassic	Weak		
OKD079	56	56.61	Potassic	Moderate	Silicification	Moderate
OKD079	56.61	77	Potassic	Weak		
OKD079	77	81	Potassic	Moderate	Silicification	Moderate
OKD079	81	86.83	Potassic	Weak		
OKD079	86.83	92	Potassic	Weak	Silicification	Weak
OKD079	92	98.15	Silicification	Moderate	Potassic	Weak
OKD079	98.15	103.1	Silicification	Moderate	Potassic	Weak

OKD079	103.1	108.22	Silicification	Strong	Potassic	Moderate
OKD079	108.22	111.84	Potassic	Moderate		
OKD079	111.84	113.55	Silicification	Strong	Potassic	Moderate
OKD079	113.55	119.47	Potassic	Moderate		
OKD079	119.47	120.77	Potassic	Weak		
OKD079	120.77	124.78	Potassic	Weak		
OKD079	124.78	126.17	Silicification	Strong	Potassic	Weak
OKD079	126.17	140.1	Potassic	Moderate		
OKD079	140.1	157.86	Potassic	Weak		
OKD079	157.86	162	Potassic	Weak	Silicification	Weak
OKD079	162	177.87	Potassic	Moderate		
OKD079	177.87	178.15	Potassic	Moderate	Silicification	Weak
OKD079	178.15	179	Potassic	Weak		
OKD079	179	183.37	No Alteration			
OKD079	183.37	184	No Alteration			
OKD079	184	187.12	Potassic	Weak		

OKD079	187.12	195.95	Potassic	Weak	Silicification	Weak
OKD079	195.95	204.79	Silicification	Moderate	Potassic	Weak
OKD079	204.79	209.86	No Alteration			
OKD079	209.86	219.2	Potassic	Moderate	Silicification	Moderate
OKD079	219.2	221.59	Potassic	Weak		
OKD079	221.59	233.42	Silicification	Moderate	Potassic	Weak
OKD079	233.42	245.34	Potassic	Strong	Silicification	Moderate
OKD079	245.34	247.88	Potassic	Weak		
OKD079	247.88	249.03	Potassic	Strong	Silicification	Moderate
OKD079	249.03	251.5	Potassic	Weak		
OKD079	251.5	252.03	Potassic	Strong	Silicification	Moderate

OKD18 – Lithology

Hole_ID	Depth From (m)	Depth To (m)	Lithology	Texture	GrainSize	Oxidation	Colour	Comments
OKD118	0	18.84	Calcrete	Gritty	Medium grained	Slightly Oxidised	cream	DMT QTZ GTE IMGK fragments
OKD118	18.84	21	Interbedded metagreywacke	Bedded	Fine grained	Slightly Oxidised	grey	calcretized
OKD118	21	59.06	Interbedded metagreywacke	Bedded	Fine grained	Slightly Oxidised	grey	VNQs Peg veins between 42-44m
OKD118	59.06	77.25	Interbedded metagreywacke	Bedded	Fine grained	Fresh	grey	VNQs calcite vnlts
OKD118	77.25	86.4	Interbedded metagreywacke	Bedded	Fine grained	Fresh	grey	
OKD118	86.4	92.81	Interbedded metagreywacke	Bedded	Fine grained	Fresh	grey	calcite vnlts biotite selvaged veins VNQs
OKD118	92.81	104.55	Interbedded metagreywacke	Bedded	Fine grained	Fresh	grey	biotite selvaged vnlts calcite vnlts
OKD118	104.55	135.59	Cordierite metagreywacke	Porphyroblastic	Medium grained	Fresh	grey	VNQs garnets CSU beds calcite vnlts
OKD118	135.59	152.54	Massive metagreywacke	Massive	Fine grained	Fresh	grey	calcite vnlts CSU beds
OKD118	152.54	157.38	Interbedded metagreywacke	Bedded	Fine grained	Fresh	grey	garnets calcite vnlts
OKD118	157.38	168.58	Massive metagreywacke	Massive	Fine grained	Fresh	grey	garnets VNQs
OKD118	168.58	175.91	Interbedded metagreywacke	Bedded	Fine grained	Fresh	grey	biotite selvaged vnlts
OKD118	175.91	191.61	Interbedded metagreywacke	Bedded	Fine grained	Fresh	light grey	biotite selvages VNQs calcite vnlts

OKD118	191.61	202.56	Interbedded metagreywacke	Sheared	Fine grained	Fresh	light grey	VNQs biotite selvages calcite vnlts
OKD118	202.56	208.04	Interbedded metagreywacke	Bedded	Fine grained	Fresh	light grey	VNCC calcite vnlts
OKD118	208.04	222.24	Interbedded metagreywacke	Bedded	Fine grained	Fresh	light grey	biotite selvaged QTZ vnlts and VNQs
OKD118	222.24	247.47	Interbedded metagreywacke	Bedded	Fine grained	Fresh	light grey	biotite selvaged vnlts VNQs calcite vnlts folded
OKD118	247.47	260.82	Interbedded metagreywacke	Bedded	Fine grained	Fresh	light grey	biotite selvaged calcite vnlts
OKD118	260.82	273	Interbedded metagreywacke	Bedded	Fine grained	Fresh	grey	VNQs biotite selvages
OKD118	273	296.22	Massive metagreywacke	Massive	Fine grained	Fresh	grey	VNQs biotite selvages calcite vnlts
OKD118	296.22	329.78	Interbedded metagreywacke	Bedded	Fine grained	Fresh	grey	biotite selvaged vnlts
OKD118	329.78	337.65	Interbedded metagreywacke	Bedded	Fine grained	Fresh	grey	biotite selvaged VNQs
OKD118	337.65	348.68	Interbedded metagreywacke	Bedded	Fine grained	Fresh	grey	biotite selvaged vnlts
OKD118	348.68	368	Interbedded metagreywacke	Bedded	Fine grained	Fresh	light grey	biotite selvaged Qtz vnlts
OKD118	368	377.52	Interbedded metagreywacke	Bedded	Fine grained	Fresh	grey	calcite vnlts
OKD118	377.52	391.43	Massive metagreywacke	Massive	Fine grained	Fresh	light grey	
OKD118	391.43	420.76	Interbedded metagreywacke	Bedded	Fine grained	Fresh	grey	QTZ calcite vnlts CSU beds with aspmin
OKD118	420.76	422.81	Interbedded metagreywacke	Sheared	Fine grained	Fresh	grey	VNQs
OKD118	422.81	428.91	Interbedded metagreywacke	Bedded	Fine grained	Fresh	grey	VNQs

OKD118	428.91	438.7	Interbedded metagreywacke	Bedded	Fine grained	Fresh	grey	calcite vnlts CSU bed
OKD118	438.7	441.35	Interbedded metagreywacke	Fractured	Fine grained	Fresh	grey	calcite vnlts
OKD118	441.35	455	Interbedded metagreywacke	Bedded	Fine grained	Fresh	grey	CSU beds VNQs
OKD118	455	470.28	Interbedded metagreywacke	Bedded	Fine grained	Fresh	grey	CSU beds VNQs
OKD118	470.28	479.81	Massive metagreywacke	Massive	Fine grained	Fresh	grey	VNQs calcite vnlts
OKD118	479.81	487.65	Massive metagreywacke	Massive	Fine grained	Fresh	grey	calcite vnlts
OKD118	487.65	511.54	Interbedded metagreywacke	Bedded	Fine grained	Fresh	grey	QTZ vnlts CSU beds folded

OKD18 – Mineralogy

Hole_ID	Depth_From (m)	Depth_To (m)	Min1	Min1 (%)	Min2	Min2 (%)	Min3	Min3 (%)
OKD118	0	20.11	No Mineralization					
OKD118	20.11	21	Oxidized Sulphide	1				
OKD118	21	33.23	No Mineralization					
OKD118	33.23	38.16	Oxidized Sulphide	1				
OKD118	38.16	49.4	Pyrite	1				
OKD118	49.4	58.59	Pyrite	1				
OKD118	58.59	77.25	Pyrite	1				
OKD118	77.25	84	Pyrite	1				
OKD118	84	92.81	Pyrite	1	Arsenopyrite	1		

OKD118	92.81	97.29	Pyrrhotite	1				
OKD118	97.29	104.7	Pyrite	1				
OKD118	104.7	111.59	Pyrrhotite	1				
OKD118	111.59	152.59	Pyrite	1				
OKD118	152.59	168.58	Pyrite	1				
OKD118	168.58	171.54	Pyrrhotite	1				
OKD118	171.54	176.04	Pyrrhotite	1	Pyrite	1		
OKD118	176.04	202.56	Pyrrhotite	1	Pyrite	1		
OKD118	202.56	243	Pyrite	1	Arsenopyrite	1		
OKD118	243	247.34	Pyrrhotite	1				
OKD118	247.34	274.07	Pyrrhotite	1	Pyrite	1		
OKD118	274.07	281.35	Pyrrhotite	1				
OKD118	281.35	338.33	Pyrrhotite	1	Pyrite	1		
OKD118	338.33	342.95	Pyrrhotite	1				
OKD118	342.95	349.41	Pyrrhotite	1				
OKD118	349.41	393.23	Pyrrhotite	1	Pyrite	1		

OKD118	393.23	398.95	Pyrrhotite	1				
OKD118	398.95	436.74	Pyrrhotite	1	Pyrite	1		
OKD118	436.74	441.08	Pyrrhotite	1				
OKD118	441.08	442.71	Pyrrhotite	1	Arsenopyrite			
OKD118	442.71	455.55	Pyrite	1				
OKD118	455.55	457.24	Pyrrhotite	1				
OKD118	457.24	511.54	Pyrite	1				

OKD118 – Alteration

Hole_ID	Depth From (m)	Depth To (m)	Alteration 1	Intensity	Alteration 2	Intensity
OKD118	0	18.84	No Alteration			
OKD118	18.84	54.42	FeOx	Weak		
OKD118	54.42	85.35	Silicification	Weak		
OKD118	85.35	92.81	Silicification	Weak	Potassic	Weak
OKD118	92.81	101.45	Potassic	Weak		
OKD118	101.45	136.1	No Alteration			
OKD118	136.1	146.81	Silicification	Weak		
OKD118	146.81	159.28	Silicification	Weak	Potassic	Weak
OKD118	159.28	167.1	Silicification	Weak	Potassic	Weak
OKD118	167.1	171.58	No Alteration			
OKD118	171.58	176.04	Potassic	Weak		
OKD118	176.04	208.04	Silicification	Moderate	Potassic	Moderate
OKD118	208.04	222.67	Potassic	Weak	Silicification	Weak
OKD118	222.67	232.72	No Alteration			

OKD118	232.72	240.55	Potassic	Weak		
OKD118	240.55	241.16	Potassic	Weak		
OKD118	241.16	248.19	Potassic	Weak		
OKD118	248.19	260.05	Potassic	Weak	Silicification	Weak
OKD118	260.05	262.7	Potassic	Weak	Silicification	Weak
OKD118	262.7	273.22	Potassic	Weak	Silicification	Weak
OKD118	273.22	281.41	No Alteration			
OKD118	281.41	288.66	Potassic	Weak	Silicification	Weak
OKD118	288.66	298.13	Potassic	Moderate	Silicification	Weak
OKD118	298.13	300.41	No Alteration			
OKD118	300.41	302.31	Potassic	Weak		
OKD118	302.31	313.38	Potassic	Moderate	Silicification	Weak
OKD118	313.38	316.77	Potassic	Weak		
OKD118	316.77	337	Silicification	Moderate	Potassic	Moderate
OKD118	337	342.95	Potassic	Weak		
OKD118	342.95	348.68	Silicification	Weak	Potassic	Weak

OKD118	348.68	351.15	Silicification	Moderate	Potassic	Weak
OKD118	351.15	359.81	Silicification	Moderate	Potassic	Moderate
OKD118	359.81	367.64	Silicification	Moderate	Potassic	Weak
OKD118	367.64	377.55	Silicification	Moderate	Potassic	Weak
OKD118	377.55	383.95	Silicification	Moderate	Potassic	Weak
OKD118	383.95	391.43	Silicification	Moderate	Potassic	Moderate
OKD118	391.43	398.95	Potassic	Weak		
OKD118	398.95	404.1	Potassic	Weak	Silicification	Weak
OKD118	404.1	410.39	Silicification	Moderate	Potassic	Moderate
OKD118	410.39	416.11	Potassic	Weak		
OKD118	416.11	428.91	Silicification	Weak	Potassic	Weak
OKD118	428.91	437.15	Potassic	Weak	Silicification	Weak
OKD118	437.15	454.23	No Alteration			
OKD118	454.23	458.75	Potassic	Weak	Silicification	Weak
OKD118	458.75	461.19	No Alteration			
OKD118	461.19	496.54	Potassic	Weak	Silicification	Weak

OKD118	496.54	510.41	Potassic	Weak		
OKD118	510.41	511.54	No Alteration			

OKD142 – Lithology

Hole_ID	Depth From (m)	Depth To (m)	Lithology	Texture	GrainSize	Oxidation	Colour	Comments
OKD142	15.53	41.78	Cordierite metagreywacke	Sheared	Fine grained	Moderately Oxidised	grey	UCDD in parts
OKD142	41.78	63.18	Cordierite metagreywacke	Sheared	Fine grained	Slightly Oxidised	grey	
OKD142	63.18	69.8	Interbedded metagreywacke	Bedded	Fine grained	Slightly Oxidised	grey	
OKD142	69.8	81.4	Cordierite metagreywacke	Bedded	Fine grained	Slightly Oxidised	grey	Broken core in parts
OKD142	81.4	103.04	Massive metagreywacke	Bedded	Fine grained	Fresh	grey	
OKD142	103.04	144.35	Interbedded metagreywacke	Bedded	Fine grained	Fresh	light grey	slightly oxidised in parts folded

OKD142	144.35	162	Interbedded metagreywacke	Bedded	Fine grained	Fresh	grey	
OKD142	162	189.62	Interbedded metagreywacke	Bedded	Fine grained	Fresh	light grey	PEG qtz veins
OKD142	189.62	205.17	Interbedded metagreywacke	Bedded	Fine grained	Fresh	grey	garnets qzt veins
OKD142	205.17	236	Interbedded metagreywacke	Bedded	Fine grained	Fresh	grey	Broken in parts qtz veins garnets
OKD142	0	5	Calcrete	Conglomeratic	Fine grained	Slightly Oxidised	cream	
OKD142	5	7.16	Calcrete	Conglomeratic	Fine grained	Moderately Oxidised	grey	CGWK very friable
OKD142	7.16	15.53	Cordierite metagreywacke	Massive	Fine grained	Moderately Oxidised	grey	weak friable zone
OKD142	236	239.13	Massive metagreywacke	Sheared	Fine grained	Fresh	grey	Dextral faulting

OKD142	239.13	261.46	Interbedded metagreywacke	Bedded	Fine grained	Fresh	grey	Boudinage CSU beds
OKD142	261.46	282.45	Interbedded metagreywacke	Bedded	Fine grained	Fresh	grey	qzt veins broken zone folded
OKD142	282.45	303.08	Massive metagreywacke	Massive	Fine grained	Fresh	grey	CSU beds garnet E.O.H

OKD142 – Mineralogy

Hole_ID	Depth_From (m)	Depth_To (m)	Min1	Min1 (%)	Min2	Min2 (%)	Min3	Min3 (%)
OKD142	0	5	No Mineralization					
OKD142	5	52.25	Oxidized Sulphide	1				
OKD142	52.25	55.44	Oxidized Sulphide	1		1	Pyrite	1
OKD142	55.44	63.9	Pyrrhotite	1		1	Oxidized Sulphide	1
OKD142	63.9	69.32	Pyrrhotite	1		1		
OKD142	69.32	75.15	Pyrrhotite	1		1	Oxidized Sulphide	1
OKD142	75.15	93.2	Pyrrhotite	1		1		
OKD142	93.2	95.68	Pyrrhotite	1		1	Arsenopyrite	1

OKD142	95.68	97.68	Pyrrhotite	1		1		
OKD142	97.68	105.1	Pyrrhotite	1		1	Arsenopyrite	1
OKD142	105.1	113.7	Pyrrhotite	1		1		
OKD142	113.7	116.98	Pyrrhotite	1		1	Arsenopyrite	1
OKD142	116.98	121.57	Pyrrhotite	1		1		
OKD142	121.57	124.85	Pyrrhotite	1		1	Arsenopyrite	1
OKD142	124.85	128.5	Pyrrhotite	1		1		
OKD142	128.5	135.33	Pyrrhotite	1		1	Arsenopyrite	1
OKD142	135.33	144.31	Pyrrhotite	1		1		
OKD142	144.31	151.4	Pyrrhotite	1		1	Arsenopyrite	1
OKD142	151.4	153.96	Pyrrhotite	1		1		
OKD142	153.96	162.77	Pyrrhotite	1		1	Arsenopyrite	1
OKD142	162.77	199	Pyrrhotite	1		1		
OKD142	199	201.87	Pyrrhotite	1		1	Arsenopyrite	1
OKD142	201.87	211.47	Pyrrhotite	1		1		
OKD142	211.47	221.13	Pyrrhotite	1		1	Arsenopyrite	1

OKD142	221.13	223.87	Pyrrhotite	1		1		
OKD142	223.87	232.1	Pyrrhotite	1		1	Arsenopyrite	1
OKD142	232.1	238.2	Pyrrhotite	1		1		
OKD142	238.2	239.54	Pyrrhotite	2		1	Arsenopyrite	1
OKD142	239.54	260.82	Pyrrhotite	1		1		
OKD142	260.82	261.34	Pyrrhotite	1		1	Arsenopyrite	1
OKD142	261.34	269.18	Pyrrhotite	1		1		
OKD142	269.18	272.25	Pyrrhotite	1		1	Arsenopyrite	1
OKD142	272.25	279.12	Pyrrhotite	1		1		
OKD142	279.12	279.5	Pyrrhotite	1		1	Arsenopyrite	1
OKD142	279.5	287.77	Pyrrhotite	1		1		
OKD142	287.77	291.4	Pyrrhotite	1		1	Arsenopyrite	1
OKD142	291.4	303.08	Pyrrhotite	1		1		

OKD142 – Alteration

Hole_ID	Depth From (m)	Depth To (m)	Alteration 1	Intensity	Alteration 2	Intensity
OKD142	0	5	No Alteration			
OKD142	5	12.54	FeOx	Moderate		
OKD142	12.54	29	FeOx	Weak		
OKD142	29	43	FeOx	Moderate		
OKD142	43	52.25	FeOx	Weak		
OKD142	52.25	63.87	FeOx	Weak		
OKD142	63.87	68.74	Potassic	Weak		
OKD142	68.74	75.15	Potassic	Weak	FeOx	Weak
OKD142	75.15	78.94	Potassic	Weak		
OKD142	78.94	86.43	Potassic	Weak		
OKD142	86.43	90.3	Potassic	Weak		
OKD142	90.3	93.07	Potassic	Weak		
OKD142	93.07	100.33	Potassic	Weak		
OKD142	100.33	105.68	Potassic	Moderate	Silicification	Moderate

OKD142	105.68	109.31	Potassic	Weak		Weak
OKD142	109.31	113.67	Potassic	Moderate	Silicification	Moderate
OKD142	113.67	121.86	Potassic	Weak		Weak
OKD142	121.86	133.23	Potassic	Moderate		Moderate
OKD142	133.23	134.16	Potassic	Moderate	Silicification	Moderate
OKD142	134.16	136.82	Potassic	Moderate		Moderate
OKD142	136.82	161.93	Potassic	Weak		Weak
OKD142	161.93	189	Potassic	Moderate	Silicification	Moderate
OKD142	189	201.03	Potassic	Weak		Weak
OKD142	201.03	207	Potassic	Weak	Silicification	Weak
OKD142	207	221.52	Potassic	Weak		Weak
OKD142	221.52	227.62	Potassic	Moderate		Moderate
OKD142	227.62	235.86	Potassic	Weak		Weak
OKD142	235.86	239.26	Potassic	Moderate	Silicification	Moderate
OKD142	239.26	286.88	Potassic	Weak		
OKD142	286.88	295.5	Potassic	Weak		

OKD142	295.5	303.08	No Alteration			

OKD211 – Lithology

Hole_ID	Depth From (m)	Depth To (m)	Lithology	Texture	GrainSize	Oxidation	Colour	Comments
OKD211	0	4.34	Calcrete	Conglomeratic	Medium grained	Slightly Oxidised	cream	
OKD211	4.34	17.6	Interbedded metagreywacke	Bedded	Fine grained	Moderately Oxidised	cream	bleached oxidized
OKD211	17.6	18.89	Quartz vein	Massive	Coarse grained	Slightly Oxidised	white	
OKD211	18.89	35.07	Interbedded metagreywacke	Bedded	Fine grained	Moderately Oxidised	cream	bleached oxidized
OKD211	35.07	51	Interbedded metagreywacke	Bedded	Fine grained	Slightly Oxidised	light grey	slightly bleached
OKD211	51	60.27	Interbedded metagreywacke	Bedded	Fine grained	Fresh	light grey	

OKD211	60.27	118.6	Interbedded metagreywacke	Bedded	Fine grained	Fresh	grey	
OKD211	118.6	123.62	Interbedded metagreywacke	Bedded	Fine grained	Fresh	grey	graphitized
OKD211	123.62	173.6	Interbedded metagreywacke	Bedded	Fine grained	Fresh	grey	
OKD211	173.6	187.54	Massive metagreywacke	Massive	Fine grained	Fresh	grey	
OKD211	187.54	221.25	Interbedded metagreywacke	Bedded	Fine grained	Fresh	grey	CSUs
OKD211	221.25	255.56	Massive metagreywacke	Massive	Fine grained	Fresh	grey	
OKD211	255.56	269.02	Massive metagreywacke	Massive	Fine grained	Slightly Oxidised	grey	fault zone
OKD211	269.02	296	Massive metagreywacke	Massive	Fine grained	Fresh	grey	

OKD211	296	300.15	Cordierite metagreywacke	Porphyroblastic	Fine grained	Fresh	grey	E.O.H

OKD211 – Mineralogy

Hole_ID	Depth_From (m)	Depth_To (m)	Min1	Min1 (%)	Min2	Min2 (%)	Min3	Min3 (%)
OKD211	0	18.87	No Mineralization					
OKD211	18.87	35.07	Oxidized Sulphide	2				
OKD211	35.07	45.7	Pyrrhotite	1	Pyrite	1	Oxidized Sulphide	1
OKD211	45.7	51	Pyrrhotite	1	Pyrite	1	Oxidized Sulphide	1
OKD211	51	68.07	Pyrrhotite	1	Arsenopyrite	1	Pyrite	1
OKD211	68.07	79.8	Pyrrhotite	1	Pyrite	1		
OKD211	79.8	82.7	Pyrrhotite	1	Pyrite	1	Arsenopyrite	1
OKD211	82.7	92.04	Pyrrhotite	1	Pyrite	1		
OKD211	92.04	92.56	Pyrrhotite	1	Pyrite	1	Arsenopyrite	1

OKD211	92.56	105.83	Pyrrhotite	1	Pyrite	1		
OKD211	105.83	147.82	Pyrrhotite	1	Pyrite	1	Arsenopyrite	1
OKD211	147.82	204.7	Pyrrhotite	1	Pyrite	1		
OKD211	204.7	211.4	Pyrrhotite	1	Pyrite	1	Arsenopyrite	1
OKD211	211.4	224.86	Pyrrhotite	1	Pyrite	1		
OKD211	224.86	228.92	Pyrrhotite	1	Pyrite	1	Arsenopyrite	1
OKD211	228.92	296	Pyrrhotite	1	Pyrite	1		
OKD211	296	300.15	Pyrite	1				

OKD142 – Alteration

Hole_ID	Depth From (m)	Depth To (m)	Alteration 1	Intensity	Alteration 2	Intensity
OKD211	0	4.34	No Alteration			
OKD211	4.34	17.6	FeOx	Moderate		
OKD211	17.6	18.87	FeOx	Weak	Potassic	Weak
OKD211	18.87	35.07	FeOx	Moderate		
OKD211	35.07	51	Silicification	Moderate	Potassic	Weak
OKD211	51	60.27	Silicification	Moderate	Potassic	Moderate
OKD211	60.27	106.36	Potassic	Weak		
OKD211	106.36	111.7	Potassic	Weak	Silicification	Weak
OKD211	111.7	136.81	Silicification	Moderate	Potassic	Moderate
OKD211	136.81	144.14	Potassic	Weak		
OKD211	144.14	148.26	Potassic	Moderate	Silicification	Weak
OKD211	148.26	171.17	Potassic	Weak		

OKD211	171.17	175.87	No Alteration			
OKD211	175.87	180.32	Potassic	Weak	Silicification	Weak
OKD211	180.32	187.54	No Alteration			
OKD211	187.54	203.75	Potassic	Weak		
OKD211	203.75	212.77	Potassic	Moderate	Silicification	Moderate
OKD211	212.77	296	Potassic	Weak		
OKD211	296	300.15	No Alteration			